4 Supersymmetric Models with an Extra Singlet

4.1 Introduction

Stephanie Baffioni, John F. Gunion, David J. Miller, Apostolos Pilaftsis and Dirk Zerwas

The Minimal Supersymmetric Standard Model (MSSM) suffers from a serious theoretical flaw known as the "μ-problem". The dimensionful parameter μ is required in the MSSM in order to have mixing between the two chiral Higgs doublet superfields. The difficulty is that μ has no *a priori* knowledge of electroweak symmetry breaking, but must, for phenomenological reasons, be around the electroweak scale. The very simplest means for resolving this problem is the introduction of a singlet Higgs chiral superfield. It is easy to arrange for the scalar component of the singlet superfield to acquire a vacuum expectation value of electroweak or SUSY breaking magnitude, and this automatically generates an effective μ with electroweak magnitude. The resulting models are very attractive and not only succeed in solving the μ problem but do not encounter the various problems of the MSSM associated with the LEP lower bounds on the masses of Higgs bosons. For instance, unlike the MSSM, the singlet-extended scenarios with low values of $\tan\beta \lesssim 3$ are viable due to additional tree-level contributions to the theoretical upper bound on the Higgs-boson mass. A SM-like Higgs boson with mass of order 100 GeV is also a possibility, evading conflict with LEP limits by virtue of Higgs to Higgs-pair decays. In addition, the parameters of the singlet models can be chosen so that the so-called "little hierarchy" problem can be significantly alleviated and electroweak baryogenesis is successful. In general, the Higgs sector phenomenology of the singlet models is much less constrained than that of the MSSM, leading to a far greater range of possible experimental signatures and needed search strategies.

In section 4.1.1 we begin by describing the μ problem in more detail and in section 4.1.2 show how it can be solved by the introduction of a new Higgs singlet chiral superfield. In section 4.1.3 we then outline the major variants of such models that emerge when cosmological issues associated with domain walls in the early universe are taken into consideration. In section 4.1.4, a summary of the main model and phenomenological features of the two simplest models, the NMSSM and the MNSSM, is provided. Experimentalists may wish to focus on this summary section.

4.1.1 The μ-problem

Any renormalizable supersymmetric model can be completely specified by a choice of particle content, gauge symmetries and a *superpotential*. The gauge symmetries dictate the form of the gauge interactions in the Lagrangian, while the superpotential yields non-gauge interaction terms proportional to its second derivatives with respect to the scalar fields. A superpotential W results in terms,

$$\mathcal{L} \supset -\frac{1}{2}\left(\frac{\partial^2 W}{\partial\phi_i\partial\phi_j}\psi_i\psi_j + \frac{\partial^2 W^*}{\partial\phi_i^*\partial\phi_j^*}\psi_i^\dagger\psi_j^\dagger\right) - \frac{\partial W}{\partial\phi_i}\frac{\partial W^*}{\partial\phi^{*\,i}}, \tag{4.1}$$

where ϕ_i are the scalar fields, ψ_i are their fermion partners, and summation over repeated indices is understood. The scalar and fermion fields have dimension [mass] and [mass]$^{3/2}$ respectively, and the Lagrangian is dimension [mass]^4, so it is easy to see that the superpotential has dimension [mass]^3. Since supersymmetry (SUSY) is broken, one must also introduce soft SUSY breaking terms, which generally include soft mass terms in addition to terms of the same form as those in the superpotential multiplied by arbitrary (but $\mathcal{O}(M_{\rm SUSY})$) dimensionful coefficients.

The superpotential of the MSSM can be written as,[1]

$$W_{\rm MSSM} \;=\; \widehat{Q}\widehat{H}_u\mathbf{h_u}\widehat{U}^C \;+\; \widehat{H}_d\widehat{Q}\mathbf{h_d}\widehat{D}^C \;+\; \widehat{H}_d\widehat{L}\mathbf{h_e}\widehat{E}^C \;+\mu\widehat{H}_u\widehat{H}_d\,. \tag{4.2}$$

Here and in the following, fields with a hat denote superfields, whilst those without a hat stand for scalar superfield components. In addition to the Yukawa couplings of the two Higgs doublets to quarks and

[1] Our notation of the Higgs superfields with respect to the one given in Section 3 is: $\widehat{H}_u \equiv \widehat{H}_2$ and $\widehat{H}_d \equiv \widehat{H}_2$.

leptons, Eq. (4.2) contains a term involving a dimensionful parameter μ. This performs two essential functions in the MSSM. Firstly, it provides a contribution to the masses of the Higgs bosons and their higgsino partners (for this reason μ is often called the "Higgs-higgsino mass parameter"). Without this contribution the lightest chargino, which is a mixture of a higgsino and a gaugino, would have a mass of order $M_W^2/M_{\rm SUSY}$ which is small enough to be excluded by experimental searches. Secondly, the accompanying soft supersymmetry breaking term $B\mu\, H_u H_d$ provides a mixing between the two Higgs doublets. Without this term, any electroweak symmetry breaking generated in the up-quark sector (caused by $M_{H_u}^2 < 0$) could not be communicated to the down-quark sector; the field H_d would not gain a vacuum expectation value (vev) and the down-type quarks and leptons would remain massless. It is therefore essential that μ be non-zero and of order the electroweak or supersymmetry breaking scales.

However, since the parameter μ appears in the superpotential it does not break supersymmetry and is present when supersymmetry is unbroken. Its value is therefore completely unrelated to the electroweak or supersymmetry breaking scales. In fact, within a supergravity (SUGRA) framework, the μ-parameter is naturally expected to be of order $M_{\rm Planck}$. This huge disparity between the natural and phenomenologically needed scales of μ is known as the "μ-problem".

4.1.2 Solving the μ-problem with an extra singlet

Many scenarios, all based on extensions of the MSSM, have been proposed in the existing literature [1–5] to provide a natural explanation of the μ-term. The simplest approach, and that which concerns us here, is to introduce an extra Higgs iso-singlet superfield, $\widehat{S}$, into the model. If we replace the μ-term of the MSSM with a term coupling this new superfield to the Higgs boson doublets, i.e.

$$W_\lambda \;=\; \widehat{Q}\widehat{H}_u\mathbf{h_u}\widehat{U}^C \;+\; \widehat{H}_d\widehat{Q}\mathbf{h_d}\widehat{D}^C \;+\; \widehat{H}_d\widehat{L}\mathbf{h_e}\widehat{E}^C \;+\; \lambda\widehat{S}\widehat{H}_u\widehat{H}_d\,, \tag{4.3}$$

where λ is some dimensionless coupling, then an effective μ-term will be generated if the real scalar component of $\widehat{S}$ develops a vacuum expectation value (vev). The *effective* μ parameter is given by

$$\mu \;=\; \mu_{\rm eff} \;=\; \lambda\langle S\rangle. \tag{4.4}$$

The constraints which arise when the resulting Higgs potential is minimized to find the vacuum state relate the vevs of the three neutral scalars, H_u^0, H_d^0 and S, to their soft supersymmetry breaking masses. Therefore, in the absence of fine tuning, one expects that these vevs should all be of order $M_{\rm SUSY}$, and the μ problem is solved. These three vevs are usually then replaced by the phenomenological parameters $\mu_{\rm eff}$, M_Z and $\tan\beta$.

Additionally, one must introduce soft supersymmetry breaking terms into the Lagrangian. These must be of the same form as for the MSSM except that the term involving the supersymmetry breaking parameter B must be removed (since it was associated with the μ-term) and instead a soft mass for the new singlet should be added, together with soft supersymmetry breaking terms for the extra interactions. The soft supersymmetry breaking terms associated with the Higgs sector are then,

$$-\mathcal{L}_{\rm soft} \;\supset\; m_{H_u}^2|H_u|^2 + m_{H_d}^2|H_d|^2 + m_S^2|S|^2 + \Big(\lambda A_\lambda S H_u H_d + \text{h.c.}\Big)\,, \tag{4.5}$$

where A_λ is a dimensionful parameter of order $\sim M_{\rm SUSY}$.

The new singlet superfield provides an additional scalar Higgs field, a pseudoscalar Higgs field, and an accompanying higgsino. The new Higgs fields will mix with the neutral Higgs fields from the usual Higgs doublets, and so the model will in total have five neutral Higgs bosons (three scalars and two pseudoscalars if CP is conserved). The extra higgsino will mix with the higgsinos from the doublets and the gauginos to provide an extra neutralino state, for a total of five. The charged Higgs and chargino mass spectrum remain unchanged.

However, the superpotential presented in Eq. (4.3), and its derived Lagrangian, contain an extra global U(1) symmetry, known as a Peccei-Quinn (PQ) Symmetry [6]. Assigning PQ charges, Q^{PQ}, according to

$$\widehat{Q} : -1, \quad \widehat{U}^C : 0, \quad \widehat{D}^C : 0, \quad \widehat{L} : -1, \quad \widehat{E}^C : 0, \quad \widehat{H}_u : 1, \quad \widehat{H}_d : 1, \quad \widehat{S} : -2, \tag{4.6}$$

the model is invariant under the global $U(1)$ transformation $\widehat{\Psi}_i \to e^{iQ_i^{PQ}\theta}\widehat{\Psi}_i$, where

$$\widehat{\Psi}_i \in \{\widehat{Q}, \widehat{U}^C, \widehat{D}^C, \widehat{L}, \widehat{E}^C, \widehat{H}_u, \widehat{H}_d, \widehat{S}\}.$$

The PQ symmetry will spontaneously break when the Higgs scalars gain vevs, and a pseudo[2]-Nambu-Goldstone boson, known as the PQ axion (it is actually one of the pseudoscalar Higgs bosons), will be generated. For values of $\lambda \sim \mathcal{O}(1)$, this axion would have been detected in experiment and this model ruled out. There are three ways that this model can be saved.

Firstly, one can simply decouple the axion by making λ very small [7–12]. One finds that astrophysical constraints from the cooling of stars in globular clusters are most restrictive, requiring $\lambda \lesssim 10^{-6}$. Interestingly, since the singlet vev is always multiplied by λ, i.e. appears as $\lambda\langle S\rangle$, in the minimization equations which set the vevs, in the absence of fine tuning μ_{eff} will still naturally be of order the electroweak scale. Additionally, the presence of an axion automatically solves the strong CP problem via its effective coupling to the gluon. However, since there is no good explanation of why λ should be so small, we are really just replacing one problem with another.

There is also an issue of how much dark matter is present in this model. Usually in R-parity conserving supersymmetry, the lightest supersymmetric partner (LSP) will, if neutral, provide a contribution to dark matter. In this case the LSP is the supersymmetric partner of the axion, often called the axino (it is actually a neutralino). It is very light, typically $\sim 10^{-6}$eV, and, like its partner state, is very decoupled. Therefore its annihilation rate in the early universe would be very small and it should naively provide a dark matter contribution so large that the model can be ruled out. However, the axino is so decoupled that it may never have come into equilibrium in the early universe. In this case, there would be no need to have a large annihilation cross-section to reduce its dark matter contribution; one could simply have very few axinos before annihilation starts.

A second possibility is to promote the PQ symmetry to a local symmetry. This requires the introduction of a new gauge boson, traditionally called Z', mediating a new force, which will gain a mass when the PQ symmetry is broken. As usual, the Goldstone boson will be "eaten" by the gauge boson to provide the extra degree of freedom needed for its longitudinal polarization, and consequently there would be no axion to be found in low energy experiments.

The existence of additional U(1) gauge groups at TeV energies is well motivated by GUT and string models [13–16]. In particular, compactification of the extra dimensions in string theories often leads to large gauge groups such as E_6 or E_8. These gauge groups can then break down to the gauge groups of the SM with extra (local) U(1)'s. For example, one possible breaking would be $E_6 \to SO(10)\times U(1)_\phi$ followed by $SO(10) \to SU(5)\times U(1)_\chi$. In general, the gauge bosons of these two new $U(1)$ symmetries mix, and one can arrange the symmetry breaking such that one combination maintains a GUT scale mass, while the other is manifest at (just above) the electroweak scale and becomes the Z'.

The existence of an extra Z' is already strongly constrained by experiment [17]. Direct searches at the Tevatron [18, 19] constrain the Z' mass by looking for its decay to leptons or jets. These direct searches typically require a Z' of the form described above to be heavier than a few hundred GeV. Indirect searches for virtual Z' exchange and/or Z-Z' mixing yield similar limits. Models with extra gauge groups are discussed in Section 6.

[2] The axion is only a "pseudo"-Nambu-Goldstone boson since the PQ symmetry is explicitly broken by the QCD triangle anomaly. The axion then acquires a small mass from its mixing with the pion.

4.1.3 Breaking the Peccei-Quinn symmetry

The last (but by no means least) way of avoiding the PQ axion constraints is to explicitly break the PQ symmetry. The new superfield $\widehat{S}$ has no gauge couplings but has a PQ charge, so one can naively introduce any term of the form $\widehat{S}^n$ with $n \in \mathbb{Z}$ into the superpotential in order to break the PQ symmetry. However, since the superpotential is of dimension 3, any power with $n \neq 3$ will require a dimensionful coefficient naturally of the GUT or Planck scale, naively making the term either negligible (for $n > 3$) or unacceptably large (for $n < 3$). For this reason, it is usual to postulate some extra discrete symmetry, e.g. $\mathbb{Z}_3$, in order to forbid terms with dimensionful coefficients. The superpotential of the model then becomes,

$$W_{\text{NMSSM}} \;=\; W_\lambda \;+\; \frac{1}{3}\kappa\widehat{S}^3\;, \tag{4.7}$$

where κ is a dimensionless constant which measures the size of the PQ breaking.

Additionally, one must also introduce an extra soft supersymmetry breaking term to accompany the new trilinear self coupling. The complete soft SUSY-breaking Higgs sector becomes then,

$$-\mathcal{L}_{\text{soft}} \;\supset\; m^2_{H_u}|H_u|^2 + m^2_{H_d}|H_d|^2 + m^2_S|S|^2 + \Big(\lambda A_\lambda S H_u H_d + \frac{1}{3}\kappa A_\kappa S^3 + \text{h.c.}\Big)\;, \tag{4.8}$$

where, like A_λ, A_κ is a dimensionful coefficient of order $\sim M_{\text{SUSY}}$.

This model is known as the Next-to-Minimal Supersymmetric Standard Model (NMSSM) and has generated much interest in the literature [13, 15, 20–31]. Just as for the PQ symmetric model discussed above, the neutral Higgs sector will consist of three scalars and two pseudoscalars. The masses and singlet contents of the physical fields depend strongly on the parameters of the model, in particular how well the PQ symmetry is broken. Also, there will be five neutralinos instead of the usual four. The charged Higgs sector and the chargino sector remain unchanged. Some aspects of the phenomenology of the NMSSM will be summarized later and in separate contributions.

Phenomenologically, this model is rather interesting. Notice that we have introduced extra fields with no gauge couplings and mixed them with the usual fields of the MSSM. This will dilute the couplings of the Higgs bosons and neutralinos when compared to the MSSM. Furthermore, it is possible to have a rather light pseudoscalar Higgs boson, which is a bit more difficult to have in the MSSM. Potentially, heavier Higgs bosons may decay into this light pseudoscalar rather than via more conventional decays to, say, b quarks. Therefore, one may find that the usual search channels at the LHC are not as successful as they are for the MSSM. Some of the related phenomenological issues will be summarized later and some will be discussed in separate contributions.

Here, we focus on the solution to a possible cosmological problem for the NMSSM. The $\mathbb{Z}_3$ symmetry, which we enforced on the model to ensure the absence of dimensionful couplings, cannot be completely unbroken. If it were, a "domain wall problem" would arise. In particular, if $\mathbb{Z}_3$ symmetry is exact, observables are unchanged when we (globally) transform all the fields according to $\Psi \to e^{i2\pi/3}\Psi$. Therefore the model will have three separate but degenerate vacua, and which one of these ends up being the "true" vacuum is a random decision taken at the time of electroweak symmetry breaking. However, one expects that causally disconnected regions of space would not necessarily choose the same vacuum, and our observable universe should consist of different domains with different ground states, separated by domain walls [32]. Such domain wall structures create unacceptably large anisotropies in the cosmic microwave background [33]. Historically, it was always assumed that the $\mathbb{Z}_3$ symmetry could be broken by an appropriate type of unification with gravity at the Planck scale. Non-renormalizable operators will generally be introduced into the superpotential and Kähler potential which break $\mathbb{Z}_3$ and lead to a preference for one particular vacuum, thereby solving the problem. However, the same operators may give rise at the loop level to quadratically divergent tadpole contributions in the Lagrangian, of the form [34–41]

$$\mathcal{L}_{\text{soft}} \;\supset\; t_S\, S \;\sim\; \frac{1}{(16\pi^2)^n}\, M_{\text{P}}\, M^2_{\text{SUSY}}\, S\;, \tag{4.9}$$

where n is the number of loops. Clearly, this tadpole breaks the $\mathbb{Z}_3$ symmetry as desired. But, if $n < 5$, t_S is several orders of magnitude larger than the soft-SUSY breaking scale M_{SUSY}. This leads to an unacceptably large would-be μ-term since $t_S\, S$ combines with the $\sim M^2_{\mathrm{SUSY}} S^* S$ soft mass term to yield a shift in the vev of S to a value of order $\langle S\rangle \sim \frac{t_S}{M^2_{\mathrm{SUSY}}} \sim \frac{1}{(16\pi^2)^n}\, M_{\mathrm{P}}$ and corresponding $\mu_{\mathrm{eff}} \sim \lambda\langle S\rangle$. For example, if the tadpole were generated at the one-loop level, the effective μ-term would be huge, of order 10^{16}–10^{17} GeV i.e. close to the GUT scale, whereas μ should be of order of the electroweak scale to realize a natural Higgs mechanism. Hence, it was argued in [42] that the NMSSM is either ruled out cosmologically or suffers from a naturalness problem related to the destabilization of the gauge hierarchy. However, there are at least two simple escapes.

One obvious way out of this problem would be to gauge the $U(1)_{\mathrm{PQ}}$ symmetry [13–16]. In this case, the $\mathbb{Z}_3$ symmetry is embedded into the local $U(1)$ symmetry. The would-be PQ axion is then eaten by the longitudinal component of the extra gauge boson. However, from a low-energy perspective, the price one has to pay here is that the field content needs to be extended by adding new chiral quark and lepton states in order to ensure anomaly cancellation related to the gauged $U(1)_{\mathrm{PQ}}$ symmetry.

The second approach is to find symmetry scenarios [43] where all harmful destabilizing tadpoles are absent. This can be achieved by imposing a discrete Z_2^R symmetry under which all superfields and the superpotential flip sign. To avoid destabilization while curing the domain wall problem, this symmetry has to be extended to the non-renormalizable part of the superpotential and to the Kähler potential. As happens to all R-symmetries, Z_2^R symmetry is broken by the soft-SUSY breaking terms, giving rise to harmless tadpoles of order $\frac{1}{(16\pi^2)^n}\, M^3_{\mathrm{SUSY}}$, with $2 \le n \le 4$. Although these terms are phenomenologically irrelevant, they are entirely sufficient to break the global Z_3 symmetry and make the domain walls collapse.

Another potentially interesting alternative for breaking the PQ symmetry is the realization of the so-called Minimal Nonminimal Supersymmetric Standard Model (MNSSM) [44]. The basic idea is to find discrete R symmetries, such that the destabilizing tadpoles do appear but are naturally suppressed because they arise at loops higher than 5 [45]. In particular, these symmetries may lead to a superpotential whose renormalizable part has exactly the form W_λ in (4.3). Hence, the effective renormalizable superpotential of such a model reads [44]:

$$W^{\mathrm{eff}}_{\mathrm{MNSSM}} \;=\; W_\lambda \;+\; t_F \widehat{S}\,. \tag{4.10}$$

where t_F is a radiatively induced tadpole of the electroweak scale. In addition, there will be a soft SUSY-breaking tadpole term $t_S S$ as given in (4.9). The key point in the construction of the renormalizable MNSSM superpotential is that the simple form (4.10) can be enforced by discrete R-symmetries [44–47]. These discrete R-symmetries govern the complete gravity-induced non-renormalizable superpotential and Kähler potential. Within the SUGRA framework of SUSY-breaking, it has then been possible to show [44] that the potentially dangerous tadpole t_S will appear at a loop level n higher than 5. From (4.9), the size of the tadpole parameter t_S can be estimated to be in the right ballpark, i.e. $|t_S| \lesssim$ 1–10 TeV^3 for $n = 6, 7$, such that the gauge hierarchy does not get destabilized. To be specific, the tadpole $t_S\, S$ together with the soft SUSY-breaking mass term $m_S^2 S^* S \sim M^2_{\mathrm{SUSY}} S^* S$ lead to a vacuum expectation value (VEV) for S, $\big\langle S\big\rangle = \frac{1}{\sqrt{2}} v_S$, of order $M_{\mathrm{SUSY}} \sim 1$ TeV. The latter gives rise to a μ-parameter at the required electroweak scale. Thus, another natural explanation for the origin of the μ-parameter can be obtained.

4.1.4 *Model features and phenomenological highlights of the NMSSM and the MNSSM*

In the following, we summarize the basic field-theoretic, phenomenological and cosmological features of the NMSSM and the MNSSM, and how these compare with the MSSM.

(i) Even though the mechanisms are different, both the NMSSM and the MNSSM can provide a *minimal* and an *elegant* solution to the μ-problem of the MSSM. The μ-parameter arises from the superpotential term $\lambda \widehat{S}\widehat{H}_u\widehat{H}_d$, through the vev of the scalar component S of the singlet superfield $\widehat{S}$, i.e. $\lambda\langle S\rangle \widehat{H}_u\widehat{H}_d = \mu_{\rm eff}\widehat{H}_u\widehat{H}_d$. Such a term is essential for acceptable phenomenology.

(ii) The difference between the NMSSM and MNSSM arises from the symmetries imposed upon the superpotential and Kähler potential within a SUGRA framework. In the NMSSM case, they are such as to allow an additional superpotential component of form $\frac{1}{3}\kappa\widehat{S}^3$ and disallow all superpotential terms with dimensionful parameters, with the result that the scale of electroweak symmetry breaking is generated by the scale of SUSY breaking only. In the MNSSM case, symmetries are chosen so as to forbid the cubic singlet superpotential term but allow a linear tadpole term $t_S\,S$ ($t_F\widehat{S}$) where t_S (t_F) is dimensionful. The symmetries in the two cases are set up so that the tadpole term proportional to S coming from multi-loop-induced operators arising from physics above the unification scale is phenomenologically irrelevant in the NMSSM case, whereas it is crucial in the MNSSM case. In both cases, however, these symmetries play an important role in naturally solving the cosmological domain wall and visible axion problems.

(iii) After employing the minimization conditions for the Higgs potential and demanding the known value of the Z mass, the parameters specifying the Higgs sectors in the two models are as follows. In the NMSSM a convenient set is

$$\lambda, \quad \kappa, \quad A_\lambda, \quad A_\kappa, \quad \mu = \mu_{\rm eff}, \quad \tan\beta\,. \tag{4.11}$$

In the case of the MNSSM, a convenient parameter set is

$$\lambda, \quad A_\lambda\ (\text{or } M_{H^+}), \quad \mu = \mu_{\rm eff}, \quad \tan\beta, \quad \lambda\, t_S/\mu\,, \tag{4.12}$$

whereas the extra parameter t_F can be ignored as it appears usually suppressed in generic SUGRA-mediated SUSY-breaking scenarios. In addition, the stop squark masses strongly influence the Higgs boson masses and mixings through radiative corrections.

(iv) Since the NMSSM and the MNSSM introduce only a singlet superfield $\widehat{S}$ which is uncharged under the SM gauge group, the good property of gauge coupling unification in the MSSM is preserved. In the same context, the radiative electroweak symmetry breaking mechanism remains natural in both cases.

(v) The "little fine tuning problem", which results in the MSSM due to the fact that LEP II failed to detect a CP-even Higgs boson, is less severe within the NMSSM and the MNSSM. In particular, the scenarios that arise from the requirement of minimal fine tuning point to certain phenomenologies [48, 49]. For example, one might have complete absence of the fine-tuning problem, if the lightest CP-odd Higgs particle A_1 is light enough to allow for the decay $H_1 \to A_1A_1$ [48, 49]. Indeed, the models with absolute minimum fine tuning and with A_1 mass below $2m_b$ are especially interesting since they predict a rate for ZH_1 with $H_1 \to b\bar{b}$, which is also consistent with a possible event excess in the LEP data for Higgs mases in the vicinity of 100 GeV. Such a possibility of a light 'CP-odd' Higgs may arise within the MSSM [50], which can also describe possible LEP excesses, but the associated scenarios are not related with reduced fine tuning in the Higgs sector.

(vi) In the NMSSM and the MNSSM, the upper bound on the mass of the lightest SM-like Higgs boson, e.g. H_1, increases by an amount of ~ 30 GeV with respect to the MSSM, for small values of $\tan\beta$, i.e. $M_{H_1} \lesssim 145$ GeV, for maximal stop mixing and $\tan\beta = 2$. Notice that MSSM scenarios using such low values of $\tan\beta$ have already been ruled out by LEP data or are at the verge of being ruled out at the Tevatron.

(vii) The NMSSM and the MNSSM both predict the existence of stable or quasi-stable light neutralinos that could be responsible for the Dark Matter (DM) of the universe [51–54]. There are many new possibilities as compared to the MSSM. In particular, in the NMSSM and MNSSM it is possible that the lightest neutralino is extremely light (100 MeV to 10 GeV) and can annihilate sufficiently through a light A_1 that the correct DM relic density is obtained. In general, the parameter regions for which correct DM relic abundance can be obtained in the NMSSM and MNSSM are far more extensive as compared to the MSSM and each such region will have interesting and significant consequences for the phenomenology to be expected at colliders.

(viii) Finally, an important cosmological feature of the MNSSM and the NMSSM is that they can comfortably explain the Baryon Asymmetry in the Universe by means of a strong first order electroweak phase transition [51, 55–57]. In contrast, baryogenesis considerations leave the MSSM in slight disfavor, requiring the right handed stop squark to be lighter than the top quark and the Higgs lighter than about 117 GeV [58, 59]. In these scenarios, the heavier stop quark is extremely heavy, leading to large fine-tuning.

Apart from the common features listed above, the two models, the NMSSM and the MNSSM, have some characteristic phenomenological differences, especially when compared with the MSSM. More explicitly, the following points can be made:

(a) Unlike the NMSSM, the MNSSM satisfies the tree-level mass sum rule [44]:

$$M^2_{H_1} \,+\, M^2_{H_2} \,+\, M^2_{H_3} \;=\; M^2_Z \,+\, M^2_{A_1} \,+\, M^2_{A_2}\,, \tag{4.13}$$

where $H_{1,2,3}$ and $A_{1,2}$ are the three CP-even and two CP-odd Higgs fields, respectively. The tree-level mass sum rule (4.13) is very analogous to the corresponding one of the MSSM [60,61], where the two heavier Higgs states H_3 and A_2 are absent in the latter. Radiative effects may violate (4.13) by an additional term of order M_Z^2. Hence, possible observation of a large violation of the sum rule (4.13) can rule out the MNSSM, pointing explicitly towards the NMSSM.

(b) The decoupling properties of a large tadpole in the MNSSM open up further possibilities in the Higgs-boson mass spectrum. In particular, the charged Higgs boson H^+ can be much lighter than the neutral Higgs boson with a SM-type coupling to the Z boson. In fact, the H^+ boson could be as light as 80 GeV, so it could be the *lightest* particle in the *entire* Higgs spectrum. The planned colliders, i.e. the upgraded Tevatron collider and the LHC, are expected to be able to to test scenarios with a relatively light H^+, e.g. through the top-quark decay channel $t \to H^+b$ [62]. It is crucial to notice that such light charged Higgs-boson scenarios, with $M_{H^+} \lesssim$ 100–120 GeV, are very difficult to obtain both in the MSSM and the NMSSM, for phenomenologically favoured values of the μ-parameter, i.e. for $\mu > 100$ GeV.

(c) A clear phenomenological distinction of the NMSSM from the MNSSM and the MSSM as well can be obtained by means of the complementarity relations of the Higgs-boson couplings to the Z boson:

$$g^2_{H_1ZZ} \;=\; g^2_{H_2A_1Z}\,, \qquad g^2_{H_2ZZ} \;=\; g^2_{H_1A_1Z}\,. \tag{4.14}$$

Specifically, the above relations (4.14) are not generically valid in the NMSSM [44]. A future e^+e^- linear collider will have the capability to experimentally determine the $H_{1,2}ZZ$- and $H_{2,1}A_1Z$- couplings to a precision as high as 3% and so test, to a high degree of accuracy, the complementarity relations (4.14) which are an essential phenomenological feature of the MNSSM (with an unsuppressed t_S) and the MSSM.

The following sections will shed more light upon the field-theoretic, cosmological and phenomenological properties and implications of the NMSSM and the MNSSM.

4.2 The NMSSM Higgs mass spectrum

David J. Miller

We have seen in the introduction that the NMSSM provides an elegant solution to the μ problem of the MSSM by introducing an extra complex scalar Higgs superfield. After explicity breaking the Peccei-Quinn symmetry, the NMSSM results in the superpotential of Eq. (4.7) and the corresponding Higgs potential of Eq. (4.8). The Higgs sector consists of three scalars, H_1, H_2 and H_3, two pseudoscalars, A_1 and A_2, and two charged Higgs bosons, $H^{\pm}$, while the gaugino/higgsino sector consists of five neutralinos, $\tilde{\chi}_i^0$, $i = 1..5$, and four charginos $\tilde{\chi}_i^{\pm}$, $i = 1, 2$.

The first question to ask is, what is the mass spectrum of these particles, and how does it change as we alter the parameters of the model? In general, one would like to answer this question directly from the analytic formulae for the masses. However, even in the MSSM, these formulae are sufficiently complicated that it is difficult to untangle the effects of the different paramaters, and one must resort to numerical analysis. Principally, this is due to the large top quark Yukawa couplings which cause the Higgs masses to have large radiative corrections that must be taken into account.

This complicated nature largely carries over to the NMSSM, so that one must also include radiative corrections to get a complete picture of the mass hierarchy. However, the *extra* singlet fields introduced have no initial couplings to top quarks, and only gain a coupling through mixing with the other Higgs states. If the extra Higgs states are rather decoupled then their coupling to the top quark will be small and radiative corrections can be ignored for an approximate first look at their masses. Indeed, even if they are not decoupled, the top quark coupling will still be 'shared out' amongst the larger number of Higgs bosons and diluted. Since the radiative corrections are to the mass-squared rather than the mass, this will lead to a decrease in their importance. Therefore, neglecting radiative corrections in the NMSSM Higgs sector does a better job of approximating the masses than one would otherwise first suppose [30].

4.2.1 The Higgs sector

Since no new charged states have been added, the **charged Higgs boson** field content remains exactly the same as in the MSSM. Once the extra singlet field obtains a vev, the charged Higgs mass terms in the Higgs potential will be identical to the MSSM for both the D-terms and the soft-supersymmetry breaking terms. However, the term in the superpotential $\lambda S H_u^+ H_d^-$ provides an interaction between the charged Higgs bosons and the new singlet, so it will lead to slightly different F-terms. This causes a slightly altered parameterisation of the charged Higgs mass as compared to the MSSM,

$$M_{H^\pm}^2 = \frac{2\mu_{\text{eff}}}{\sin 2\beta}\left(A_\lambda + \frac{\kappa\mu_{\text{eff}}}{\lambda}\right) + M_W^2 - \frac{1}{2}\lambda^2 v^2. \tag{4.15}$$

Of course, since the overall scale is an input (via A_λ), one can regard the charged Higgs mass spectrum as being identical to that of the MSSM, and reparameterize the other Higgs masses accordingly. Indeed, this is what is normally done in the MNSSM and we will ocasionally follow the same approach here and regard $M_{H^\pm}$ as an input replacing A_λ.

The **pseudoscalar Higgs bosons** now have a 2×2 mass matrix, which rather easily lends itself to an analytic solution. However, the expression is still rather opaque, and it is useful to further approximate the masses by expanding in the (usually) small ratios $v/M_{H^\pm}$ and $1/\tan\beta$. This gives, for the two mass states,

$$\begin{aligned} M_{A_1}^2 &\approx -3\frac{\kappa\mu_{\text{eff}}}{\lambda}A_\kappa, && (4.16)\\ M_{A_2}^2 &\approx \frac{2\mu_{\text{eff}}}{\sin 2\beta}\left(A_\lambda + \frac{\kappa\mu_{\text{eff}}}{\lambda}\right)\left(1 + \lambda^2\frac{v^2}{8\mu_{\text{eff}}^2}\sin^2 2\beta\right). && (4.17)\end{aligned}$$

The ordering of the solutions, normally in order of *ascending* mass, clearly depends on the choice of parameters, but one can see that one of the pseudoscalar Higgs bosons has a mass of order $M_{H^\pm}$, while the other depends on the root of the magnitude of the supersymmetry breaking term corresponding to the Peccei-Quinn breaking term in the supersopential, i.e. κA_κ. Notice that vacuum stability requires that the quantity A_κ should be (approximately) negative in order to keep $M^2_{A_1} > 0$.

The **scalar Higgs bosons** have a 3×3 mass matrix, so the exact tree-level masses are rather complicated, but again simplify considerably when we make our approximation. This gives,

$$\begin{aligned} M^2_{H_{1/2}} &\approx \frac{1}{2}\Bigg[M_Z^2 \cos^2 2\beta + \frac{\kappa\mu_{\rm eff}}{\lambda}\left(A_\kappa + 4\frac{\kappa\mu_{\rm eff}}{\lambda}\right) \mp \Bigg\{\left(M_Z^2\cos^2 2\beta - \frac{\kappa\mu_{\rm eff}}{\lambda}\left(A_\kappa + 4\frac{\kappa\mu_{\rm eff}}{\lambda}\right)\right)^2 \\ &\qquad + 2\lambda^2 v^2\left(2\mu_{\rm eff} - \left(A_\lambda + 2\frac{\kappa\mu_{\rm eff}}{\lambda}\right)\sin 2\beta\right)^2\Bigg\}^{1/2}\Bigg], \qquad (4.18) \\ M^2_{H_3} &\approx \frac{2\mu_{\rm eff}}{\sin 2\beta}\left(A_\lambda + \frac{\kappa\mu_{\rm eff}}{\lambda}\right)\left(1 + \lambda^2\frac{v^2}{8\mu^2_{\rm eff}}\sin^2 2\beta\right). \qquad (4.19) \end{aligned}$$

Again, the distinction of which scalar is H_1, H_2 or H_3 depends on the values of the parameters. We can see that H_3 is approximately degenerate with A_2 and $H^\pm$, which is directly analagous to the degeneracy of the heavy Higgs sector of the MSSM. All of these masses increase with increaing A_λ.

The dependence of the lighter scalars on A_λ is entirely in the last term under the square root of Eq.(4.18). One finds that if this term becomes too large, i.e. if A_λ deviates too far from $2\mu_{\rm eff}/\sin 2\beta - 2\kappa\mu_{\rm eff}/\lambda$, then the lightest Higgs boson will become tachyonic and the vacuum unstable. When this term is minimised, at $A_\lambda = 2\mu_{\rm eff}/\sin 2\beta - 2\kappa\mu_{\rm eff}/\lambda$, the two lightest scalars will take masses,

$$M^2_{H_1} \approx \frac{\kappa\mu_{\rm eff}}{\lambda}\left(A_\kappa + 4\frac{\kappa\mu_{\rm eff}}{\lambda}\right), \qquad M^2_{H_2} \approx M_Z^2\cos^2 2\beta. \qquad (4.20)$$

Similarly to the lightest pseudoscalar, the lightest scalar mass depends on the square-root of A_κ. However, notice the opposite sign compared with Eq.(4.16). This effectively sets a constraint on the values which A_κ for which the vacuum is stable,

$$-4\frac{\kappa\mu_{\rm eff}}{\lambda} \lesssim A_\kappa \lesssim 0. \qquad (4.21)$$

A small value of $|A_\kappa|$ is phenomenologically interesting [48] since it leads to a very light pseudoscalar but a moderately heavy lightest scalar. Even if the scalar is still significantly below the current LEP Higgs boounds, it may have escaped detection by decaying into the light pseudoscalar. See Section 4.3 for further details.

The one-loop masses of H_1 and A_1 are shown in Fig.(4.1) as a function of A_κ for a typical scenario. Increasing or decreasing $\kappa\mu_{\rm eff}/\lambda$ allows one to increase or decrease the masses of H_1 and A_1 simultaneously, while changing A_κ allows one to shift mass from one state to the other. These effects are nicely summarized by the approximate sum rule (at $A_\lambda = 2\mu_{\rm eff}/\sin 2\beta - 2\kappa\mu_{\rm eff}/\lambda$),

$$M^2_{H_1} + \frac{1}{3}M^2_{A_1} \approx 4\left(\frac{\kappa\mu_{\rm eff}}{\lambda}\right)^2. \qquad (4.22)$$

The approximate expressions are also plotted (dotted curves) and show at least a qualitative agreement with the one-loop results.

The approximate tree-level mass of the second lightest scalar (for this critical A_λ value) should look familiar; it is the same as the tree-level approximation to the lightest scalar mass in the MSSM, and will similarly gain large radiative corrections.

Fig. 4.2 (*left*) shows the one-loop Higgs masses for the same scenario as Fig. 4.1 but now as a function of $M_{H^\pm}$, with $A_\kappa = 100$ GeV. As predicted, the heaviest scalar and pseudoscalar are approximately degenerate with the charged Higgs boson, and one scalar is roughly of the mass one would

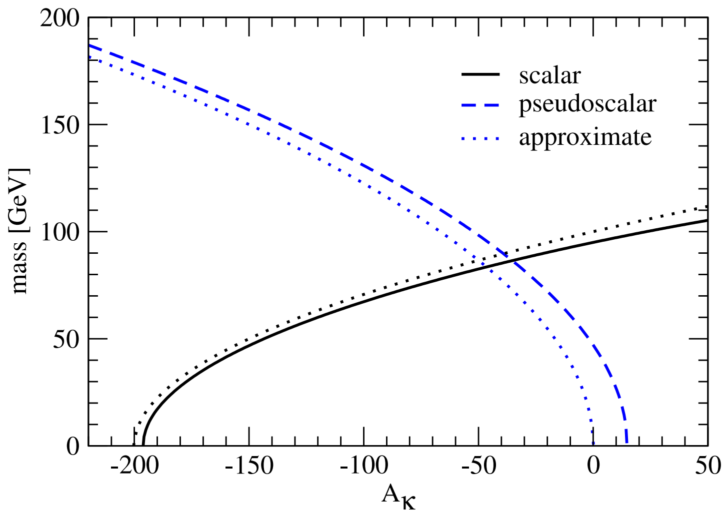

Fig. 4.1: The lightest scalar (solid) and pseudoscalar (dashed) Higgs masses at one-loop, as a function of A_κ, for $\lambda = 0.3$, $\kappa = 0.1$, $\tan\beta = 3$, $\mu_{\rm eff} = 150$ GeV, $A_\lambda = 450$ GeV and $M_{\rm SUSY} = 1$ TeV. Also shown by the dotted curves are the corresponding approximate expressions given in Eqs.(4.16) and (4.20).

expect of h in the MSSM. The other two Higgs bosons are predominantly singlets, with masses set by the size of the Peccei-Quinn breaking terms, as previously discussed. Also shown (*dotted*) are the approximate masses of Eqs. (4.16-4.19). These approximate masses do very well indeed at predicting the pseudoscalar masses and the heaviest scalar mass. They do not do so well with the two lighter scalars, which is entirely due to the radiative corrections. If one were to plot the tree-level Higgs masses, one would see that the approximate solutions match the tree-level result almost perfectly. It is interesting to note that the lightest scalar mass is very well predicted at its maximal value (which is why the curves in Fig. 4.1 match so well). At this point, the lightest scalar is almost entirely the new singlet state, which has no coupling to top quarks and therefore no sizable radiative corrections. The second lightest scalar is, for this value of $M_{H^\pm}$, almost identical to the lightest scalar h of the MSSM, and so will gain the same large radiative corrections from top/stop loops. As one moves away from this point, to the left or right, the Higgs bosons mix, the lightest scalar inherits a top quark coupling and the radiative corrections are shared out between them.

In Fig. 4.2 (*right*) we show the same masses for a larger value of $\kappa = 0.4$. As predicted, the increased size of the Peccei-Quinn breaking terms raises the masses of the singlet dominated fields. The singlet dominated scalar is now the heaviest scalar for low values of $M_{H^\pm}$ and the second lightest for high values of $M_{H^\pm}$. The increased mass contribution from the enhanced Peccei-Quinn breaking terms also reduces its mixing with the 'h-like' scalar, and therefore its radiative corrections. In fact, now both scalar and pseudoscalar singlet dominated fields have masses which match very well with the approximate expressions (apart from where they become approximately degenerate with the other states). Once again, we can reduce the singlet dominated scalar mass while increasing the pseudoscalar mass, or vice versa, by altering the parmeter A_κ. Note that the charged Higgs mass is contrained by the requirement that the lightest scalar mass-squared be positive (i.e. vacuum stability).

4.2.2 The Neutralino Sector

The Neutralinos do not suffer from the same large radiative corrections seen in the Higgs sector. However, the Neutralino mass matrix is now 5×5, so analytic expressions for the tree-level masses cannot be obtained in closed form. In order to get a handle on the behaviour of the masses with respect to variations in the parameters we must again resort to approximate expressions [31]. The Chargino masses and

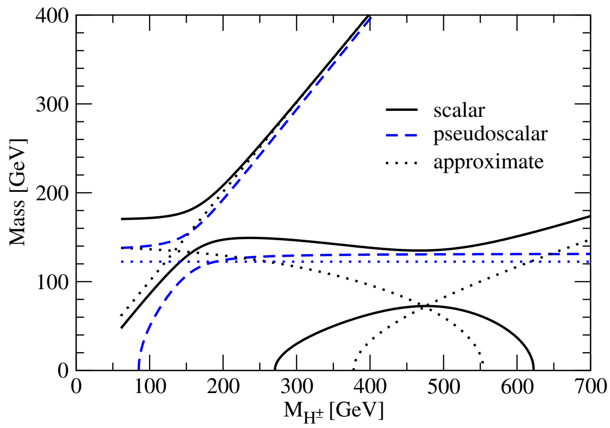

Fig. 4.2: The scalar (solid) and pseudoscalar (dashed) Higgs masses at one-loop, as a function of $M_{H^\pm}$, for $\lambda = 0.3$, $\tan\beta = 3$, $\mu_{\rm eff} = 150$ GeV, $A_\kappa = 100$ GeV, $M_{\rm SUSY} = 1$ TeV and $\kappa = 0.1$ (left) or 0.4 (right). Also shown by the dotted curves are the corresponding approximate expressions given in Eqs. (4.16-4.19).

mixings are unaffected by the additional fields (although they may have extra decays if kinematically allowed) so we will not discuss them further here.

When considering the neutralino sector we can forget about the soft supersymmetry breaking parameters A_λ and A_κ, which have no effect, but must instead include the soft supersymmetry breaking gaugino masses M_1 and M_2. The relevant parameters are then λ, κ, $\mu_{\rm eff}$, $\tan\beta$, M_1 and M_2. For illustrative purposes we will here consider the case where $M_{1,2} \gg |\mu_{\rm eff}| \gg M_Z$, and $|\mu_{\rm eff}| \gg \lambda v/\sqrt{2}$ (this last condition is saying that the vev of the new field should be substantially larger than that of the usual doublets, i.e. $\langle S\rangle \gg v/\sqrt{2}$). With this approximation, we find,

$$
\begin{aligned}
m_1 &\approx M_1 + \frac{M_Z^2}{M_1} s_W^2, \\
m_2 &\approx M_2 + \frac{M_Z^2}{M_2} c_W^2, \\
m_3 &\approx -\mu_{\rm eff} - \frac{M_{12}}{2M_1M_2} M_Z^2 (1-\sin 2\beta) - \frac{\lambda^2 v^2}{4\mu_{\rm eff}}(1+\sin 2\beta), \\
m_4 &\approx \mu_{\rm eff} - \frac{M_{12}}{2M_1M_2} M_Z^2 (1+\sin 2\beta) + \frac{\lambda^2 v^2}{4\mu_{\rm eff}}(1-\sin 2\beta), \\
m_5 &\approx 2\frac{\kappa\mu_{\rm eff}}{\lambda} + \frac{\lambda^2 v^2}{2\mu_{\rm eff}} \sin 2\beta,
\end{aligned} \tag{4.23}
$$

where s_W and c_W are the sine and cosine of the Weinberg angle and $M_{12} = M_1 c_W^2 + M_2 s_W^2$. As in the Higgs sector, one would normally reorder these states in order of ascending mass (and, unlike the Higgs sector, include phase rotations to render them positive), depending on the parameters. One finds that the singlet dominated neutralino is that labeled ‘5’ above with a mass which grows as the Peccei-Quinn breaking (i.e. κ) is increased. For particularly low values of κ, the second term may dominate.

The tree-level neutralino masses are plotted in Fig. 4.3 as a function of κ, together with the approximate expressions. We see that two of the neutrinos match the input soft supersymmetry breaking gaugino masses very well, with two more slightly above and below $\mu_{\rm eff}$. The last neutralino is singlet dominated and increases linearly with κ. The approximate forms match rather well with the exact (though tree-level) results, except when the states are nearly degenerate, and with the proviso that one must relable the approximate expressions depending on the hierarchy. Only the prediction for the lightest state is rather low. For other hierarchies of the paremeters e.g. $\mu_{\rm eff} \gg M_{1,2} \gg M_z$, different approximations

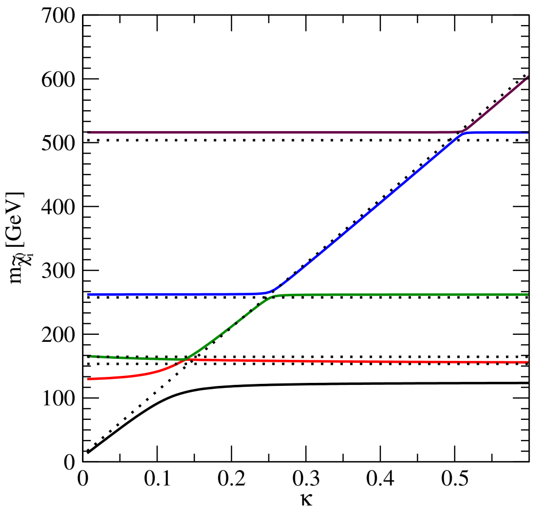

Fig. 4.3: The tree-level neutralino masses (*solid*) as a function of κ with $M_1 = 250$ GeV, $M_2 = 500$ GeV, $\lambda = 0.3$, $\mu_{\rm eff} = 120$ GeV, $\tan\beta = 3$. Also shown (*dashed*) are the approximate forms of Eq. (4.23).

are more appropriate but give similar results [31].

4.3 Low fine-tuning scenarios in the NMSSM and LHC/ILC implications

Radovan Dermisek and John F. Gunion

In this contribution, we describe how the NMSSM can achieve extremely low fine-tuning and how it is that low fine-tuning scenarios can provide a very nice explanation of the LEP Higgs event excess in the vicinity of Higgs mass ~ 100 GeV. In these highly preferred scenarios, e^+e^- collisions produce a CP-even Higgs boson (generically denoted by H) with SM-like ZZ, WW couplings in association with the Z, but the Higgs decays predominantly to two light CP-odd Higgs bosons (generically denoted by A), where each CP-odd Higgs boson decays to $\tau^+\tau^-$ or jets (because its mass is below $2m_b$). This serves to suppress the decays of the CP-even Higgs to $b\bar{b}$ to more or less exactly the right level to describe the LEP event excess in the $Z + b\bar{b}$ channel. Implications of such scenarios for future colliders are reviewed.

Recall from the introduction that the Higgs sector of the NMSSM contains the CP-even Higgs bosons H_1, H_2, H_3, the CP-odd Higgs bosons A_1, A_2 and the usual charged Higgs pair $H^\pm$, and that the properties of the Higgs bosons are fixed by the six parameters

$$\lambda,\ \kappa,\ A_\lambda,\ A_\kappa,\ \tan\beta,\ \mu_{\rm eff}\ . \tag{4.24}$$

along with input values for the gaugino masses and for the soft terms related to the (third generation) squarks and sleptons that contribute to the radiative corrections in the Higgs sector and to the Higgs decay widths. Exploration of the NMSSM Higgs sector is greatly simplified by employing the `NMHDECAY` [63, 64] program. All available radiative corrections are implemented therein.

In general, an important issue for NMSSM Higgs phenomenology is the mass and nature of the lightest CP-even and CP-odd Higgs bosons. In particular, if the A_1 is very light or even just moderately light there are are dramatic modifications in the phenomenology of Higgs discovery at both the LHC and ILC [30, 63–72]. A light A_1 is natural in the context of the model. Indeed, the NMSSM can contain either an approximate global $U(1)$ R-symmetry in the limit that the Higgs-sector trilinear soft SUSY breaking terms are small ($\kappa A_\kappa, \lambda A_\lambda \to 0$), or a $U(1)$ Peccei-Quinn symmetry in the limit that the cubic singlet term in the superpotential and its soft partner vanish ($\kappa, \kappa A_\kappa \to 0$) [66, 67]. In either case, one ends up with the lightest CP-odd Higgs boson, A_1, as the pseudo-Nambu-goldstone boson of this broken symmetry, implying that it can naturally be light. If one of these symmetries were unbroken, it would lead to a massless CP-odd A_1 which is ruled out. However, a very light A_1 is not ruled out. The low fine-tuning scenarios are associated with a small breaking of the $U(1)$ R-symmetry that can arise from explicit non-zero values for A_λ and A_κ and/or radiative corrections to A_λ and to the pseudoscalar Higgs mass-squared matrix that are present even when A_κ and A_λ are zero at tree-level.

4.3.1 Fine-tuning in the MSSM and NMSSM

We begin with a discussion of how it is that in the NMSSM, adding a Higgs singlet superfield allows one to reduce [48, 55] the fine tuning problem, which is present in the case of the MSSM due to the fact that LEP II excludes a SM-like CP-even Higgs boson with mass below 114 GeV that decays primarily to $b\bar{b}$.

One standard measure of fine-tuning is [73]

$$F = \mathrm{Max}_p F_p \equiv \mathrm{Max}_p \left| \frac{d \log M_Z}{d \log p} \right| , \tag{4.25}$$

where the parameters p comprise all GUT-scale soft-SUSY-breaking parameters. We will show that F can be much smaller in the NMSSM than in the MSSM [48,55]. In particular, in the NMSSM, fine-tuning can even be eliminated if the lightest CP-odd Higgs is light enough to allow $H_1 \to A_1 A_1$ decays [48] and the A_1 has mass below $2m_b$ so that it decays to $\tau^+\tau^-$, $q\bar{q}$ and/or gg.

In the MSSM model constraints are such that the lightest CP-even Higgs boson (h) is most naturally very SM-like, in which case $M_h \gtrsim 114$ GeV is required by LEP limits (except for a small window in parameter space where the CP-odd MSSM A has mass between ~ 90 GeV and ~ 114 GeV and $\tan\beta$ is large). Such a large M_h is not easily obtained without having a very substantial value for the root-mean stop mass, $\sqrt{m_{\tilde{t}_1} m_{\tilde{t}_2}}$ and/or large stop mixing (parameterized by the soft stop mixing parameter A_t), upon which the radiative corrections to M_h in the MSSM primarily depend. As a result, the MSSM is very fine-tuned and the associated hierarchy problem is substantial (see, for example, [48]).

The NMSSM can be much less fine-tuned in several interesting ways. Let us recall the formula for the maximum tree-level mass-squared of a SM-like Higgs boson in the NMSSM:

$$[{M_H}^2]_{tree} \le M_Z^2 \left(\cos^2 2\beta + \frac{2\lambda^2}{g^2 + {g'}^2} \sin^2 2\beta \right) , \tag{4.26}$$

where typically this applies to $H = H_1$ or $H = H_2$, depending upon which is SM-like. To this tree-level result one must add the radiative corrections from the stop squarks and top quark loops. For small λ and/or large $\tan\beta$, Eq. (4.26) reduces to the MSSM result of $[{M_H}^2]_{tree} \le M_Z^2 \cos^2 2\beta$. However, if λ is taken large compared to g, g', and $\tan\beta$ is not far from unity, the 2nd term can dominate and a value of ${M_H}^2 > (114 \text{ GeV})^2$ is possible without having to employ extreme $\sqrt{m_{\tilde{t}_1} m_{\tilde{t}_2}}$ or stop mixing parameter A_t values. The result is a lower level of fine-tuning [29, 55] as compared to the MSSM. However, to get values substantially below those found in the MSSM requires λ (at scale M_Z) to be $\mathcal{O}(1)$, above the limit $\lambda \le 0.7$ for which λ remains perturbative under evolution all the way up to the GUT scale M_U.

The alternative [48] is to choose parameters for which fine-tuning is "automatically" minimized. The lowest fine-tuning is achieved for scenarios in which the lightest Higgs boson of the NMSSM is SM-like in its normal couplings and has mass below 114 GeV and yet escapes LEP constraints by virtue of having unusual decay modes for which LEP limits are weaker. In particular, parameters for which $H_1 \to A_1 A_1$ decays are dominant are consistent with LEP constraints for M_{H_1} as low as 90 GeV (110 GeV) if the dominant A_1 decay is to $\tau^+\tau^-$ ($b\bar{b}$). This immediately allows lower $\sqrt{m_{\tilde{t}_1} m_{\tilde{t}_2}}$ and A_t and, therefore, smaller F values. The very low values of F that can be achieved are illustrated in Fig. 4.4. The points plotted are those from a large scan over NMSSM parameters at fixed $\tan\beta = 10$ and $M_{1,2,3}(M_Z) = 100, 200, 300$ GeV. All points plotted pass `NMHDECAY` constraints, which include

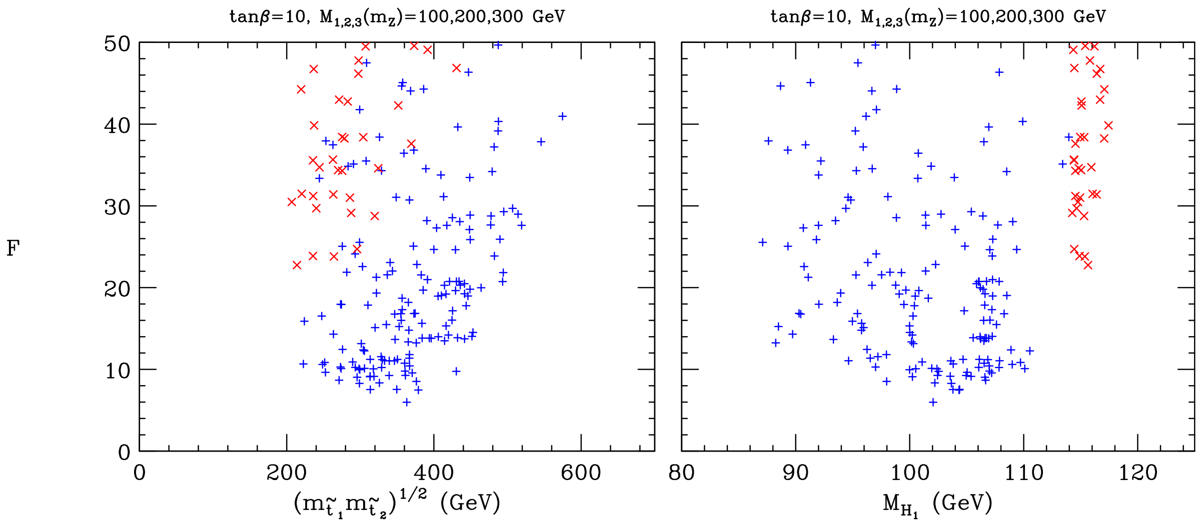

Fig. 4.4: For the NMSSM, we plot the ne-tuning measure F vs. $\sqrt{m_{\tilde{t}_1} m_{\tilde{t}_2}}$ (left) and vs. M_{H_1} (right) for NMHDECAY-accepted scenarios with $\tan\beta = 10$ and $M_{1,2,3}(M_Z) = 100, 200, 300$ GeV. Points marked by '+' ('×') have $M_{H_1} < 114$ GeV ($M_{H_1} \geq 114$ GeV) and escape LEP *single-channel* limits primarily due to dominance of $H_1 \to A_1 A_1$ decays (due to $M_{H_1} > 114$ GeV).

in particular perturbativity for λ up to M_U and all single-channel (the meaning and importance of this restriction will be explained in Section 4.3.2) LEP constraints. The points with lowest F ($F < 10$) correspond to $\sqrt{m_{\tilde{t}_1} m_{\tilde{t}_2}} \sim 250 - 400$ GeV and have 98 GeV $\leq M_{H_1} \leq$ 105 GeV. For about 2/3 of these points $M_{A_1} < 2m_b$ and the main A_1 decay is to $\tau^+\tau^-$. For the remaining 1/3 of the $F < 10$ points, $M_{A_1} > 2m_b$ and $BR(A_1 \to b\bar{b}) \sim 0.92$ and $BR(A_1 \to \tau^+\tau^-) \sim 0.08$. As discussed in the next section, the $M_{A_1} > 2m_b$ scenarios are not consistent with the full LEP-Higgs Working Group (LHWG) LEP analysis, whereas the $M_{A_1} < 2m_b$ scenarios describe very nicely the $M_H \sim 100$ GeV excess in the $Z + b$'s final state. Implications for the LHC and the ILC are discussed in the final section of this report.

Overall, the $M_{A_1} < 2m_b$ scenarios are very appealing since they are extremely consistent with the two primary features of the LEP data: i) the consistency of the LEP precision electroweak data with the presence of a CP-even Higgs boson with SM-like ZZH coupling and $M_H \sim 100$ GeV and ii) a $M_H \sim 100$ GeV Higgs boson that has SM-like WW, ZZ couplings but decays to $b\bar{b}$ with about 1/10 the branching ratio of a SM Higgs boson as a result of primary decays to state(s) that do not contain b-quarks.

4.3.2 NMSSM scenarios with low fine-tuning

Let us now give more details regarding how the NMSSM can achieve much lower fine-tuning than the MSSM. In Ref. [48], two types of scenarios were examined for parameter choices such that $F < 10$. In both scenarios, $BR(H_1 \to b\bar{b}) \sim 0.07 - 0.2$ and $BR(H_1 \to A_1 A_1) \sim 0.88 - 0.75$. In scenarios of type I (II), $M_{A_1} > 2m_b$ ($M_{A_1} < 2m_b$) and $BR(A_1 \to b\bar{b}) \sim 0.92$ (0).

To relate this to LEP data, let us discuss the observed and expected 95% CL limits in the $Z4b$ channel from [74] and in the $Z2b$ channel from [75]. Both show event excesses. In particular, for M_H in the vicinity of $105 - 110$ GeV and M_A in the 30 GeV to 50 GeV zone there is a sharp deviation of the observed limit on $C_{\rm eff}^{4b} = [g_{ZZH}^2/g_{ZZH_{SM}}^2] BR(H \to ZAA)[BR[A \to b\bar{b})]^2$ to values above the expected limit, implying the presence of excess events. A similar deviation has been evident in the $Zb\bar{b}$ final state for a number of years [75]. One finds a higher observed 95% CL for $C_{\rm eff}^{2b} = [g_{ZZH}^2/g_{ZZH_{SM}}^2] BR(H \to b\bar{b})$ in the $Zb\bar{b}$ final state as a function of M_H than expected in the $M_H \sim 100{-}110$ GeV vicinity. The statistical significance of this excess is in the $1\sigma{-}2\sigma$ range. It would

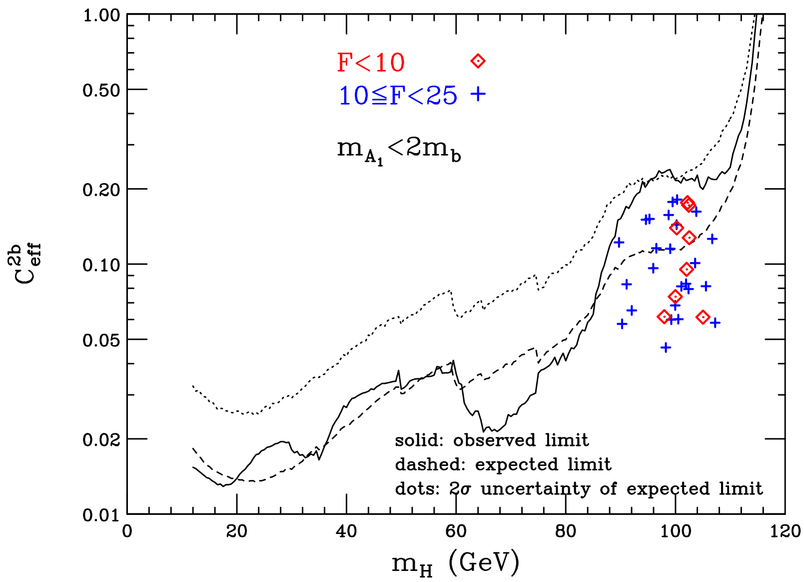

Fig. 4.5: Expected and observed 95% CL limits on $C_{\rm eff}^{2b} = [g^2_{ZZH}/g^2_{ZZH_{SM}}]BR(H \to b\bar{b})$ from Ref. [75] are shown vs. M_H. Also plotted are the predictions for NMSSM parameter choices in our scan that give ne-tuning measure $F < 25$ and $M_{A_1} < 2m_b$ with xed $\tan\beta = 10$ and gaugino masses of $M_{1,2,3}(M_Z) = 100, 200, 300$ GeV.

seem that there is a significant possibility that both the $Z2b$ and $Z4b$ excesses arise from the decays of a single CP-even Higgs boson with SM-like coupling strength to gauge bosons and fermions, but with additional coupling to a light, perhaps CP-odd, Higgs boson. This is precisely the scenario that applies in the NMSSM (with $H = H_1$ and $A = A_1$) for those parameter choices that correspond to low values of F and $M_{A_1} > 2m_b$. Typically, the low-F scenarios with $M_{A_1} > 2m_b$ have $BR(H_1 \to b\bar{b}) \sim 0.05 - 0.2$ and $M_{A_1} \sim 30 - 45$ GeV with $BR(H_1 \to A_1A_1) \sim 0.85 - 0.75$ [with $BR(A_1 \to b\bar{b}) \sim 0.93$]. Note, however, that for simultaneous consistency with the separate $C_{\rm eff}^{2b}$ and $C_{\rm eff}^{4b}$ limits, $M_{H_1} \gtrsim 106$ GeV is required, a value which is not particularly ideal for the $M_H \sim 100$ GeV location of the largest $Z2b$ excess.

In fact, there is an even more severe problem. Although these type-I ($M_{A_1} > 2m_b$) scenarios satisfy the separate $Z2b$ and $Z4b$ LHWG limits, the overlap between these two analyzes is such that when both channels are present with the rates predicted, all type-I scenarios with $F < 10$ are excluded. This conclusion was reached only after processing the type-I scenario predictions through the full $1-CL_b$ LHWG analysis machinery. The result is that the only $F < 10$ scenarios consistent with the full LHWG analysis are of type-II ($M_{A_1} < 2m_b$). Type-I scenarios with $F < 10$ are typically excluded at better than the 99% CL after data from all experiments are combined. However, it should be remarked that the OPAL experiment, which has the best $Z2b$ vs. $Z4b$ discrimination, does not on its own exclude such a scenario and does see excesses in both the $Z2b$ and $Z4b$ channels. For $10 < F < 100$ the range of possibilities is expanded. In particular, there are $M_{H_1} \gtrsim 108$ GeV points that make a net contribution to the $Z2b$ and $Z4b$ channels that is reduced compared to the $F < 10$ cases and that probably would not be excluded by the combined analysis. However, again the M_{H_1} mass is too large to explain the largest $Z2b$ excess in the $M_H \sim 100$ GeV region.

As a result of the problems with the $M_{A_1} > 2m_b$ scenarios as outlined above, it is clearly important to analyze the scenarios with $M_{A_1} < 2m_b$. As noted earlier, a light A_1 is natural in the NMSSM in the $\kappa A_\kappa, \lambda A_\lambda \to 0$ limit due to the presence of a global $U(1)_R$ symmetry of the scalar potential which is spontaneously broken by the vevs, resulting in a Nambu-Goldstone boson in the spectrum [66]. This symmetry is explicitly broken by the trilinear soft terms so that for small $\kappa A_\kappa, \lambda A_\lambda$ the lightest

CP odd Higgs boson is naturally much lighter than other Higgs bosons. For the $F < 10$ scenarios, $\lambda(M_Z) \sim 0.15 - 0.25$, $\kappa(M_Z) \sim 0.15 - 0.3$, $|A_\kappa(M_Z)| < 4$ GeV and $|A_\lambda(M_Z)| < 200$ GeV, implying small κA_κ and moderate λA_λ. The effect of λA_λ on M_{A_1} is further suppressed when the A_1 is largely singlet in nature, as is the case for low-F scenarios. Therefore, we always obtain small M_{A_1}. We note that small soft SUSY-breaking trilinear couplings at the unification scale are generic in SUSY breaking scenarios where SUSY breaking is mediated by the gauge sector, as, for instance, in gauge or gaugino mediation. Although the value $A_\lambda(M_Z)$ might be sizable due to contributions from gaugino masses after renormalization group running between the unification scale and the weak scale, A_κ receives only a small correction from the running (such corrections being one loop suppressed compared to those for A_λ). Altogether, a light, singlet A_1 is very natural in models with small soft SUSY-breaking trilinear couplings at the unification scale. Finally, we note that the above $\lambda(M_Z)$ values are such that λ will remain perturbative when evolved up to the unification scale, implying that the resulting unification-scale λ values are natural in the context of model structures that might yield the NMSSM as an effective theory below the unification scale.

A very important feature of the $M_{A_1} < 2m_b$, $F < 10$ scenarios is that a significant fraction of them can easily explain the well-known excess in the $ZH \to Zb\bar{b}$ final state in the vicinity of $M_H \sim 100$ GeV. This is illustrated in Fig. 4.5 from [49], where all $F < 10$ NMSSM parameter choices (from a lengthy scan) with $M_{A_1} < 2m_b$ are shown to predict $M_{H_1} \sim 98 - 105$ GeV with about half the points predicting $M_{H_1} \sim 100 - 102$ GeV along with a $C^{2b}_{\rm eff}$ that would explain the observed excess with respect to the expected limit. The other primary decay mode for all the plotted points is $H_1 \to A_1 A_1$ with $A_1 \to \tau^+\tau^-$ or light quarks and gluons (when $M_{A_1} < 2m_\tau$). Thus, unlike the type-I ($M_{A_1} > 2m_b$) scenarios, there is no additional contribution to the $Z + b$'s final state — the $C^{2b}_{\rm eff}$ limits are the most relevant single-channel limits. However, to really decide if a given scenario is consistent with the LEP data, and at what level, it must be processed through the complete LHWG confidence level/likelihood analysis. This processing was performed for us by P. Bechtle. In Table 4.1, we give the precise masses and branching ratios of the H_1 and A_1 for all the $F < 10$ points. We also give the number of standard deviations, $n_{\rm obs}$ ($n_{\rm exp}$), by which the observed rate (expected rate obtained for the predicted signal+background) exceeds the predicted background. These are derived from $(1 - CL_b)_{\rm observed}$ and $(1 - CL_b)_{\rm expected}$ using the usual tables: e.g. $(1 - CL_b) = 0.32$, 0.045, 0.0027 correspond to 1σ, 2σ, 3σ excesses, respectively. The quantity $s95$ is the factor by which the signal predicted in a given case would have to be multiplied in order to exceed the 95% CL. All these quantities are obtained by processing each scenario through the full preliminary LHWG confidence level/likelihood analysis. If $n_{\rm exp}$ is larger than $n_{\rm obs}$ then the excess predicted by the signal plus background Monte Carlo is larger than the excess actually observed and vice versa. The points with $M_{H_1} \lesssim 100$ GeV have the largest $n_{\rm obs}$. Point 2 gives the best consistency between $n_{\rm obs}$ and $n_{\rm exp}$, with a predicted excess only slightly smaller than that observed. Points 1 and 3 also show substantial consistency. For the 4th and 7th points, the predicted excess is only modestly larger (roughly within 1σ) compared to that observed. The 5th and 6th points are very close to the 95% CL borderline and have a predicted signal that is significantly larger than the excess observed. LEP is not very sensitive to point 8. Thus, a significant fraction of the $F < 10$ points are very consistent with the observed event excess.

We wish to emphasize that in our scan there are many, many points that satisfy all constraints and have $M_{A_1} < 2m_b$. The remarkable result is that those with $F < 10$ have a substantial probability that they predict the Higgs boson properties that would imply a LEP $ZH_1 \to Z + b$'s excess of the sort seen. The smaller number of $F < 10$ points with M_{A_1} substantially above $2m_b$ all predict a net $Z + b$'s signal that is ruled out at better than 99% CL by LEP data. Indeed, all $F < 25$ points have a net $H_1 \to b$'s branching ratio, $BR(H_1 \to b\bar{b}) + BR(H_1 \to A_1 A_1 \to b\bar{b}b\bar{b}) \gtrsim 0.85$, which is too large for LEP consistency if M_{H_1} is near 100 GeV. (Analysis of points with M_{A_1} very near $b\bar{b}$ decay threshold, but such that $A_1 \to b\bar{b}$ is dominant, is very subtle. Such points arise for $F < 10$ and require further analysis in cooperation with the LHWG.)

Table 4.1: Some properties of the H_1 and A_1 for the eight allowed points with $F < 10$ and $M_{A_1} < 2m_b$ from our $\tan\beta = 10$, $M_{1,2,3}(M_Z) = 100, 200, 300$ GeV NMSSM scan. The $n_{\rm obs}$, $n_{\rm exp}$ and $s95$ values are obtained after full processing of all ZH nal states using the preliminary LHWG analysis code (thanks to P. Bechtle). See text for details. N_{SD}^{LHC} is the statistical signi cance of the best standard LHC Higgs detection channel for integrated luminosity of $L = 300$ fb^{-1}.

M_{H_1}/M_{A_1} (GeV)	Branching Ratios $H_1 \to b\overline{b}$	$H_1 \to A_1A_1$	$A_1 \to \tau\overline{\tau}$	$n_{\rm obs}/n_{\rm exp}$ units of 1σ	$s95$	N_{SD}^{LHC}
98.0/2.6	0.062	0.926	0.000	2.25/1.72	2.79	1.2
100.0/9.3	0.075	0.910	0.852	1.98/1.88	2.40	1.5
100.2/3.1	0.141	0.832	0.000	2.26/2.78	1.31	2.5
102.0/7.3	0.095	0.887	0.923	1.44/2.08	1.58	1.6
102.2/3.6	0.177	0.789	0.814	1.80/3.12	1.03	3.3
102.4/9.0	0.173	0.793	0.875	1.79/3.03	1.07	3.6
102.5/5.4	0.128	0.848	0.938	1.64/2.46	1.24	2.4
105.0/5.3	0.062	0.926	0.938	1.11/1.52	2.74	1.2

As already noted, these low-F NMSSM scenarios have an A_1 that is fairly singlet in nature. This means that $Z^* \to ZA_1A_1$ at LEP (and indeed all A_1 production mechanisms based on the ZZA_1A_1 and WWA_1A_1 quartic interactions) would have a very low rate. The A_1WW and A_1ZZ couplings arise first at one loop and the $A_1t\overline{t}$ coupling is also very suppressed. At $\tan\beta = 10$, the suppression from the A_1's predominantly singlet composition is compensated by the $\tan\beta$ factor yielding $A_1b\overline{b}\,\gamma_5$ coupling strength that is of order the $H_{SM}b\overline{b}$ scalar coupling strength. A final feature of the low-F points that should be noted is that all the other Higgs bosons are fairly heavy, typically above 400 GeV in mass.

4.3.3 Higgs detection in the low-F scenarios

An important question is the extent to which the type of $H \to AA$ Higgs scenario (whether NMSSM or other) described here can be explored at the Tevatron, the LHC and a future e^+e^- linear collider. This has been examined in the case of the NMSSM in [65,68,72], with the conclusion that observation of any of the NMSSM Higgs bosons may be difficult at hadron colliders. At a naive level, the $H_1 \to A_1A_1$ decay mode renders inadequate the usual Higgs search modes that might allow H_1 discovery at the LHC. Since the other NMSSM Higgs bosons are rather heavy and have couplings to b quarks that are not greatly enhanced, they too cannot be detected at the LHC. The last column of Table 4.1 shows the statistical significance of the most significant signal for *any* of the NMSSM Higgs bosons in the "standard" SM/MSSM search channels for the eight $F < 10$ NMSSM parameter choices. For the H_1 and A_1, the most important detection channels are $H_1 \to \gamma\gamma$, $WH_1{+}t\overline{t}H_1 \to \gamma\gamma\ell^\pm X$, $t\overline{t}H_1/A_1 \to t\overline{t}b\overline{b}$, $b\overline{b}H_1/A_1 \to b\overline{b}\tau^+\tau^-$ and $WW \to H_1 \to \tau^+\tau^-$ – see [72]. Even after $L = 300$ fb^{-1} of accumulated luminosity, the typical maximal signal strength is at best 3.5σ. For the eight points of Table 4.1, this largest signal derives from the $WH_1 + t\overline{t}H_1 \to \gamma\gamma\ell^\pm X$ channel. There is a clear need to develop detection modes sensitive to the dominant $H_1 \to A_1A_1 \to \tau^+\tau^-\tau^+\tau^-$ decay channel.

Let us consider the possibilities. Two detection modes that can be considered are $WW \to H_1 \to A_1A_1 \to 4\tau$ and $gg \to t\overline{t}H_1 \to t\overline{t}A_1A_1 \to t\overline{t}4\tau$. Second, recall that the $\widetilde\chi_2^0 \to H_1\widetilde\chi_1^0$ channel provides a signal in the MSSM when $H_1 \to b\overline{b}$ decays are dominant. See, for example, [76]. It has not been studied for $H_1 \to A_1A_1 \to 4\tau$ decays. If a light $\widetilde\chi_1^0$ provides the dark matter of the universe (as possible because of the $\widetilde\chi_1^0\widetilde\chi_1^0 \to A_1 \to X$ annihilation channels for a light A_1, see [53, 54] and references therein as well as the separate contribution on this subject, the $m_{\widetilde\chi_2^0} - m_{\widetilde\chi_1^0}$ mass difference might be large enough to allow such decays. Diffractive production [77–79], $pp \to ppH_1 \to ppX$, where the mass M_X can be reconstructed with roughly a $1-2$ GeV resolution, can potentially reveal a Higgs peak, independent of the decay of the Higgs. A study [80] is underway to see if this discovery mode works for the $H_1 \to A_1A_1 \to 4\tau$ decay mode as well as it appears to work for the simpler SM $h_{SM} \to b\overline{b}$ case. The main issue may be whether events can be triggered despite the soft nature of the decay products of the τ's present in X when $H_1 \to A_1A_1 \to 4\tau$ as compared to $h_{SM} \to b\overline{b}$.

At the Tevatron it is possible that ZH_1 and WH_1 production, with $H_1 \to A_1A_1 \to 4\tau$, will provide the most favorable channels. If backgrounds are small, one must simply accumulate enough events. However, efficiencies for triggering on and isolating the 4τ final state will not be large. Perhaps one could also consider $gg \to H_1 \to A_1A_1 \to 4\tau$ which would have substantially larger rate. Studies are needed. If supersymmetry is detected at the Tevatron, but no Higgs is seen, and if LHC discovery of the H_1 remains uncertain, Tevatron studies of the 4τ final state might be essential. However, rates imply that the H_1 signal could only be seen if Tevatron running is extended until $L > 10\ \mathrm{fb}^{-1}$ has been accumulated. Even if both the Tevatron and the LHC are unable to detect the H_1, the LHC *would* observe numerous supersymmetry signals and *would* confirm that $WW \to WW$ scattering is perturbative, implying that something like a light Higgs boson must be present.

Of course, discovery of the H_1 will be straightforward at an e^+e^- linear collider via the inclusive $ZH_1 \to \ell^+\ell^-X$ reconstructed M_X approach (which allows Higgs discovery independent of the Higgs decay mode). Direct detection in both the $ZH_1 \to \ell^+\ell^-b\overline{b}$ and $ZH_1 \to \ell^+\ell^-4\tau$ modes will also be possible. At a $\gamma\gamma$ collider, the $\gamma\gamma \to H_1 \to 4\tau$ signal will be easily seen [81].

In contrast, since (as already noted) the A_1 in these low-F NMSSM scenarios is fairly singlet in nature, its *direct* (i.e. not in H_1 decays) detection will be very challenging even at the ILC. Further, the low-F points are all such that the other Higgs bosons are fairly heavy, typically above 400 GeV in mass, and essentially inaccessible at both the LHC and all but a $\gtrsim 1$ TeV ILC.

We should note that much of the discussion above regarding Higgs discovery when $H \to AA$ decays are dominant is quite generic. Whether the A is truly the NMSSM CP-odd A_1 or just a lighter Higgs boson into which the SM-like H pair-decays, hadron collider detection of the H in its $H \to AA$ decay mode will be very challenging — only an e^+e^- linear collider can currently guarantee its discovery.

4.4 Di-photon Higgs signals at the LHC as a probe of an NMSSM Higgs sector

Stefano Moretti and Shoaib Munir

In view of the upcoming CERN LHC, quite some work has been dedicated to probing the NMSSM Higgs sector over recent years. Primarily, there have been attempts to extend the so-called 'No-lose theorem' of the MSSM [82] to the case of the NMSSM [68–71]. From this perspective, it was realised that at least one NMSSM Higgs boson should remain observable at the LHC over the NMSSM parameter space that does not allow any Higgs-to-Higgs decay. However, when the only light non-singlet (and, therefore, potentially visible) CP-even Higgs boson, H_1 or H_2, decays mainly to two very light CP-odd Higgs bosons, A_1A_1, one may not have a Higgs signal of statistical significance at the LHC [83]. While the jury is still out on whether a 'No-lose theorem' can be proved for the NMSSM, we are here concerned with an orthogonal approach. We asked ourselves if a, so to say, 'More-to-gain theorem' can be formulated in the NMSSM. That is, whether there exist regions of the NMSSM parameter space where more Higgs states of the NMSSM are visible at the LHC than those available within the MSSM. In our attempt to overview all such possibilities, we start by considering here the case of the di-photon decay channel of a neutral Higgs boson. This mode can be successfully probed in the MSSM, but limitedly to the case of one Higgs boson only, which is CP-even and rather light. We will argue that in the NMSSM one can instead potentially have up to three di-photon signals of Higgs bosons, involving not only CP-even but also CP-odd states, the latter with masses up to 600 GeV or so. In fact, even when only one di-photon signal can be extracted in the NMSSM, this may well be other than the H_1 state. When only the latter is visible, finally, it can happen that its mass is larger than the maximum value achievable within the MSSM. In all such cases then, the existence of a non-minimal SUSY Higgs sector would be manifest.

For a general study of the NMSSM Higgs sector (without any assumption on the underlying SUSY-breaking mechanism) we used here the `NMHDECAY` code (version 1.1) [63]. This program computes the masses, couplings and decay Branching Ratios (BRs) of all NMSSM Higgs bosons in terms of model parameters taken at the EW scale. For our purpose, instead of postulating unification, we fixed the soft SUSY breaking terms to a very high value, so that they have little or no contribution to the outputs of the parameter scans. Consequently, we are left with six free parameters: the Yukawa couplings λ and κ, the soft trilinear terms A_λ and A_κ, plus tanβ and $\mu_{\rm eff} = \lambda\langle S\rangle$. The computation of the spectrum includes leading two-loop terms, EW corrections and propagator corrections. `NMHDECAY` also takes into account theoretical as well as experimental constraints from negative Higgs searches at collider experiments.

We have used `NMHDECAY` to scan over the NMSSM parameter space defined in [84] (borrowed from [72]), where also the configuration of the remaining SUSY soft terms can be found. The allowed decay modes for neutral NMSSM Higgs bosons are into any SM particle, plus into any final state involving all possible combinations of two Higgs bosons (neutral and/or charged) or of one Higgs boson and a gauge vector as well as into all possible sparticles. We have performed our scan over several millions of randomly selected points in the specified parameter space. The data points surviving all constraints are then used to determine the cross-sections for NMSSM Higgs hadro-production. As the SUSY mass scales have been set well above the EW one, the production modes exploitable in simulations at the LHC are those involving couplings to heavy ordinary matter only, i.e., the so-called ‘direct’ Higgs production modes of [85]. Production and decay rates for NMSSM neutral Higgs bosons have then been multiplied together to yield inclusive event rates, assuming a LHC luminosity of 100 fb^{-1} throughout.

As an initial step we computed the total cross-section times BR into $\gamma\gamma$ pairs against each of the six parameters of the NMSSM, for each neutral Higgs boson. We have assumed all production modes mentioned above and started by computing fully inclusive rates. We are focusing on the $\gamma\gamma$ decay mode since it is the most promising channel for the discovery of a (neutral) Higgs boson at the LHC in the moderate Higgs mass range (say, below 130 GeV). However, since the tail of the $\gamma\gamma$ background falls rapidly with increasing invariant mass of the di-photon pair, signal peaks for heavier Higgses could also be visible in addition to (or instead of) the lightest one [86]. As the starting point of our signal-to-background study, based on the ATLAS analysis of Ref. [87], we argue that cross-section times BR rates of 10 fb or so are interesting from a phenomenological point of view, in the sense that they may yield visible signal events, the more so the heavier the decaying Higgs state (also because the photon detection efficiency grows with the Higgs mass [87]). Hereafter, we will refer to such NMSSM parameter configurations as ‘potentially visible’.

We have then plotted the NMSSM configurations with three potentially visible Higgses H_1, H_2 and A_1 (in selected combinations, as detailed in the captions) against the various model parameters in Figs. 4.6–4.8. Their spread is quite homogeneous over the NMSSM parameter space and not located in some specific parameter areas (i.e., in a sense, not ‘fine-tuned’). The distribution of the same points in terms of cross-sections times BR as a function of the corresponding Higgs masses can be found in Fig. 4.9. Of particular relevance is the distribution of points in which only the NMSSM H_1 state is visible, when its mass is beyond the upper mass limit for the corresponding CP-even MSSM Higgs state, which is shown in Fig. 4.10[3]. This plot reveals that about 93% of the NMSSM H_1 masses visible alone are expected to be within 2–3 GeV beyond the MSSM bound, hence the two models would be

[3]Notice that the value obtained for $M_{H_1}^{\rm max}$ from `NMHDECAY` version 1.1, of $\sim$ 130 GeV, based on the leading two-loop approximations described in [63], is a few GeV lower than the value declared in Sect. 4.1.4. Besides, for consistency, we use the value of 120 GeV (obtained at the same level of accuracy) as upper mass limit on the lightest CP-even Higgs boson of the MSSM. (Notice that a slightly modified $M_{H_1}^{\rm max}$ value is obtained for the NMSSM from `NMHDECAY` version 2.1 [64], because of the improved mass approximations with respect to the earlier version of the program adopted here.) Eventually, when the LHC is on line, the exercise that we are proposing can be performed with the then state-of-the-art calculations.

Table 4.2: Higgs events potentially visible at the LHC through the $\gamma\gamma$ decay mode. Percentage refers to the portion of NMSSM parameter space involved for each discovery scenario.

Higgs Flavor	Points Visible		Percentage
H_1	Total:	1345884	99.7468
	Alone:	1345199	99.6961
	With H_2:	528	0.0391
	With A_1:	152	0.0113
	With H_2 and A_1:	5	0.0004
H_2	Total:	1253	0.0929
	Alone:	717	0.0531
	With H_1:	528	0.0391
	With A_1:	3	0.0002
	With A_1 and A_1:	5	0.0004
H_3	Total:	0	0
A_1	Total:	165	0.0122
	Alone:	5	0.0004
	With H_1:	152	0.0113
	With H_2:	3	0.0002
	With H_1 and H_2:	5	0.0004
A_2	Total:	0	0

indistinguishable[4]. Nonetheless, there is a fraction of a percent of such points with M_{H_1} values even beyond 125 GeV or so (the higher the mass the smaller the density, though), which should indeed allow one to distinguish between the two models. Moreover, by studying the cross-section times BR of the Higgses when two of them are observable against their respective mass differences (see Figs. 9–11 of [84]) and widths, one sees that the former are larger than the typical mass resolution in the di-photon channel, so that the two decaying objects should indeed appear in the data as separate resonances.

Table 4.2 recaps the potential observability of one or more NMSSM Higgs states in the di-photon mode at the LHC. It is obvious from the table that one light CP-even Higgs should be observable almost throughout the NMSSM parameter space. However, there is also a fair number of points where two Higgses may be visible simultaneously (H_1 and H_2 or – more rarely – H_1 and A_1), while production and decay of the three lightest Higgses (H_1, H_2 and A_1) at the same time, although possible, occurs for only a negligible number of points in the parameter space. Furthermore, the percentage of points for which only the second lightest Higgs state is visible is also non-negligible. These last two conditions are clearly specific to the NMSSM, as they are never realised in the MSSM. Finally, none of the two heaviest NMSSM neutral Higgs states (H_3 and A_2) will be visible in the di-photon channel at the LHC (given their large masses).

Next, we have proceeded to a dedicated parton level analysis of signal and background processes, the latter involving both tree-level $q\bar{q} \to \gamma\gamma$ and one-loop $gg \to \gamma\gamma$ contributions. We have adopted standard cuts on the two photons [87]: $p_T^\gamma > 25$ GeV and $|\eta^\gamma| < 2.4$ on transverse energy and pseudorapidity, respectively. As illustrative examples of a possible NMSSM Higgs phenomenology appearing at the LHC in the di-photon channel, we have picked up the following three configurations:

1. $\lambda = 0.6554$, $\kappa = 0.2672$, $\mu_{\rm eff} = -426.48$ GeV, $\tan\beta = 2.68$, $A_\lambda = -963.30$ GeV, $A_\kappa = 30.48$ GeV;
2. $\lambda = 0.6445$, $\kappa = 0.2714$, $\mu_{\rm eff} = -167.82$ GeV, $\tan\beta = 2.62$, $A_\lambda = -391.16$ GeV, $A_\kappa = 50.02$ GeV;
3. $\lambda = 0.4865$, $\kappa = 0.3516$, $\mu_{\rm eff} = 355.63$ GeV, $\tan\beta = 2.35$, $A_\lambda = 519.72$ GeV, $A_\kappa = -445.71$ GeV.

[4]Other than an experimental di-photon mass resolution of 2 GeV or so [87] one should also bear in mind here that the mass bounds in both models come at present with a theoretical error of comparable size.

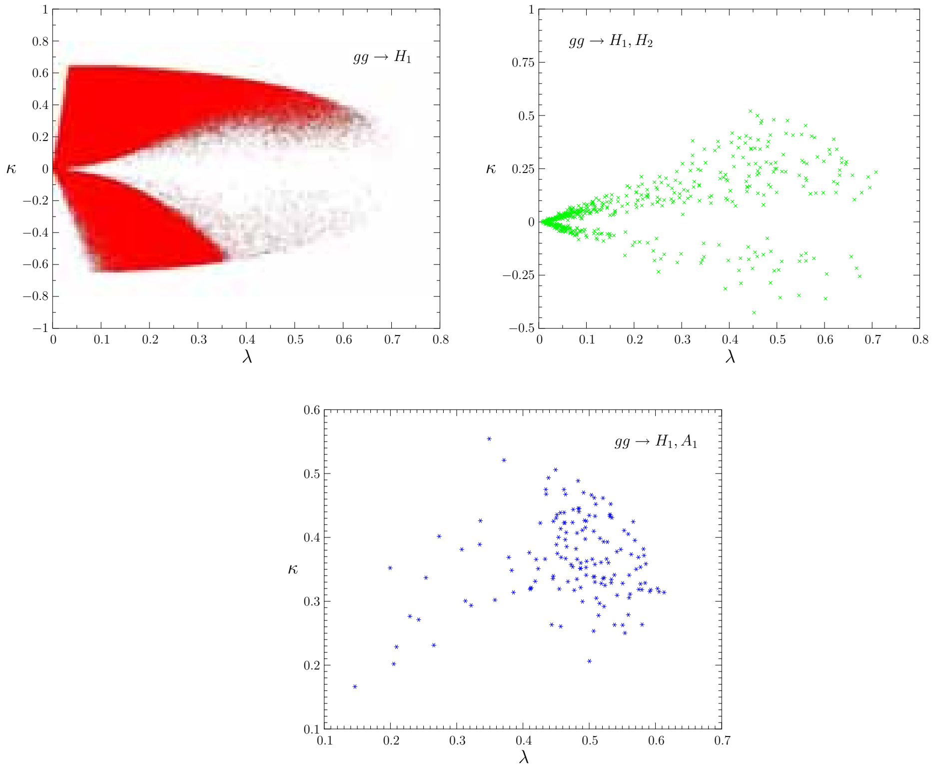

Fig. 4.6: The NMSSM parameter space when H_1 (red/dots), H_1, H_2 (green/crosses) and H_1, A_1 (blue/stars) are potentially visible (individually and simultaneously), plotted against λ and κ.

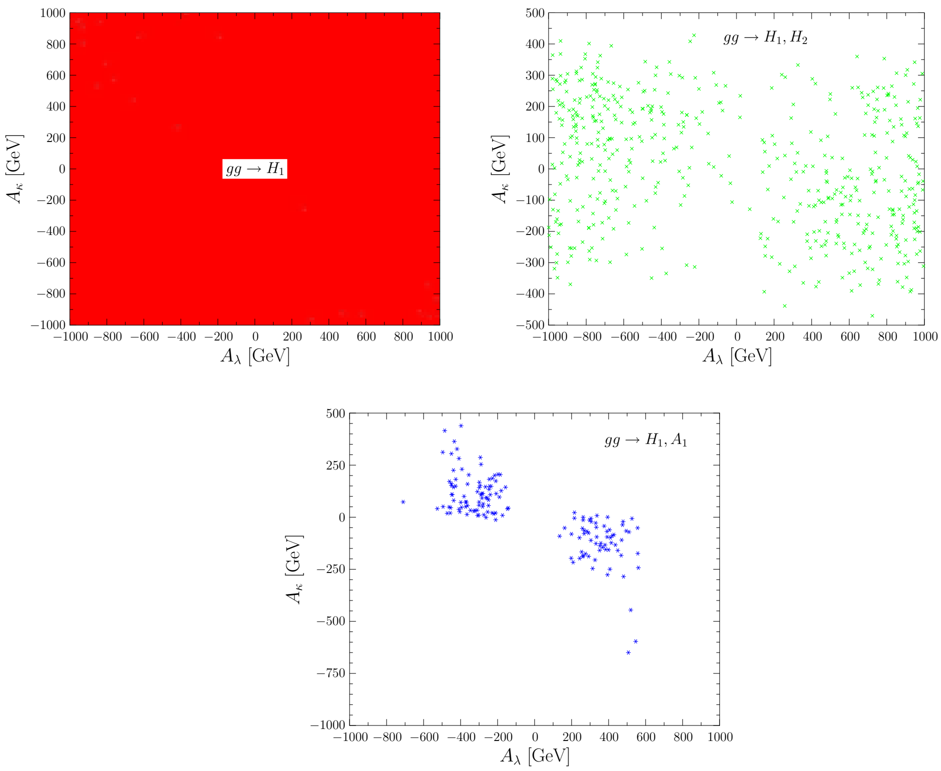

Fig. 4.7: As above, plotted against A_λ and A_κ.

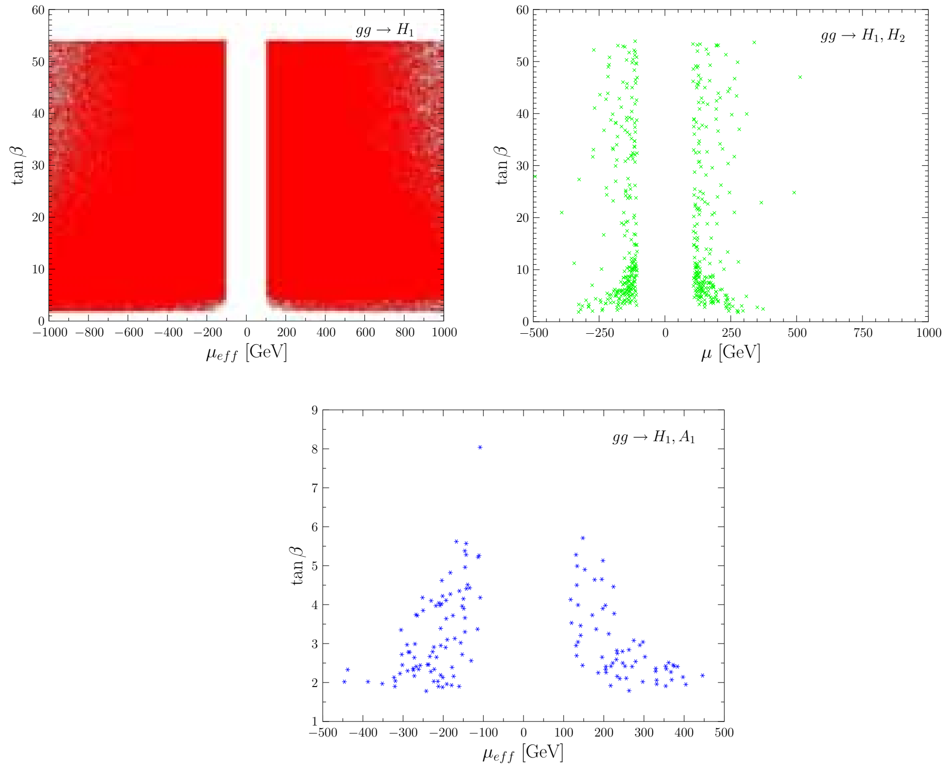

Fig. 4.8: As above, plotted against $\mu_{\rm eff}$ and $\tan\beta$.

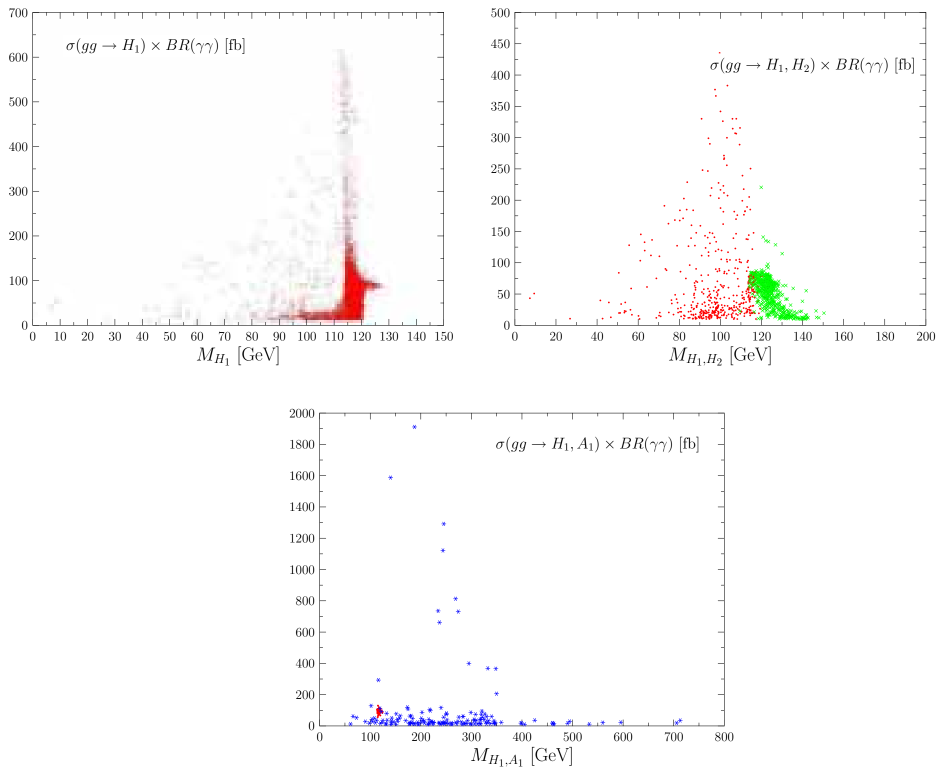

Fig. 4.9: Cross-section times BR for H_1 (red/dots), H_2 (green/crosses) and A_1 (blue/stars), when potentially visible (individually and simultaneously) plotted against their respective masses.

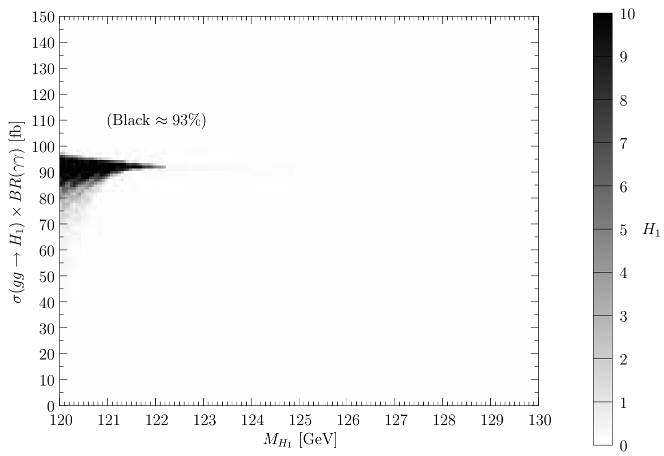

Fig. 4.10: The distribution of points with one potentially visible NMSSM H_1 state with mass beyond the MSSM upper mass limit on the corresponding Higgs state. The scale on the right represents a measure of point density.

The first is representative of the case in which only the NMSSM H_1 boson is visible, but with mass larger than the MSSM upper limit on the corresponding Higgs state. The second and third refer instead to the case when also the H_2 or A_1 state are visible, respectively. The final results are found in Fig. 4.11. The corresponding mass resonances are clearly visible above the continuum di-photon background and discoverable beyond the 5σ level. Indeed, similar situations can be found for each of the combinations listed in Tab. 4.2 and most of these correspond to phenomenological scenarios which are distinctive of the NMSSM and that cannot be reproduced in the MSSM.

In short, while the bulk of the NMSSM parameter space is in a configuration degenerate with the MSSM case (as far as di-photon Higgs signals at the LHC are concerned), non-negligible areas exist with the potential to unveil a non-minimal nature of the underlying SUSY model in this search channel alone.

4.5 Dark matter in the NMSSM and relations to the NMSSM Higgs sector

John F. Gunion, Dan Hooper and Bob McElrath

Since the NMSSM has five neutralinos and two CP-odd Higgs bosons, there are many new ways in which the relic density of the $\widetilde{\chi}_1^0$ could match the observed dark matter density. Dedicated work on NMSSM scenarios appears in [53, 54]. The latter group has made their code publicly available. Let us recall that in the MSSM there is a significant constraint on the mass M_A of the single CP-odd state. This in turn constrains the values of $m_{\widetilde{\chi}_1^0}$ that would lie in the "funnel" region of $m_{\widetilde{\chi}_1^0} \sim 2M_A$ where $\widetilde{\chi}_1^0\widetilde{\chi}_1^0 \to A \to X$ can be sufficiently efficient to adequately reduce the $\widetilde{\chi}_1^0$ relic density to a level at or below that observed. In contrast, in the NMSSM there are two CP-odd states and their masses, M_{A_1} and M_{A_2}, are quite unconstrained by LEP data and theoretical model structure, implying that $\widetilde{\chi}_1^0\widetilde{\chi}_1^0 \to A_{1,2} \to X$ could be the primary annihilation mechanism for large swaths of parameter space.

Let us first discuss the MSSM situation in a bit more detail. Neutralinos produced in the early Universe must annihilate into Standard Model particles at a sufficient rate to avoid overproducing the density of dark matter. Within the framework of the Minimal Supersymmetric Standard Model (MSSM), the lightest neutralino can annihilate through a variety of channels, exchanging other sparticles, Z bosons, or Higgs bosons. The masses of sparticles such as sleptons or squarks, as well as the masses of Higgs bosons, are limited by collider constraints, with typical lower limits of around ~100 GeV. For lighter neutralinos, it becomes increasingly difficult for these heavy propagators to generate neutralino annihilation cross sections that are large enough. The most efficient annihilation channel for very light neutralinos in the MSSM is the s-channel exchange of a pseudoscalar Higgs boson. It has been shown that this channel

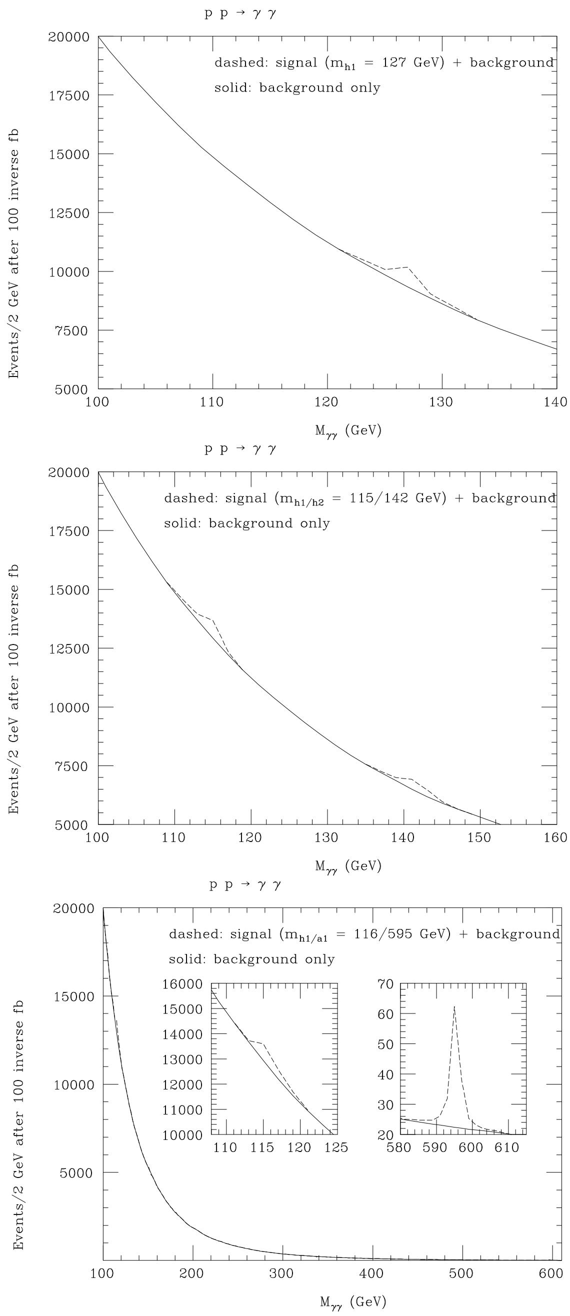

Fig. 4.11: The differential distribution in invariant mass of the di-photon pair after the cuts in p_T^γ and η^γ mentioned in the text, for 100 fb^{-1} of luminosity, in the case of the background (solid) and the sum of signal and background (dashed), for the example points 1. 3. described in the text (from left to right, in correspondence).

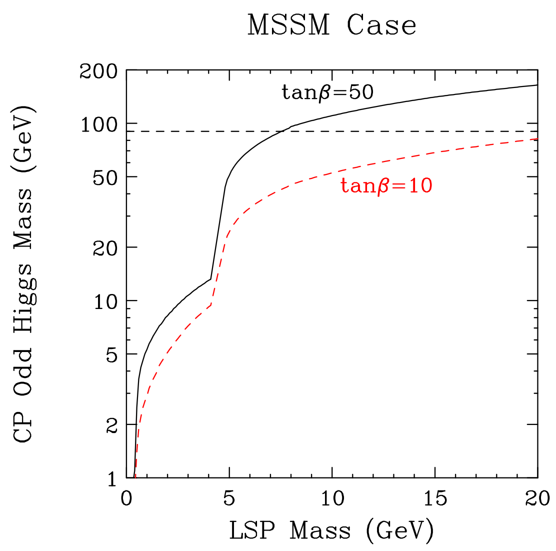

Fig. 4.12: The CP-odd Higgs mass required to obtain the measured relic density for a light neutralino in the MSSM. Models above the curves produce more dark matter than in observed. These results are for the case of a bino-like neutralino with a small higgsino admixture ($\epsilon_B^2 = 0.94$, $\epsilon_u^2 = 0.06$). Results for two values of $\tan\beta$ (10 and 50) are shown. The horizontal dashed line represents the lower limit on the CP-odd Higgs mass in the MSSM from collider constraints. To avoid overproducing dark matter, the neutralino must be heavier than about 8 (22) GeV for $\tan\beta = 50$ (10).

can, in principle, be sufficiently efficient to allow for neutralinos as light as 6 GeV [88, 89]. Such models require a careful matching of a number of independent parameters, however, making viable models with neutralinos lighter than ~20 GeV rather unlikely [90]. Measurements of rare B-decays are also particularly constraining in this regime.

This result should be contrasted with that found for the NMSSM. In the NMSSM (and other supersymmetric models with an extended Higgs sector), a very light CP-odd Higgs boson can naturally arise making it possible for a very light neutralino to annihilate efficiently enough to avoid being overproduced in the early Universe. In fact, it is relatively easy to construct NMSSM models yielding the correct relic density even for a very light neutralino, 100 MeV $< m_{\widetilde{\chi}_1^0} <$ 20 GeV. Even after including constraints from Upsilon decays, $b \to s\gamma$, $B_s \to \mu^+\mu^-$ and the magnetic moment of the muon, a light bino or singlino neutralino is allowed that can generate the appropriate relic density.

4.5.1 Models with a light LSP

Above we outlined the general possibilities for dark matter in the NMSSM context, focusing on the fact that a light or very light neutralino would not yield an over abundance of dark matter. In contrast, it was stated that in the MSSM context it is very difficult to have a light neutralino that is consistent with $\Omega h^2 < 0.1$. As a more specific benchmark for comparison, we consider a light bino in the MSSM which annihilates through the exchange of the CP-odd A. The results for this case are shown in Fig. 4.12. In this figure, the thermal relic density of LSP neutralinos exceeds the measured density for M_A above the solid and dashed curves, for values of $\tan\beta$ of 50 and 10, respectively. Shown as a horizontal dashed line is the lower limit on M_A from collider constraints. This figure demonstrates that even in the case of very large $\tan\beta$, the lightest neutralino must be heavier than about 7 GeV. For moderate values of $\tan\beta$, the neutralino must be heavier than about 20 GeV.

Turning to the NMSSM, as we have noted the physical LSP is a mixture of the bino, neutral wino, neutral higgsinos and singlino. The lightest neutralino therefore has, in addition to the four MSSM

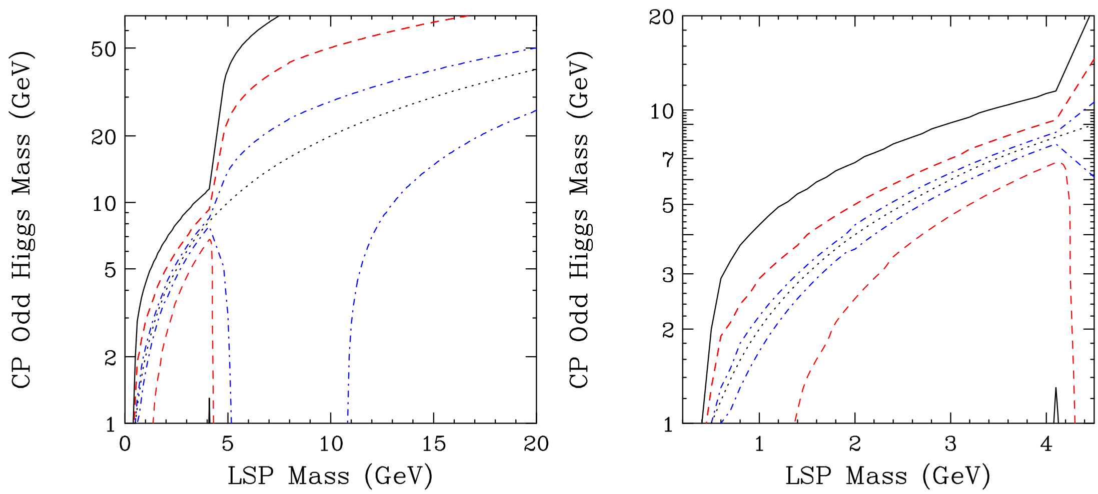

Fig. 4.13: We display contours in M_{A_1} $m_{\widetilde{\chi}_1^0}$ parameter space for which $\Omega h^2 = 0.1$. Points above or below each pair of curves produce more dark matter than is observed; inside each set of curves less dark matter is produced than is observed. These results are for a bino-like neutralino with a small higgsino admixture ($\epsilon_B^2 = 0.94$, $\epsilon_u^2 = 0.06$). Three values of $\tan\beta$ (50, 15 and 3) have been used, shown as solid black, dashed red, and dot-dashed blue lines, respectively. The dotted line is the contour corresponding to $2m_{\widetilde{\chi}_1^0} = M_{A_1}$. For each set of lines, we have set $\cos^2\theta_{A_1} = 0.6$. The $\tan\beta = 50$ case is highly constrained for very light neutralinos, and is primarily shown for comparison with the MSSM case.

components, a singlino component which is the superpartner of the singlet Higgs. The eigenvector of the lightest neutralino, $\widetilde{\chi}_1^0$, in terms of gauge eigenstates can be written in the form

$$\widetilde{\chi}_1^0 = \epsilon_u \tilde{H}_u^0 + \epsilon_d \tilde{H}_d^0 + \epsilon_W \tilde{W}^0 + \epsilon_B \tilde{B} + \epsilon_s \tilde{S}, \tag{4.27}$$

where ϵ_u, ϵ_d are the up-type and down-type higgsino components, ϵ_W, ϵ_B are the wino and bino components and ϵ_s is the singlet component of the lightest neutralino. Similarly, the CP-even and CP-odd Higgs states are mixtures of MSSM-like Higgses and singlets. For the lightest CP-even Higgs state we can define:

$$H_1 = \sqrt{2}\left[\xi_u \mathrm{Re}(H_u^0 - v_u) + \xi_d \mathrm{Re}(H_d^0 - v_d) + \xi_s \mathrm{Re}(S - x)\right], \tag{4.28}$$

where $x \equiv \langle S \rangle$. Here, Re denotes the real component of the respective state. Lastly, the lightest CP-odd Higgs can be written as (a similar formula also applies for the heavier A_2)

$$A_1 = \cos\theta_{A_1} A_{\mathrm{MSSM}} + \sin\theta_{A_1} A_s, \tag{4.29}$$

where A_s is the CP-odd [$\sqrt{2}\mathrm{Im}(S)$] component of the scalar singlet field and A_{MSSM} is the combination of the imaginary components of H_u and H_d that would be the MSSM pseudoscalar Higgs if the singlet were not present. Here, θ_{A_1} is the mixing angle between these two states. There is also a third linear combination of the imaginary components of H_u^0, H_d^0 and S that we have removed by a rotation in β. This field becomes the longitudinal component of the Z after electroweak symmetry is broken.

In the NMSSM context, when annihilation proceeds via one of the CP-odd Higgs bosons the calculation of the relic $\widetilde{\chi}_1^0$ density is much more flexible than in the MSSM. For annihilation via the A_1, the thermally averaged cross section takes the form [using the usual expansion in terms $t = T/m_{\widetilde{\chi}_1^0}$ and writing $\langle\sigma v\rangle = a + bt + \mathcal{O}(t^2)$]:

$$\begin{aligned}
a_{\chi\chi\to A_1\to f\bar{f}} &= \frac{g_2^4 c_f m_f^2 \cos^4\theta_{A_1}\tan^2\beta}{8\pi m_W^2}\frac{m_{\widetilde{\chi}_1^0}^2\sqrt{1-m_f^2/m_{\widetilde{\chi}_1^0}^2}}{(4m_{\widetilde{\chi}_1^0}^2-M_{A_1}^2)^2+M_{A_1}^2\Gamma_{A_1}^2} \qquad (4.30)\\
\times\Big[-\epsilon_u(\epsilon_W &- \epsilon_B\tan\theta_W)\sin\beta+\epsilon_d(\epsilon_W-\epsilon_B\tan\theta_W)\cos\beta\\
&+ \sqrt{2}\frac{\lambda}{g_2}\epsilon_s(\epsilon_u\sin\beta+\epsilon_d\cos\beta)+\frac{\tan\theta_{A_1}}{g_2}\sqrt{2}(\lambda\epsilon_u\epsilon_d-\kappa\epsilon_s^2)\Big]^2,\\
b_{\chi\chi\to A_1\to f\bar{f}} &\simeq 0, \qquad (4.31)
\end{aligned}$$

where c_f is a color factor, equal to 3 for quarks and 1 otherwise. For this result, we have assumed that the final state fermions are down-type. If they are instead up-type fermions, the $\tan^2\beta$ factor should be replaced by $\cot^2\beta$. A similar formula holds for the A_2.

Fig. 4.13 shows how the MSSM results can be modified within the framework of the NMSSM. There, we give results for the case where the NMSSM CP-odd Higgs A_1 is taken to be a mixture of MSSM-like and singlet components specified by $\cos^2\theta_{A_1} = 0.6$ and the neutralino composition is taken to be specified by $\epsilon_B^2 = 0.94$ and $\epsilon_u^2 = 0.06$. These specific values are representative of those that can be achieved for various NMSSM parameter choices satisfying all constraints. For each pair of contours (solid black, dashed red, and dot-dashed blue), $\Omega h^2 = 0.1$ along the contours and the region between the lines is the space in which the neutralino's relic density obeys $\Omega h^2 < 0.1$. The solid black, dashed red, and dot-dashed blue lines correspond to $\tan\beta$=50, 15 and 3, respectively. Also shown as a dotted line is the contour corresponding to the resonance condition, $2m_{\widetilde{\chi}_1^0} = M_{A_1}$.

For the $\tan\beta$=50 or 15 cases, neutralino dark matter can avoid being overproduced for any A_1 mass below $\sim 20-60$ GeV, as long as $m_{\widetilde{\chi}_1^0} > m_b$. For smaller values of $\tan\beta$, a lower limit on M_{A_1} can apply as well.

For neutralinos lighter than the mass of the b-quark, annihilation is generally less efficient. This region is shown in detail in the right frame of Fig. 4.13. In this funnel region, annihilations to $c\bar{c}$, $\tau^+\tau^-$ and $s\bar{s}$ all contribute significantly. Despite the much smaller mass of the strange quark, its couplings are enhanced by a factor proportional to $\tan\beta$ (as with bottom quarks) and thus can play an important role in this mass range. In this mass range, constraints from Upsilon and J/ψ decays can be very important, often requiring fairly small values of $\cos\theta_{A_1}$.

For annihilations to light quarks, $c\bar{c}$, $s\bar{s}$, etc., the Higgs couplings to various meson final states should be considered, which include effective Higgs-gluon couplings induced through quark loops. The calculations shown employed a conservative approximation of keeping only the Higgs-quark-quark couplings alone, even for these light quarks, but with kinematic thresholds set by the mass of the lightest meson containing a given type of quark, rather than the quark mass itself. This corresponds to thresholds of 9.4 GeV, 1.87 GeV, 498 MeV and 135 MeV for bottom, charm, strange and down quarks, respectively. A more detailed treatment, which was not undertaken, would include the proper meson form factors as well as allowing for the possibility of virtual meson states.

The above discussion focused on the case of a mainly bino LSP. If the LSP is mostly singlino, it is also possible to generate the observed relic abundance in the NMSSM. A number of features differ for the singlino-like case in contrast to a bino-like LSP, however. Most importantly, an LSP mass that is chosen to be precisely at the Higgs resonance, $M_{A_1} \simeq 2m_{\widetilde{\chi}_1^0}$, is not possible for this case: M_{A_1} is always less than $2m_{\widetilde{\chi}_1^0}$ by a significant amount. Second, in models with a singlino-like LSP, the A_1 is generally also singlet-like and the product of $\tan^2\beta$ and $\cos^4\theta_{A_1}$, to which annihilation rates are proportional, see Eq. (4.30), is typically very small. This limits the ability of a singlino-like LSP to generate the observed relic abundance. The result is that annihilation is too inefficient for an LSP that is more than

80% singlino. However, there is no problem having $m_{\widetilde\chi_1^0} \sim M_{A_1}/2$ so as to achieve the correct relic density when the $\widetilde\chi_1^0$ is mainly bino while the A_1 is mainly singlet.

Of course, we should also discuss the implications for direct dark matter detection in the NMSSM. As above, we focus on scenarios with a light $\widetilde\chi_1^0$ that are a somewhat unique feature of the NMSSM. The spin-independent elastic scattering cross section of a light neutralino with nuclei is generally dominated by the t-channel exchange of a CP-even Higgs boson. For a bino-like LSP and the H_1 with composition as in Eq. (4.28), the elastic cross section is approximated by

$$\begin{aligned}\sigma^{\rm bino}_{\rm elastic} \quad &\sim \quad \frac{8G_F^2 M_Z^2}{\pi {M_{H_1}}^4}\left(\frac{m_p m_{\widetilde\chi_1^0}}{m_p + m_{\widetilde\chi_1^0}}\right)^2 \epsilon_B^2 \sin^2\theta_W \, (\epsilon_d\xi_u - \epsilon_u\xi_d)^2 \; \times \\ &\left(\sum_{q=d,s,b}\frac{m_q\xi_d}{\cos\beta} < N|q\bar q|N > + \sum_{q=u,c}\frac{m_q\xi_u}{\sin\beta} < N|q\bar q|N >\right)^2 . \end{aligned} \tag{4.32}$$

If the LSP is singlino-like, on the other hand, the appropriate approximation is

$$\begin{aligned}\sigma^{\rm singlino}_{\rm elastic} \quad &\sim \quad \frac{8G_F^2 M_Z^2}{\pi {M_{H_1}}^4}\left(\frac{m_p m_{\widetilde\chi_1^0}}{m_p + m_{\widetilde\chi_1^0}}\right)^2 \frac{2\lambda^2\,\epsilon_s^2\,\cos^2\theta_W}{g_2^2} \, (\epsilon_d\xi_d + \epsilon_u\xi_u)^2 \; \times \\ &\left(\sum_{q=d,s,b}\frac{m_q\xi_d}{\cos\beta} < N|q\bar q|N > + \sum_{q=u,c}\frac{m_q\xi_u}{\sin\beta} < N|q\bar q|N >\right)^2 . \end{aligned} \tag{4.33}$$

In assessing the implications of the above, it is useful to note that LEP limits on the H_1 if it decays to $b\bar b$ (we return to the $H_1 \to A_1A_1$ type scenario later) with $M_{H_1} < 120$ GeV roughly imply

$$\xi_{u,d} \lesssim \left(\frac{M_{H_1}}{120\mathrm{GeV}}\right)^{3/2} + 0.1, \tag{4.34}$$

and for a light $\widetilde\chi_1^0$ LEP limits on invisible Z decays roughly imply $\epsilon_{u,d} < 0.06$. If we assume that the s-quark contribution dominates and use $m_s < N|s\bar s|N > \approx 0.2$ GeV, the resulting cross section for a bino-like or singlino-like $\widetilde\chi_1^0$ is then roughly given by:

$$\sigma_{\rm elastic} \lesssim 1.4\times 10^{-42} cm^2 \left(\frac{120\text{ GeV}}{M_{H_1}}\right)^4 \left(\left(\frac{M_{H_1}}{120\text{ GeV}}\right)^{3/2} + 0.1\right)^2 \left(\frac{\tan\beta}{50}\right)^2 F_\lambda \tag{4.35}$$

assuming $m_{\widetilde\chi_1^0} > m_p$ and $\tan\beta > 1$, using the $\xi_{u,d}$ limit of Eq. (4.34) and adopting $\epsilon_{u,d} \sim 0.06$. In the above, $F_\lambda = 1$ for the bino-like case and $F_\lambda = 2\lambda^2/(g_2^2\tan^2\theta_W) \approx 0.67\times(\lambda/0.2)^2$ for the singlino-like case. For $\tan\beta = 50$, $\lambda = 0.2$ and a Higgs mass of 120 GeV, we estimate a neutralino-proton elastic scattering cross section on the order of 4×10^{-42} cm^2 (4×10^{-3} fb) for either a bino-like or a singlino-like LSP. This value may be of interest to direct detection searches such as CDMS, DAMA, Edelweiss, ZEPLIN and CRESST. To account for the DAMA data, the cross section would have to be enhanced by a local over-density of dark matter.

It is interesting to consider whether there are any special features related to the very attractive scenarios motivated by minimizing the fine-tuning measure F. In those scenarios, the H_1 can have mass below the LEP limit (e.g. of order 100 GeV) even though its WW, ZZ couplings are very SM-like. This is possible provided $M_{A_1} < 2m_b$ so that the H_1 decays predominantly via $H_1 \to A_1A_1$ with $A_1 \to \tau^+\tau^-$ (or, if $M_{A_1} < 2m_\tau$, $A_1 \to gg, c\bar c, \ldots$) since the $H_1 \to A_1A_1 \to \tau^+\tau^-\tau^+\tau^-$ decay channel is not constrained by LEP data for $M_{H_1} \lesssim 90$ GeV. For our purposes, the important feature of such a scenario is that, the A_1 turns out to be very singlet-like, with $\cos^2\theta_{A_1} \lesssim 0.015$. In this case, adequate annihilation of a very light $\widetilde\chi_1^0$ via $\widetilde\chi_1^0\widetilde\chi_1^0 \to A_1 \to X$ occurs only if $m_{\widetilde\chi_1^0} \simeq M_{A_1}/2$. This requires a rather fine adjustment of the M_1 bino soft mass relative to M_{A_1} that has no immediately obvious theoretical motivation. Because the A_1 is so light in the low fine-tuning scenarios, if $m_{\widetilde\chi_1^0}$ is significantly above $2m_b$ then consistency with relic abundance limits requires that $\widetilde\chi_1^0\widetilde\chi_1^0$ annihilation proceed via one of the more conventional co-annihilation channels or via $\widetilde\chi_1^0\widetilde\chi_1^0 \to A_2 \to X$. The latter case is only applicable if $m_{\widetilde\chi_1^0} \gtrsim 200$ GeV, since the A_2 is typically quite heavy in the low-F scenarios, $M_{A_2} \gtrsim 400$ GeV.

Another issue is direct detection of dark matter. Since the A_1 is so singlet in nature, the only exchange of importance is H_1 exchange. In the low-F scenarios, H_1 is almost entirely H_u. In particular, the H_d composition component of the H_1 is $\xi_d \sim 0.1$, and correspondingly $\xi_u \sim 0.99$. For the $\widetilde\chi_1^0$, $\epsilon_B > 0.8$ and ϵ_u and ϵ_d can take a range of values from 0.1 up to 0.5. Referring to Eq. (4.32), again keeping only the s-quark contribution and keeping only the dominant $\epsilon_d\xi_u$ piece in the external factor, we obtain

$$\sigma_{\rm elastic} \sim 5 \times 10^{-6}\epsilon_B^2 \left(\frac{\epsilon_d}{0.25}\right)^2 \left(\frac{100~{\rm GeV}}{M_{H_1}}\right)^4 \left(\frac{\tan\beta}{10}\right)^2 ~{\rm fb}\,. \tag{4.36}$$

If $m_{\widetilde\chi_1^0}$ is in the $15-100$ GeV mass range that is optimal for experiments like ZEPLIN and CRESST, direct dark matter detection would might be possible. If $m_{\widetilde\chi_1^0} < m_b$ (the $\widetilde\chi_1^0\widetilde\chi_1^0 \to A_1 \to X$ possibility), the sensitivity of ZEPLIN and CRESST is greatly reduced and dark matter detection would be very difficult.

So, where does all this leave us with respect to the ILC program. First consider the case where $m_{\widetilde\chi_1^0} \sim M_{A_1}/2 < m_b$, the best that a hadron collider can do will probably be to set an upper limit on $m_{\widetilde\chi_1^0}$. Determining its composition is almost certain to be very difficult. Note that the $m_{\widetilde\chi_2^0} - m_{\widetilde\chi_1^0}$ mass difference should be large, implying adequate room for $\widetilde\chi_2^0 \to Z\widetilde\chi_1^0$ and a search for lepton kinematic edges and the like. (Of course, $\widetilde\chi_2^0 \to H_1\widetilde\chi_1^0$ will also probably be an allowed channel, with associated implications for H_1 detection in SUSY cascade decays.) A light singlet-like A_1 is very hard to detect. At best, it might be possible to bound $\cos\theta_{A_1}$ by experimentally establishing an upper bound on the $WW \to A_1A_1$ rate (proportional to $\cos^4\theta_{A_1}$). Thus, the ILC would be absolutely essential. Precise measurement of the $\widetilde\chi_1^0$ mass and composition using the standard ILC techniques should be straightforward. A bigger question is how best to learn about the A_1 at the precision level. Of course, we will have lots of A_1's to study from ZH_1 production followed by $H_1 \to A_1A_1$ decays. The events will give precise measurements of $g_{ZZH_1}^2 BR(H_1 \to A_1A_1)BR(A_1 \to X)BR(A_1 \to Y)$, where $X, Y = \tau^+\tau^-, gg, c\overline{c}, \ldots$. The problem will be to unfold the individual branching ratios so as to learn about the A_1 itself. Particularly crucial would be some sort of determination of $\cos\theta_{A_1}$ which enters so critically into the annihilation rate. (I assume that a $\tan\beta$ measurement could come from other supersymmetry particle production measurements and so take it as given.) There is some chance that $WW \to A_1A_1$ and $Z^* \to ZA_1A_1$, with rates proportional to $\cos^4\theta_{A_1}$, could be detected. The $\cos^2\theta_{A_1} = 1$ rates are very large, implying that observation might be possible despite the fact that the low-F scenarios have $\cos^2\theta_{A_1} \lesssim 0.01$. One could also consider whether $\gamma\gamma \to A_1$ production would have an observable signal despite the suppression due to the singlet nature of the A_1. Hopefully, enough precision could be achieved for the A_1 measurements that they could be combined with the $\widetilde\chi_1^0$ precision measurements so as to allow a precision calculation of the expected $\widetilde\chi_1^0$ relic density. A study of the errors in the dark matter density computation using the above measurements as compared to the expected experimental error for the Ωh^2 measurement is needed.

If the $\widetilde\chi_1^0$ is not light, but the low fine-tuning scenario applies with A_1 mass below $2m_b$, then early universe $\widetilde\chi_1^0\widetilde\chi_1^0$ annihilation cannot occur via the A_1 channel. In this case, proper relic density must be achieved using co-annihilation or $\widetilde\chi_1^0\widetilde\chi_1^0 \to A_2$ annihilation (where $A_2 \sim A_{MSSM}$ and M_{A_2} is relatively large) — there is no point in repeating the relevant analyses here. We only note that the precision needed to compute the $\widetilde\chi_1^0\widetilde\chi_1^0$ annihilation rate and compare to the measured Ωh^2 should be achievable at the ILC. As already noted, the $2m_{\widetilde\chi_1^0} \simeq M_{A_1}$ scenario seems relatively fine-tuned and we regard the large $m_{\widetilde\chi_1^0}$ scenarios as much more likely.

As an overall summary, we simply reiterate the fact that the NMSSM provides a huge increase in the possibilities for achieving the correct relic density for the $\widetilde{\chi}_1^0$ and can drastically alter expectations for direct detection of dark matter.

4.6 Relic density of neutralino dark matter in the NMSSM

Geneviève Bélanger, Fawzi Boudjema, Cyril Hugonie, Alexander Pukhov and Alexander Semenov

In any supersymmetric (SUSY) extension of the Standard Model with conserved R-parity, the lightest SUSY particle (LSP) constitutes a good candidate for cold dark matter. Recent measurements from WMAP [91, 92] have constrained the value for the relic density of dark matter within 10% ($0.0945 < \Omega h^2 < 0.1287$ at 2σ). The forthcoming PLANCK experiment should reduce this interval down to 2-3%. It is therefore important to calculate the relic density as accurately as possible in any given SUSY model, in order to match this experimental accuracy. Here we perform a precise calculation of the relic density of dark matter within the NMSSM using an extension of `micrOMEGAs` [93] and an interface with the program `NMHDECAY` [63] that calculates the spectrum of the model, in particular that of the Higgs sector. The NMSSM contains, in addition to the MSSM fields, an extra scalar and pseudo-scalar neutral Higgs bosons, as well as an additional neutralino. The phenomenology of the model can be markedly different from the MSSM [26, 27, 29]. In particular the possibility of light Higgs states [72] or light neutralinos that may have escaped LEP searches [94, 95] could impact significantly on the value of the relic density. We present a selection of scenarios that pedict a value of the relic density in agreement with WMAP [54].

4.6.1 The model

We consider the general NMSSM with parameters defined at the weak scale. As free parameters, we take the parameters of the Higgs sector, Eq. (4.11), as well as the gaugino masses M_1, M_2 that enter the neutralino mass matrix. In the gaugino sector, we assume universality at the GUT scale, which at the EW scale corresponds to $M_2 = 2M_1$ and $M_3 = 3.3M_2$. The soft terms in the squark and slepton sector (which enter the radiative corrections in the Higgs sector) are also fixed at the EW scale. We assume very heavy sfermions $m_{\tilde{f}} = 1$ TeV and fix the trilinear mixing to $A_f = 1.5$ TeV. We thus consider as independent parameters the following set of variables

$$\lambda,\ \kappa,\ \tan\beta,\ \mu,\ A_\lambda,\ A_\kappa,\ M_1. \tag{4.37}$$

For the SM parameters, we assume $\alpha_s = 0.118$, $m_t^{\rm pole} = 175$ GeV and $m_b(m_b) = 4.24$ GeV.

We set all these parameters in the program `NMHDECAY` [63]. For each point in the parameter space, the program `NMHDECAY` first checks the absence of Landau singularities for λ, κ, h_t and h_b below the GUT scale. For $m_t^{\rm pole} = 175$GeV, this translates into $\lambda < .75$, $\kappa < .65$, and $3. < \tan\beta < 85$. `NMHDECAY` also checks the absence of an unphysical global minimum of the scalar potential with vanishing Higgs vevs. `NMHDECAY` then computes scalar, pseudo-scalar and charged Higgs masses and mixings, taking into account one and two loop radiative corrections, as well as chargino and neutralino masses and mixings. Finally, all available experimental constraints from LEP are checked.

The couplings of the LSP to the scalar and pseudo-scalar Higgs states will enter the computation of LSP annihilation through a Higgs resonance or t-channel annihilation into Higgs pairs. The Feynman rule for the LSP-scalar-scalar vertex reads

$$\begin{aligned} g_{\widetilde{\chi}_1^0\widetilde{\chi}_1^0 h_i} &= g(N_{12} - N_{11}\tan\theta_W)(S_{i1}N_{13} - S_{i2}N_{14}) \\ &\quad + \sqrt{2}\lambda N_{15}(S_{i1}N_{14} + S_{i2}N_{13}) + \sqrt{2}S_{i3}(\lambda N_{13}N_{14} - \kappa N_{15}^2)\,. \end{aligned} \tag{4.38}$$

Here N describes the neutralino mixing and S the scalar mixing [63]. The first term is equivalent to the $\widetilde{\chi}_1^0\widetilde{\chi}_1^0 h$ coupling in the MSSM by replacing $S_{11} = S_{22} = \cos\alpha$ and $S_{12} = -S_{21} = \sin\alpha$ while the last two terms are specific of the NMSSM. The second term is proportional to the singlino component of the LSP while the last one is proportional to the singlet component of the scalar Higgs. Similarly, the LSP coupling to a pseudo-scalar also contains terms proportional to the singlino component or to the singlet component of the Higgs.

4.6.2 Relic density

In the context of the MSSM, the publicly available program `micrOMEGAs` [96, 97] computes the relic density of the lightest neutralino LSP by evaluating the thermally averaged cross section for its annihilation as well as, when necessary, for its coannihilation with other SUSY particles. It then solves the density evolution equation numerically, without using the freeze-out approximation. We have extended `micrOMEGAs` [93] to perform the relic density calculation within the NMSSM. An interface with `NMHDECAY` allows a precise calculation of the particle spectrum in the NMSSM, as well as a complete check of all the available experimental constraints from LEP [63].

In the MSSM with universal gaugino masses, one can classify the main scenarios for dark matter annihilation as follows: a bino scenario with light sfermions where neutralino annihilate into fermion pairs, a sfermion coannihilation scenario, a mixed bino/Higgsino scenario where neutralino annihilate dominantly into gauge boson pairs or into $t\bar{t}$ and finally a Higgs funnel scenario where neutralino annihilate in fermion pairs near a s-channel Higgs resonance. When sfermions are very heavy only the latter two scenarios predict $\Omega h^2 \approx 0.1$, in agreement with WMAP. To achieve this, the bino-Higgsino scenario requires $M_1 \approx \mu$, indeed higher higgsino content ($M_1 \gg \mu$) leads to very efficient annihilation and coannihilation while a smaller higgsino content ($M_1 \ll \mu$) to values of the relic density that are too high. The Higgs funnnel scenario requires that $M_H \approx 2m_{\tilde{\chi}_1^0}$, here H corresponds to either the light scalar or the heavy scalar/pseudoscalar. The latter is enhances at large values of $\tan\beta$.

In the NMSSM, the same mechanisms as for the MSSM are at work for neutralino annihilation: into fermion pairs through s-channel exchange of a Z or Higgs, into gauge boson pairs through either Z/H s-channel exchange or t-channel exchange of heavier neutralinos or charginos. The new features of the NMSSM are first a richer scalar/pseudoscalar Higgs sector that leads to more resonances but also to new decay modes for Higgses (into lighter Higgses) and second a neutralino LSP which because of its mixing with a singlino feature different couplings to gauge bosons, Higgs and sparticles. These new features imply new possibilities to either increase or decrease the relic density of neutralinos as compared to the MSSM. We next describe some typical scenarios that lead to a value for the relic density of dark matter in agreement with WMAP.

4.6.3 Results

We concentrate on models which can differ markedly from the MSSM predictions, in particular models with $\tan\beta \leq 5$ for which annihilation through a Higgs resonance is marginal in the MSSM. We also consider models where the presence of light Higgs states opens up new channels for efficient neutralino annihilation as well as models where the LSP is dominantly singlino.

Case 1: annihilation through Higgs resonances

The presence of additional Higgs states in the NMSSM means additional regions of parameter space where rapid annihilation through a s-channel resonance can take place. In fact we found that such annihilation is dominant in large regions of the parameter space and this even at low to intermediate values of $\tan\beta$. For example, starting with a value of μ and M_1 for which one would expect $\Omega h^2 > .13$ in the MSSM, and varying the parameters A_λ, A_κ one can tune the value of the scalars/pseudoscalars masses such that for at least one scalar/pseudoscalar satisfies $m_{H_i,A_i} \approx 2m_{\tilde{\chi}_1^0}$. Note that the neutralino sector does not depend on A_λ, A_κ. We found scenarios consistent with the WMAP measurement where rapid neutralino annihilation proceeds through either the H_2 resonance (an example is given in Table 4.3, Case 1), the light pseudoscalar, A_1, or the lightest scalar H_1. The latter can also occur in the MSSM.

Table 4.3: Benchmark points satisfying both LEP and WMAP constraints

Case	1	2	3a	3b	3c
λ	0.1	0.35	0.6	0.23	0.035
κ	0.11	0.2	0.12	0.003	0.0124
$\tan\beta$	5	5	2	3.2	5
μ [GeV]	300	230	265	195	285
A_λ [GeV]	-100	400	450	590	-28
A_κ [GeV]	-100	0	-50	-20	-150
M_1 [GeV]	150	160	500	100	235
$m_{\widetilde{\chi}_1^0}$ [GeV]	142	141	127	8	206
$N_{13}^2 + N_{14}^2$	0.02	0.09	0.105	0.04	0.02
N_{15}^2	0	0.02	0.90	0.95	0.94
$m_{\widetilde{\chi}_2^0}$ [GeV]	250	209	270	85	215
$m_{\widetilde{\chi}_1^\pm}$ [GeV]	246	218	269	138	273
m_{H_1} [GeV]	118	113	102	18	115
m_{H_2} [GeV]	561	258	130	115	158
m_{A_1} [GeV]	297	54	122	14	211
Ωh^2	0.104	0.116	0.1155	0.124	0.111
Channels	qq (83%) ll (10%) VV (4%) HH (2%) ZH (1%)	VV (51%) HA (31%) HH (15%) ZH (2%)	HA (60%) VV (26%) ZH (10%) HH (3%) ff(2%)	qq (92%) ll (8%)	$\widetilde{\chi}_2^0\widetilde{\chi}_2^0 \to X$ (77%) $\widetilde{\chi}_1^0\widetilde{\chi}_2^0 \to X$ (18%) $\widetilde{\chi}_1^0\widetilde{\chi}_1^\pm \to X$ (1%) qq (2%)

Case 2: the mixed bino/higgsino: $\mu \approx M_1$

We consider a scenario where $\mu = 230$, $M_1 = 160$ GeV, $\tan\beta = 5$, $A_\lambda = 500$ GeV and $A_\kappa = 0$. In the MSSM limit, that is when $\lambda \to 0$, $\Omega h^2 \approx 0.2$, a value slightly above WMAP. The LSP is a mixed bino/Higgsino and its main annihilation channel is into W pairs. For moderate values of κ, say $\kappa = 0.2$, increasing λ affects the Higgs spectrum and increases the singlino component of the LSP. This leads either to a sharp drop in Ωh^2 when one encounters the H_2 resonance or to a more moderate drop for large values of λ. For example, for $\lambda = 0.35$, we observe much enhanced cross sections for $\widetilde{\chi}_1^0\widetilde{\chi}_1^0 \to HH, HA$, this leads to $\Omega h^2 = 0.116$. Details of this scenario are presented in Table 4.3, Case 2. For even larger values of λ, the singlino component of the LSP becomes significant. Then the $\widetilde{\chi}_1^0\widetilde{\chi}_1^0 H_1$ and $\widetilde{\chi}_1^0\widetilde{\chi}_1^0 A_1$ couplings are large leading to an even larger contribution of the $\widetilde{\chi}_1^0\widetilde{\chi}_1^0 \to H_1 A_1$ annihilation through t-channel $\widetilde{\chi}_1^0$ exchange. However, this area of the parameter space is excluded by Higgs searches at LEP.

Case 3 : the singlino LSP

We explore now scenarios satisfying both LEP and WMAP constraints with a predominantly singlino LSP. For this we scanned over the whole parameter space of the NMSSM in the range $\lambda < 0.75$, $\kappa < 0.65$, $2 < \tan\beta < 10$, $100 < \mu < 500$ GeV, $100 < M_2 < 1000$ GeV, $0 < A_\lambda < 1000$ GeV and $0 < -A_\kappa < 500$ GeV. We found three classes of models: a mixed singlino/higgsino LSP that annihilates mainly into $H_1 A_1$ and VV ($V = W, Z$), an almost pure singlino that annihilates through a Z or Higgs resonance and a singlino where dominant channels are coannihilation ones. In Table 4.3 we show a selection of benchmark points along these lines (Case 3a,3b,3c).

The first scenario, Case 3a in Table 4.3, is one for which $\mu \ll M_1$ and the LSP is a mixed higgsino/singlino. In this example, the LSP is 90% singlino and 10% higgsino, with a mass of 127 GeV. The main annihilation mode is $H_1 A_1$ through t-channel $\widetilde{\chi}_1^0$ exchange, H_1 and A_1 being both mainly singlet (88% and 99% respectively). This is due to enhanced couplings $\widetilde{\chi}_1^0\widetilde{\chi}_1^0 A_1(H_1)$ which occur for large values of λ (Eq. 4.38). Annihilation of the higgsino component into W/Z pairs accounts for the subdominant channel.

In Table 4.3 we also give an example, Case 3b, of a scenario with a light singlino LSP, here with a mass of 10 GeV. The only efficient mode for such a light singlino is via a Higgs resonance, here a light scalar dominantly singlet. This scalar decays into $b\bar{b}$, or when kinematically accessible into $A_1 A_1$, the A_1 being also mainly singlet. The Higgs sector of such models is of course severely constrained by LEP, in particular the limit on the SM-like scalar, here the second scalar, H_2. For this reason most scenarios with light singlinos have $\tan\beta \approx 3$ which is the value for which the lightest visible (i.e. non singlet) Higgs mass, M_{H_2}, is maximized [28, 98–100]. Note that a light singlino requires $\kappa \ll \lambda$ and not too large value for μ.

For $\kappa \leq \lambda \ll 1$, the LSP is heavy with a large singlino component. No efficient annihilation mechanism is then available. However coannihilation with heavier neutralinos and charginos can be very efficient especially for a higgsino-like NLSP. Case 3c in Table 4.3 gives an example of such a scenario. The LSP is 96% singlino with a mass of 203 GeV. The mass difference with the NLSP $\widetilde{\chi}_2^0$ is 11 GeV. The coannihilation channels are overwhelmingly dominant. The $\widetilde{\chi}_2^0$ higgsino component is just enough (28%) for efficient annihilation. The main channels are $\widetilde{\chi}_2^0\widetilde{\chi}_2^0(\widetilde{\chi}_1^0) \rightarrow t\bar{t}, b\bar{b}$ and correspond to annihilation through H_3 and A_2 exchange. For this point, H_3 and A_2 belong to the heavy Higgs doublet with $M_A \approx 475$ GeV, so that we are close to a (double) resonance. Such a resonance is not necessary though, in order to have efficient $\widetilde{\chi}_2^0$ annihilation. We also found points in the parameter space with a heavy singlino where the dominant channel was $\widetilde{\chi}_2^0\widetilde{\chi}_2^0(\widetilde{\chi}_1^0) \rightarrow VV$ through Z exchange.

4.6.4 Conclusion

In the NMSSM, basically the same mechanisms as for the MSSM are at work for neutralino annihilation, nevertheless the presence of additional Higgs states provides additional possibilities for efficient neutralino annihilation. Specifically this means additional regions of parameter space where rapid annihilation through a s-channel resonance can take place, as well as new annihilation channels when light Higgs states are present. However, annihilation of neutralinos is not always favoured in the NMSSM. In general the singlino component of the LSP tends to reduce the annihilation cross-section. We found however regions of the parameter space where a singlino LSP gives the right amount of dark matter, either for large λ, s-channel resonances into a Z or a Higgs, or coannihilation with $\widetilde{\chi}_2^0$, $\widetilde{\chi}_1^{\pm}$.

For scenarios for which the relic density is within the WMAP allowed region, one can ask whether it would be possible to see signatures of the model at colliders. In the case of a mixed bino/higgsino LSP, provided the singlino state is not heavy and decouples, i.e. λ not too small and κ not too large, the five neutralino states might be visible at the LHC/ILC. This would be a clear signature of the NMSSM. Finally, in the singlino LSP case, μ cannot be too large. One therefore would expect visible higgsinos at the LHC. The singlino LSP would however appear at the end of the decay chain in any sparticle pair production process, which might complicate the detection task as it was the case at LEP [94].

4.7 Comparison of Higgs bosons in the extended MSSM models

Vernon Barger, Paul Langacker, Hye-Sung Lee and Gabe Shaughnessy

When the μ parameter of the Minimal Supersymmetric Standard Model (MSSM) is promoted to a Standard Model (SM) singlet field, the fine-tuning problem of the MSSM [2] can be naturally solved with a dynamically generated $\mu_{\rm eff} \equiv \lambda \langle S \rangle = \lambda v_s/\sqrt{2}$. The new Higgs singlet is accompanied by a new symmetry that governs the interaction of the singlet. Depending on the symmetry, the MSSM can be extended to different models such as the Next-to-Minimal Supersymmetric SM (NMSSM) [26, 30, 55], the Minimal Nonminimal Supersymmetric SM (MNSSM) [44–46, 51], and the $U(1)'$-extended Minimal Supersymmetric SM (UMSSM) [13, 101]. Table 4.4 shows the symmetry, superpotential and the Higgs spectrum of several models. The Exceptional Supersymmetric SM (ESSM) [16] is, to a large extent, similar to the UMSSM. The secluded $U(1)'$ model (sMSSM) [102] has multiple Higgs singlets and, in a decoupling limit of the extra singlets, the low energy spectrum is similar to the MNSSM.

It is important to compare the implications of the MSSM and its various extensions. In this note, we treat the different models in a consistent way to compare and contrast their features. (For a full study by the authors, see [103].) The neutralino sectors are also extended by the singlino and Z'-ino in these models and were studied in [52].

4.7.1 Models

The tree-level Higgs mass-squared matrices are found from the potential, V, which is a sum of the F-term, D-term and soft-terms in the lagrangian, as follows.

$$V_F = |\lambda H_u \cdot H_d + t_F + \kappa S^2|^2 + |\lambda S|^2 \left(|H_d|^2 + |H_u|^2\right) \quad (4.39)$$

$$V_D = \frac{G^2}{8}\left(|H_d|^2 - |H_u|^2\right)^2 + \frac{g_2^2}{2}\left(|H_d|^2|H_u|^2 - |H_u \cdot H_d|^2\right) + \frac{{g_{1'}}^2}{2}\left(Q_{H_d}|H_d|^2 + Q_{H_u}|H_u|^2 + Q_S|S|^2\right)^2 \quad (4.40)$$

$$V_{\rm soft} = m_{H_d}^2|H_d|^2 + m_{H_u}^2|H_u|^2 + m_S^2|S|^2 + \left(A_\lambda \lambda S H_u \cdot H_d + \frac{\kappa}{3}A_\kappa S^3 + t_S S + h.c.\right) \quad (4.41)$$

This scalar potential is a collective form of all extended MSSM models considered here and, for a particular model, the parameters in V are understood to be *turned-off* appropriately.

$$\begin{array}{rcl} \text{MNSSM/sMSSM} & : & g_{1'} = 0, \kappa = 0, A_\kappa = 0 \\ \text{NMSSM} & : & g_{1'} = 0, t_{F,S} = 0 \\ \text{UMSSM} & : & t_{F,S} = 0, \kappa = 0, A_\kappa = 0 \end{array} \quad (4.42)$$

The F-term and the soft terms contain the model dependence of the NMSSM and MNSSM/sMSSM, while the D-term contains that of the UMSSM. We ignore possible CP violation in the Higgs sector.

Table 4.4: Higgs bosons of the MSSM and several of its extensions

Model	Symmetry	Superpotential	CP-even	CP-odd	Charged
MSSM	–	$\mu \hat{H}_u \cdot \hat{H}_d$	H_1, H_2	A_1	$H^\pm$
NMSSM	$\mathbf{Z_3}$	$\lambda \hat{S} \hat{H}_u \cdot \hat{H}_d + \frac{\kappa}{3}\hat{S}^3$	H_1, H_2, H_3	A_1, A_2	$H^\pm$
MNSSM	$\mathbf{Z_5^R}, \mathbf{Z_7^R}$	$\lambda \hat{S} \hat{H}_u \cdot \hat{H}_d + t_F \hat{S}$	H_1, H_2, H_3	A_1, A_2	$H^\pm$
UMSSM	$U(1)'$	$\lambda \hat{S} \hat{H}_u \cdot \hat{H}_d$	H_1, H_2, H_3	A_1	$H^\pm$
sMSSM	$U(1)'$	$\lambda \hat{S} \hat{H}_u \cdot \hat{H}_d + \lambda_s \hat{S}_1 \hat{S}_2 \hat{S}_3$	$H_1, \cdots, H_6$	$A_1, \cdots, A_4$	$H^\pm$

4.7.2 Higgs mass matrices

The collective tree-level CP-even Higgs mass matrix elements in the (H_d^0, H_u^0, S) basis are:

$$
\begin{aligned}
(\mathcal{M}_+^0)_{11} &= \left[\frac{G^2}{4} + Q_{H_d}^2 {g_{1'}}^2\right] v_d^2 + \left(\frac{\lambda A_\lambda}{\sqrt{2}} + \frac{\lambda\kappa v_s}{2} + \frac{\lambda t_F}{v_s}\right)\frac{v_u v_s}{v_d} && (4.43)\\
(\mathcal{M}_+^0)_{12} &= -\left[\frac{G^2}{4} - \lambda^2 - Q_{H_d} Q_{H_u} {g_{1'}}^2\right] v_d v_u - \left(\frac{\lambda A_\lambda}{\sqrt{2}} + \frac{\lambda\kappa v_s}{2} + \frac{\lambda t_F}{v_s}\right) v_s && (4.44)\\
(\mathcal{M}_+^0)_{13} &= \left[\lambda^2 + Q_{H_d} Q_S {g_{1'}}^2\right] v_d v_s - \left(\frac{\lambda A_\lambda}{\sqrt{2}} + \lambda\kappa v_s\right) v_u && (4.45)\\
(\mathcal{M}_+^0)_{22} &= \left[\frac{G^2}{4} + Q_{H_u}^2 {g_{1'}}^2\right] v_u^2 + \left(\frac{\lambda A_\lambda}{\sqrt{2}} + \frac{\lambda\kappa v_s}{2} + \frac{\lambda t_F}{v_s}\right)\frac{v_d v_s}{v_u} && (4.46)\\
(\mathcal{M}_+^0)_{23} &= \left[\lambda^2 + Q_{H_u} Q_S {g_{1'}}^2\right] v_u v_s - \left(\frac{\lambda A_\lambda}{\sqrt{2}} + \lambda\kappa v_s\right) v_d && (4.47)\\
(\mathcal{M}_+^0)_{33} &= \left[Q_S^2 {g_{1'}}^2 + 2\kappa^2\right] v_s^2 + \left(\frac{\lambda A_\lambda}{\sqrt{2}} - \frac{\sqrt{2} t_S}{v_d v_u}\right)\frac{v_d v_u}{v_s} + \frac{\kappa A_\kappa}{\sqrt{2}} v_s && (4.48)
\end{aligned}
$$

where $v_{d,u} = \sqrt{2}\langle H_{d,u}^0\rangle$. The similarly modified matrix elements for the CP-odd and charged Higgs masses in the extended models can be found in [103]. We consider only the dominant 1-loop correction which comes from the common top/stop contributions to keep a consistent analysis.

The mass-squared sum rules are:

$$
\begin{aligned}
\text{MSSM} &: \left(M_{H_1}^2 + M_{H_2}^2\right) - \left(M_{A_1}^2\right) = M_Z^2 + \delta M^2\\
\text{MNSSM/sMSSM} &: \left(M_{H_1}^2 + M_{H_2}^2 + M_{H_3}^2\right) - \left(M_{A_1}^2 + M_{A_2}^2\right) = M_Z^2 + \delta M^2\\
\text{NMSSM} &: \left(M_{H_1}^2 + M_{H_2}^2 + M_{H_3}^2\right) - \left(M_{A_1}^2 + M_{A_2}^2\right) && (4.49)\\
&\qquad = M_Z^2 + \kappa(-\lambda v_d v_u + v_s(\sqrt{2}A_\kappa + v_s\kappa)) + \delta M^2\\
\text{UMSSM} &: \left(M_{H_1}^2 + M_{H_2}^2 + M_{H_3}^2\right) - \left(M_{A_1}^2\right) = M_Z^2 + M_{Z'}^2 + \delta M^2
\end{aligned}
$$

With a one-loop radiative correction, the common loop effect, δM^2, could be as large as $\mathcal{O}((100\text{ GeV})^2)$ unless $\tan\beta$ is very small.

The physical Higgs boson masses are found by diagonalizing the mass-squared matrices, $\mathcal{M}_D = R_+ \mathcal{M} R_+^{-1}$, where $\mathcal{M}$ also includes the radiative corrections. The rotation matrices, R_+, may then be used to construct the physical Higgs fields as

$$H_i = R_+^{i1}\phi_d + R_+^{i2}\phi_u + R_+^{i3}\phi_s \qquad (4.50)$$

where the physical states are ordered by their mass as $M_{H_1} \le M_{H_2} \le M_{H_3}$, and similarly for the CP-odd Higgses.

4.7.3 Interesting limits

The extended MSSM models share the common characteristics of the near Peccei-Quinn symmetry limit [6] when the model-dependent terms (such as κ, A_κ, $t_{F,S}$, $g_{1'}$) are very small, and the lightest CP-odd Higgs boson (Z' gauge boson for the UMSSM case) becomes nearly massless. The exact global Peccei-Quinn symmetry should be avoided though, to be compatible with the non-observation of the Weinberg-Wilczek axion [104, 105].

When the singlet VEV, v_s, is large while μ_{eff} is kept at the EW scale (i.e., λ is small), they approach the MSSM limit when the model-dependent terms are not large. In the large v_s limit (i.e., $M_c/v_s \sim \epsilon$ where M_c is the common mass scale other than v_s, and $\epsilon \ll 1$), we show the explicit tree-level approximations of the CP-even Higgs masses [103].

NMSSM (with an additional assumption of $\kappa \sim \epsilon$) :

$$\begin{aligned} M_{H_1}^2 &\approx \frac{1}{2} v_s \kappa \left(4 v_s \kappa + \sqrt{2} A_\kappa\right) \\ M_{H_{2,3}}^2 &\approx \frac{1}{2} M_Z^2 + \left(A_\lambda + \frac{v_s \kappa}{\sqrt{2}}\right) \mu_{\rm eff} \csc 2\beta \\ &\mp \sqrt{\left(\frac{1}{2} M_Z^2 - \left(A_\lambda + \frac{v_s \kappa}{\sqrt{2}}\right) \mu_{\rm eff} \csc 2\beta\right)^2 + 2 M_Z^2 \left(A_\lambda + \frac{v_s \kappa}{\sqrt{2}}\right) \mu_{\rm eff} \sin 2\beta} \end{aligned} \quad (4.51)$$

MNSSM/sMSSM (with an additional assumption of $t_S / M_c^3 \sim \epsilon$) :

$$\begin{aligned} M_{H_1}^2 &\approx \frac{1}{v_s^2} \frac{\mu_{\rm eff} \sec^2 2\beta}{2 G^2 A_\lambda} \left(32 \mu_{\rm eff}^2 \sin 2\beta A_\lambda^2 - G^2 v^2 \sin^3 2\beta \left(4 \mu_{\rm eff}^2 + A_\lambda^2\right)\right. \\ &\left. + 2 \mu_{\rm eff} A_\lambda \left(G^2 v^2 - 16 \mu_{\rm eff}^2 - 2 A_\lambda^2 + \cos 4\beta \left(-G^2 v^2 + 2 A_\lambda^2\right)\right)\right) - \frac{\sqrt{2} t_S}{v_s} \\ M_{H_{2,3}}^2 &\approx \frac{1}{2} M_Z^2 + A_\lambda \mu_{\rm eff} \csc 2\beta \mp \sqrt{\left(\frac{1}{2} M_Z^2 - A_\lambda \mu_{\rm eff} \csc 2\beta\right)^2 + 2 M_Z^2 A_\lambda \mu_{\rm eff} \sin 2\beta} \end{aligned} \quad (4.52)$$

UMSSM :

$$\begin{aligned} M_{H_{1,2}}^2 &\approx \frac{1}{2} M_Z^2 + A_\lambda \mu_{\rm eff} \csc 2\beta \mp \sqrt{\left(\frac{1}{2} M_Z^2 - A_\lambda \mu_{\rm eff} \csc 2\beta\right)^2 + 2 M_Z^2 A_\lambda \mu_{\rm eff} \sin 2\beta} \\ M_{H_3}^2 &\approx M_{Z'}^2 \quad (\text{with } Z' \text{ mass given by } M_{Z'}^2 = {g_{1'}}^2 (Q_{H_d}^2 v_d^2 + Q_{H_u}^2 v_u^2 + Q_S^2 v_s^2)) \end{aligned} \quad (4.53)$$

With large v_s, when κ (and κA_κ) $\to 0$, $g_{1'} \to 0$, $t_{F,S} \to 0$, all of the above Higgs masses reach the MSSM limits (with the identification of $A_\lambda = B$ and $\mu_{\rm eff} = \mu$) with an additional scalar decoupled with either negligible or very heavy mass. The first solution in the MNSSM/sMSSM is not valid when $\tan\beta$ is near 1 (or $\sec^2 2\beta \to \infty$), but an exact solution can be obtained in this limit.

4.7.4 Theoretical upper bounds on the lightest Higgs mass

From the mass matrix of Eq. (4.43-4.48), the upper bounds on the lightest CP-even Higgs can be obtained.

$$\begin{aligned} \text{MSSM} &: \quad M_{H_1}^2 \le M_Z^2 \cos^2 2\beta + \tilde{\mathcal{M}}^{(1)} \\ \text{NMSSM/MNSSM/sMSSM} &: \quad M_{H_1}^2 \le M_Z^2 \cos^2 2\beta + \frac{1}{2} \lambda^2 v^2 \sin^2 2\beta + \tilde{\mathcal{M}}^{(1)} \\ \text{UMSSM} &: \quad M_{H_1}^2 \le M_Z^2 \cos^2 2\beta + \frac{1}{2} \lambda^2 v^2 \sin^2 2\beta \\ &\qquad + g_{1'}^2 v^2 (Q_{H_d} \cos^2\beta + Q_{H_u} \sin^2\beta)^2 + \tilde{\mathcal{M}}^{(1)} \end{aligned} \quad (4.54)$$

where $\tilde{\mathcal{M}}^{(1)}$ is the common contribution from the 1-loop correction.

All extended models have larger upper bounds for the lightest CP-even Higgs than that of the MSSM due to the contribution of the singlet scalar. The UMSSM has an additional contribution in the quartic coupling from the gauge coupling constant, $g_{1'}$ of the $U(1)'$ symmetry. In the MSSM, large $\tan\beta$ values are suggested by the conflict between the experimental lower bound and the theoretical upper bound on M_{H_1}. Since the extended models contain additional terms which relax the theoretical bound, they allow smaller $\tan\beta$ values than the MSSM does (see Fig. 4.15b).

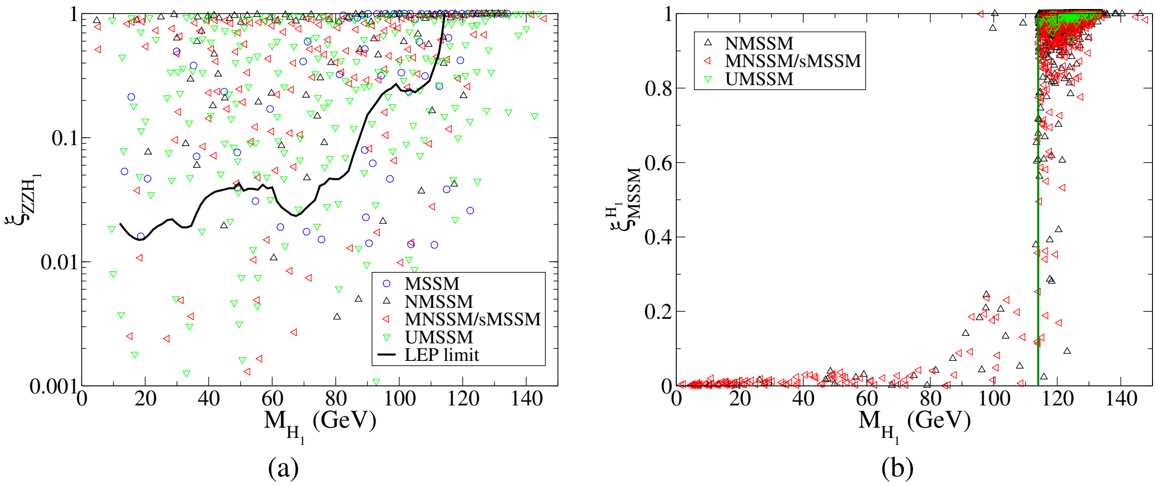

Fig. 4.14: (a) LEP limit [106] on $\xi_{ZZH_1} = \left(g_{ZZH_1}/g^{SM}_{ZZh}\right)^2 = \Gamma_{Z\to ZH_1}/\Gamma^{SM}_{Z\to Zh}$, the scaled ZZH_1 coupling in various Supersymmetric models, vs. the lightest CP-even Higgs mass. The other constraints are not applied. The solid black curve is the observed limit at 95% C.L. Points falling below this curve pass the ZZH_1 constraint. (b) The lightest CP-even Higgs masses vs. $\xi_{\rm MSSM}$ (MSSM fraction) after all constraints are applied. The vertical line is the LEP lower bound on the MSSM (SM-like) Higgs mass.

4.7.5 Experimental constraints on the Higgs

(i) LEP bound on ZZh coupling: The ZZh coupling limits from LEP [106] can be used to limit the mass of the lightest CP-even Higgs boson of the extended MSSM models. Fig. 4.14a shows the LEP limit (95% C.L.) on the ZZH_1 coupling relative to the SM coupling with the H_1 mass. The relative coupling is given by

$$\xi_{ZZH_i} = \left(g_{ZZH_i}/g^{SM}_{ZZh}\right)^2 = (R^{i1}_+ \cos\beta + R^{i2}_+ \sin\beta)^2. \tag{4.55}$$

As the scatter plot shows, when the Higgs coupling is diluted by the singlet component (i.e., $\xi_{ZZH_1} < 1$), it may have a mass smaller than the SM-like Higgs limit of 114.4 GeV.

(ii) LEP bound on M_{H_1} and M_{A_1}: For the channel of $Z \to A_i H_j$ with $A_i \to b\bar{b}$ and $H_j \to b\bar{b}$, LEP gives bounds on the MSSM Higgs masses of $M_{H_1} \geq 92.9$ GeV and $M_{A_1} \geq 93.4$ GeV assuming maximal stop mixing, yielding the most conservative limit [74]. With the maximum LEP energy, $\sqrt{s} = 209$ GeV, mass limits on the H_1 and A_1 in the extended MSSM models can be obtained with the upper bound of the cross section for $e^+e^- \to A_i H_j$ at 40 fb. In practice, we find that the LEP $Z \to A_i H_j$ constraint eliminates a significant fraction of the points generated with a low CP-odd Higgs mass.

(iii) LEP bound on $M_{H^\pm}$: The Higgs singlet does not alter the charged Higgs part, and the LEP bound on the MSSM charged Higgs mass of $M_{H^\pm} \geq 78.6$ GeV is imposed [107].

(iv) LEP bound on $M_{\chi^\pm_1}$: The LEP bound on the chargino mass of $M_{\chi^\pm_1} > 104$ GeV is imposed [108].

(v) LEP invisible Z decay width: The LEP bound on the invisible Z decay width by new physics of $\Delta\Gamma_Z < 1.9$ MeV is imposed [109].

(vi) LEP $Z - Z'$ mixing angle: The LEP bound on the $Z - Z'$ mixing angle (for the UMSSM), $\alpha_{ZZ'} < 2 \times 10^{-3}$ is imposed [110–112]. The exact bound depends on the model.

4.7.6 Numerical results

The model-independent parameters are scanned over $\tan\beta = 1 \sim 50$, $v_s = 50 \sim 2000$ GeV, $\mu_{\rm eff} = 50 \sim 1000$ GeV, $A_\lambda = 0 \sim 1000$ GeV, $A_t = -1000 \sim 1000$ GeV, $M_2 = -500 \sim 500$ GeV.

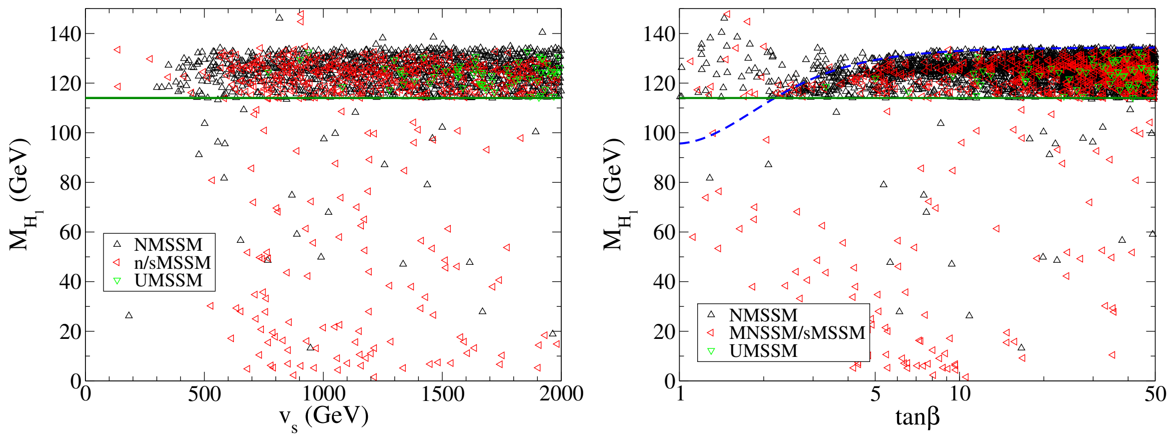

(a) (b)

Fig. 4.15: The lightest CP-even Higgs masses vs. (a) v_s and (b) $\tan\beta$. The horizontal line is the LEP lower bound on the SM-like Higgs. The dashed curve is the MSSM bound for a maximum stop mixing.

The model-dependent parameters are scanned over $\kappa = -0.75 \sim 0.75$, $A_\kappa = -1000 \sim 1000$ GeV, $t_F = -500^2 \sim 500^2$ GeV^2, $t_S = -500^3 \sim 500^3$ GeV^3, $\theta_{E_6} = 0 \sim \pi$. We assume gaugino mass unification $M_1 = M_{1'} = \frac{5g_1^2}{3g_2^2} M_2$ and fix the stop soft mass at $M_{\widetilde{Q}} = M_{\widetilde{U}} = 1000$ GeV and the renormalization scale for the loop correction at $Q = 300$ GeV. Additional constraints of $0.1 \le \lambda \le 0.75$ and $0.1 \le \sqrt{\kappa^2 + \lambda^2} \le 0.75$ for perturbativity and naturalness are also applied.

The relative coupling strength of a particular Higgs boson, H_i, to the MSSM fields may be quantified as the MSSM fraction

$$\xi^{H_i}_{\rm MSSM} = \sum_{j=1}^{2} (R_+^{ij})^2. \tag{4.56}$$

In Fig. 4.14b, we plot the MSSM fraction versus the lightest CP-even Higgs boson mass in extended MSSM models after all constraints are applied. When the singlet composition is large (i.e., $\xi^{H_1}_{\rm MSSM}$ is small), a lighter mass is allowed by the LEP constraint. The UMSSM has the additional constraint on the singlet VEV from the $Z - Z'$ mixing angle constraint, and it pushes the allowed points to more MSSM-like as shown in Fig. 4.15a. However, there are ways to allow lower v_s values, such as leptophobic couplings [113, 114] or additional singlet contributions [102]. The lightest CP-even Higgs boson mass versus $\tan\beta$ in each model shown in Fig. 4.15b has a majority of generated points in the band 114.4 GeV $< M_{H_1} < 135$ GeV and $\tan\beta > 2$. This is, as the dashed curve indicates, one of the salient features of the MSSM after the experimental constraints, which implies that most of those points are MSSM-like.

In Fig. 4.16a, we present the parameter scan results of the mass ranges for the lightest CP-even Higgs in the MSSM and its extensions after all constraints are applied. The NMSSM and the MNSSM/sMSSM have pretty similar mass ranges and they can be extremely light due to effect of the singlet. The additional constraint on s makes the lower bound of the UMSSM to be more MSSM-like. The upper bounds in the extended MSSM models are about $30 \sim 40$ GeV larger than that of the MSSM in accordance with Eq. (4.54). For the CP-odd and charged Higgses (Fig. 4.16b,c) as well as the other aspects including the Higgs production and decays, see [103].

4.7.7 Conclusions

Even though low energy Supersymmetry is well-motivated, the μ-problem suggests the MSSM may not be the full Supersymmetric model that describes TeV scale physics. The introduction of a Higgs singlet

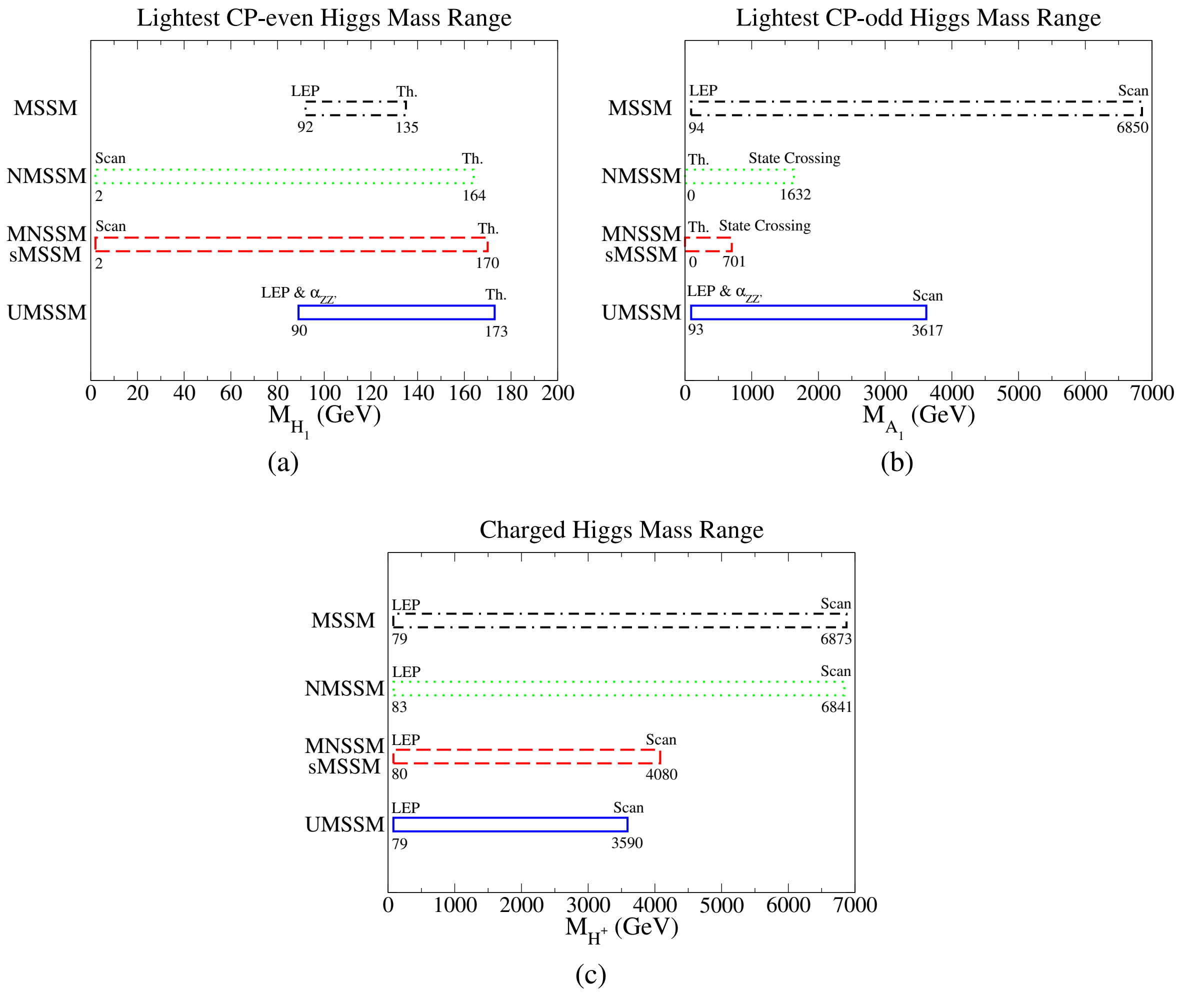

Fig. 4.16: Mass ranges of (a) the lightest CP-even, (b) the lightest CP-odd, and (c) charged Higgses

can solve this problem naturally, but depending on the new symmetry that governs the interaction of the singlet, there are more than one direction to extend the MSSM. We presented a formalism that is convenient for comparing different models in a consistent way.

The extended MSSM have many similar features including:

- The μ-problem is elegantly solved with a new Higgs singlet.
- The lightest CP-even Higgs can be considerably lighter than the SM or the MSSM bounds from LEP experiments.
- Low values of $\tan\beta$ are allowed unlike in the MSSM.
- The near Peccei-Quinn limit can be achieved when the model-dependent parameters are small, where the lightest CP-odd Higgs (or Z' for the UMSSM) are expected to be very light.
- The MSSM limit can be achieved when the singlet VEV, v_s, is large compared to other mass parameters.

Due to the different governing symmetry, the models also have distinguishable characteristics, including:

- The UMSSM predicts an EW/TeV scale Z' gauge boson (and v_s receives additional experimental constraints).
- The NMSSM may have a domain wall problem related to the discrete symmetry [42].
- The Higgs spectra and mass sum rules are model-dependent (Table 4.4 and Eq. (4.49)).

– The neutralino properties are also distinguishable [52].
– In the large v_s limit, the mass of the non-MSSM-like Higgs depends on the model parameters.

More studies are necessary to understand how to distinguish the extended MSSM models from the MSSM and from each other.

4.8 Distinction between NMSSM and MSSM in combined LHC and ILC analyses

Hans Fraas, Fabian Franke, Stefan Hesselbach and Gudrid Moortgat-Pick

In some parts of SUSY parameter space the experimentally accessible Higgs sector of the NMSSM is very similar to the MSSM Higgs sector and does not allow the identification of the underlying SUSY model. In such cases additional information from the neutralino sector can be crucial. In this contribution we analyze an NMSSM scenario for which only a combined analysis of LHC and ILC data will be sufficient to distinguish the models.

4.8.1 Neutralino sector

The NMSSM contains five neutralinos $\tilde{\chi}^0_i$, the mass eigenstates of the photino, zino and neutral higgsinos, and two charginos $\tilde{\chi}^\pm_i$, being mixtures of wino and charged higgsino. The neutralino/chargino sector depends at tree level on four parameters of Eq. (4.11), λ, κ, μ_{eff}, $\tan\beta$, and additionally on the U(1) and SU(2) gaugino masses M_1 and M_2 [31, 115–117]; see also Section 4.2. The additional fifth neutralino may significantly change the phenomenology of the neutralino sector. In scenarios where the lightest supersymmetric particle is a nearly pure singlino, the existence of displaced vertices may lead to a particularly interesting experimental signature [94, 95, 118–120] which allows the distinction between the models. Furthermore sfermion decays into fermions and singlino-dominated neutralinos can have large branching ratios resulting in modified signatures of the sfermions [121]. Especially the modified cascade decays of the squarks at the LHC can be important for the identification of the model. If however, only a part of the particle spectrum is kinematically accessible this distinction may become challenging. We start with a scenario with the parameters

$$M_1 = 360\text{ GeV},\quad M_2 = 147\text{ GeV},\quad \lambda = 0.5,\quad \kappa = 0.2,\quad \mu_{\text{eff}} = 458\text{ GeV},\quad \tan\beta = 10, \tag{4.57}$$

and the following gaugino/higgsino masses and eigenstates:

$$m_{\tilde{\chi}^0_1} = 138\text{ GeV},\qquad \tilde{\chi}^0_1 = (-0.02, +0.97, -0.20, +0.09, -0.07), \tag{4.58}$$
$$m_{\tilde{\chi}^0_2} = 337\text{ GeV},\qquad \tilde{\chi}^0_2 = (+0.62, +0.14, +0.25, -0.31, +0.65), \tag{4.59}$$
$$m_{\tilde{\chi}^0_3} = 367\text{ GeV},\qquad \tilde{\chi}^0_3 = (-0.75, +0.04, +0.01, -0.12, +0.65), \tag{4.60}$$
$$m_{\tilde{\chi}^0_4} = 468\text{ GeV},\qquad \tilde{\chi}^0_4 = (-0.03, +0.08, +0.70, +0.70, +0.08), \tag{4.61}$$
$$m_{\tilde{\chi}^0_5} = 499\text{ GeV},\qquad \tilde{\chi}^0_5 = (+0.21, -0.16, -0.64, +0.62, +0.37), \tag{4.62}$$

where the neutralino eigenstates are given in the basis $(\tilde{B}^0, \tilde{W}^0, \tilde{H}^0_d, \tilde{H}^0_u, \tilde{S})$. As can be seen from Eqs. (4.59) and (4.60), the particles $\tilde{\chi}^0_2$ and $\tilde{\chi}^0_3$ have a rather strong singlino admixture.

This scenario translates at the e^+e^- International Linear Collider (ILC) with $\sqrt{s} = 500$ GeV into the experimental observables of Table 4.5 for the measurement of the masses and production cross sections for several polarization configurations of the light neutralinos and charginos. We assume mass uncertainties of $\mathcal{O}(1-2\%)$ [122,123], a polarization uncertainty of $\Delta P_{e^\pm}/P_{e^\pm} = 0.5\%$ and one standard deviation statistical errors. The masses and cross sections in different beam polarization configurations provide the experimental input for deriving the supersymmetric parameters within the MSSM using standard methods [124–127]. Note that beam polarization may be crucial for distinguishing the two models [128–130].

Table 4.5: Masses with 1.5% ($\tilde{\chi}^0_{2,3}$, $\tilde{e}_{L,R}$, $\tilde{\nu}_e$) and 2% ($\tilde{\chi}^0_1$, $\tilde{\chi}^\pm_1$) uncertainty [122, 123] and the kinematically allowed cross sections with an error composed of the error due to the mass uncertainties, polarization uncertainty of $\Delta P_{e^\pm}/P_{e^\pm} = 0.5\%$ and one standard deviation statistical error based on $\int \mathcal{L} = 100$ fb^{-1}, for both unpolarized beams and polarized beams with $(P_{e^-}, P_{e^+}) = (\mp 90\%, \pm 60\%)$, in analogy to the study in [131].

$m_{\tilde{\chi}^0_1} = 138 \pm 2.8$ GeV		$\sigma(e^+e^- \to \tilde{\chi}^\pm_1 \tilde{\chi}^\mp_1)$/fb		$\sigma(e^+e^- \to \tilde{\chi}^0_1 \tilde{\chi}^0_2)$/fb
$m_{\tilde{\chi}^0_2} = 337 \pm 5.1$ GeV	(P_{e^-}, P_{e^+})	$\sqrt{s} = 400$ GeV	$\sqrt{s} = 500$ GeV	$\sqrt{s} = 500$ GeV
$m_{\tilde{\chi}^\pm_1} = 139 \pm 2.8$ GeV	Unpolarized	323.9 ± 33.5	287.5 ± 16.5	4.0 ± 1.2
$m_{\tilde{e}_L} = 240 \pm 3.6$ GeV	$(-90\%, +60\%)$	984.0 ± 101.6	873.9 ± 50.1	12.1 ± 3.8
$m_{\tilde{e}_R} = 220 \pm 3.3$ GeV	$(+90\%, -60\%)$	13.6 ± 1.6	11.7 ± 1.2	0.2 ± 0.1
$m_{\tilde{\nu}_e} = 226 \pm 3.4$ GeV				

Table 4.6: Masses and mixing character in the basis (H_u, H_d, S) of the NMSSM Higgs bosons for the parameters $\lambda = 0.5$, $\kappa = 0.2$, $\mu_{\text{eff}} = 458$ GeV, $\tan\beta = 10$, $A_\lambda = 4000$ GeV and $A_\kappa = -200$ GeV and the branching ratios of the lightest scalar Higgs H_1 calculated with NMHDECAY [63]. Only decay channels with $BR > 1\%$ are listed.

	m_H/GeV	mixing		$BR(H_1)$
H_1	125	$(-0.9949, -0.0992, 0.0165)$	$H_1 \to gg$	5%
H_2	293	$(-0.0145, -0.0211, -0.9997)$	$H_1 \to \tau\tau$	7%
H_3	4415	$(0.0995, -0.9948, 0.0196)$	$H_1 \to cc$	3%
A_1	333	$(0.0017, 0.0166, -0.9999)$	$H_1 \to bb$	63%
A_2	4415	$(0.0995, 0.9949, 0.0167)$	$H_1 \to WW^*$	20%
$H^\pm$	4417		$H_1 \to ZZ^*$	2%

4.8.2 Higgs sector

The Higgs sector of the NMSSM [30, 99] depends on two additional parameters, the trilinear soft scalar mass parameters A_λ and A_κ. The Higgs bosons with dominant singlet character may escape detection in large regions of these parameters, thus the Higgs sector does not allow the identification of the NMSSM. A scan with NMHDECAY [63] in our scenario, Eq. (4.57), over A_λ and A_κ results in parameter points which survive the theoretical and experimental constraints in the region 2614 GeV $< A_\lambda <$ 5583 GeV and -564 GeV $< A_\kappa <$ 5 GeV. For -396 GeV $< A_\kappa < -92$ GeV the second lightest scalar (H_2) and the lightest pseudoscalar (A_1) Higgs particle have very pure singlet character and are heavier than the mass difference $m_{\tilde{\chi}^0_3} - m_{\tilde{\chi}^0_1}$, hence the decays of the neutralinos $\tilde{\chi}^0_2$ and $\tilde{\chi}^0_3$, which will be discussed in the following, are not affected by H_2 and A_1. The dependence of the masses of H_1, H_2 and A_1 on A_κ is illustrated in Fig. 4.17 (left panel). The mass of the lightest scalar Higgs H_1, which has MSSM-like character in this parameter range, depends only weakly on A_κ and is about 125 GeV. The masses of H_3, A_2 and $H^\pm$ are of the order of A_λ. For $A_\kappa < -396$ GeV the smaller mass of the H_2 and a stronger mixing between the singlet and MSSM-like states in H_1 and H_2 might allow a discrimination in the Higgs sector while for $A_\kappa > -92$ GeV the existence of a light pseudoscalar A_1 may give first hints of the NMSSM [72]. For our specific case study we choose $A_\lambda = 4000$ GeV and $A_\kappa = -200$ GeV, which leads to to the Higgs masses and mixing characters as listed in Table 4.6. Here H_3 and A_2 are kinematically not accessible while H_2 and A_1 are not produced due to their nearly pure singlet character. Then only H_1 can be detected with the branching ratios given in Table 4.6, which are very similar to those of an SM Higgs boson of the same mass. Also the branching ratio of $\tilde{\chi}^0_2$ in the lightest Higgs particle differs only by a factor two in both scenarios. If a precise measurement of this branching ratio is possible first hints for the inconsistency of the model could be derived at the ILC.

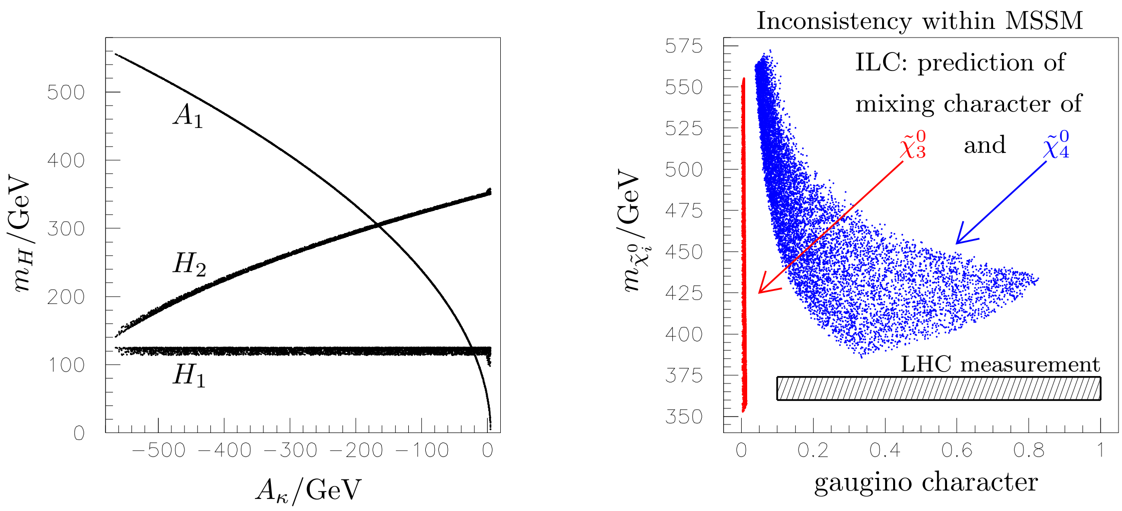

Fig. 4.17: Left: The possible masses of the two light scalar Higgs bosons, m_{H_1}, m_{H_2}, and of the lightest pseudoscalar Higgs boson m_{A_1} as function of the trilinear Higgs parameter A_κ in the NMSSM. In our chosen scenario, H_1 is MSSM-like and H_2 and A_1 are heavy singlet-dominated Higgs particles. Right: Predicted masses and gaugino admixture for the heavier neutralinos $\tilde\chi_3^0$ and $\tilde\chi_4^0$ within the consistent parameter ranges derived at the ILC$_{500}$ analysis in the MSSM and measured mass $m_{\tilde\chi_i^0} = 367 \pm 7$ GeV of a neutralino with suf ciently high gaugino admixture in cascade decays at the LHC. We require a gaugino admixture of $\gtrsim 10\%$ for the heavy neutralinos, cf. [137 139].

4.8.3 Gaugino/higgsino parameter determination at the ILC

For the determination of the supersymmetric parameters in the MSSM straightforward strategies [124, 125, 132, 133] have been worked out even if only the light neutralinos and charginos $\tilde\chi_1^0$, $\tilde\chi_2^0$ and $\tilde\chi_1^\pm$ are kinematically accessible at the first stage of the ILC [126,127]. Using the methods described in [134,135] we derive constraints for the parameters M_1, M_2, μ and $\tan\beta$ in two steps. First, the measured masses and cross sections at two energies in the chargino sector constrain the chargino mixing matrix elements U_{11}^2 and V_{11}^2 [136]. Adding then mass and cross section measurements in the neutralino sector allows to constrain the parameters

$$\begin{aligned} M_1 &= 377 \pm 42 \text{ GeV}, && (4.63)\\ M_2 &= 150 \pm 20 \text{ GeV}, && (4.64)\\ \mu &= 450 \pm 100 \text{ GeV}, && (4.65)\\ \tan\beta &\leq 30. && (4.66) \end{aligned}$$

Since the heavier neutralino and chargino states are not produced, the parameters μ and $\tan\beta$ can only be determined with a considerable uncertainty.

With help of the determined parameter ranges, Eqs. (4.63)–(4.66), the masses of heavier charginos and neutralinos can be calculated:

$$352 \text{ GeV} \leq m_{\tilde\chi_3^0} \leq 555 \text{ GeV}, \qquad 386 \text{ GeV} \leq m_{\tilde\chi_4^0} \leq 573 \text{ GeV}, \qquad 350 \text{ GeV} \leq m_{\tilde\chi_2^\pm} \leq 600 \text{ GeV}. \tag{4.67}$$

In Fig. 4.17 (right panel) the masses of $\tilde\chi_3^0$ and $\tilde\chi_4^0$ are shown as a function of its gaugino admixture for parameter points within the constraints of Eqs. (4.63)–(4.66). Obviously, the heavy neutralino $\tilde\chi_3^0$ should be almost a pure higgsino within the MSSM prediction. These predicted properties of the heavier particles can be compared with mass measurements of SUSY particles at the LHC within cascade decays [131].

We emphasize that although we started with an NMSSM scenario where $\tilde\chi_2^0$ and $\tilde\chi_3^0$ have large singlino admixtures, the MSSM parameter strategy does not fail and the experimental results from the

Table 4.7: Expected cross sections for the associated production of the heavier neutralinos and charginos in the NMSSM scenario for the $\mathrm{ILC}_{650}^{\mathcal{L}=1/3}$ option with one sigma statistical error based on $\int \mathcal{L} = 33$ fb^{-1} for both unpolarized and polarized beams.

	$\sigma(e^+e^- \to \tilde{\chi}^0_1\tilde{\chi}^0_j)$/fb at $\sqrt{s} = 650$ GeV			$\sigma(e^+e^- \to \tilde{\chi}^\pm_1\tilde{\chi}^\mp_2)$/fb
	$j = 3$	$j = 4$	$j = 5$	at $\sqrt{s} = 650$ GeV
Unpolarized beams	12.2 ± 0.6	5.5 ± 0.4	≤ 0.02	2.4 ± 0.3
$(P_{e^-}, P_{e^+}) = (-90\%, +60\%)$	36.9 ± 1.1	14.8 ± 0.7	≤ 0.07	5.8 ± 0.4
$(P_{e^-}, P_{e^+}) = (+90\%, -60\%)$	0.6 ± 0.1	2.2 ± 0.3	≤ 0.01	1.6 ± 0.2

ILC_{500} with $\sqrt{s} = 400$ GeV and 500 GeV lead to a consistent parameter determination in the MSSM. Hence in the considered scenario the analyses at the ILC_{500} or LHC alone do not allow a clear discrimination between MSSM and NMSSM. All predictions for the heavier gaugino/higgsino masses are consistent with both models. However, the ILC_{500} analysis predicts an almost pure higgsino-like state for $\tilde{\chi}^0_3$ and a mixed gaugino-higgsino-like $\tilde{\chi}^0_4$, see Fig. 4.17 (right panel). This allows the identification of the underlying supersymmetric model in combined analyses at the LHC and the $\mathrm{ILC}_{650}^{\mathcal{L}=1/3}$.

4.8.4 Combined LHC and ILC analysis

In our original NMSSM scenario, Eq. (4.57), the neutralinos $\tilde{\chi}^0_2$ and $\tilde{\chi}^0_3$ have a large bino-admixture and therefore appear in the squark decay cascades. The dominant decay mode of $\tilde{\chi}^0_2$ has a branching ratio $BR(\tilde{\chi}^0_2 \to \tilde{\chi}^\pm_1 W^\mp) \sim 50\%$, while for the $\tilde{\chi}^0_3$ decays $BR(\tilde{\chi}^0_3 \to \tilde{\ell}^\pm_{L,R}\ell^\mp) \sim 45\%$ is largest. Since the heavier neutralinos, $\tilde{\chi}^0_4$, $\tilde{\chi}^0_5$, are mainly higgsino-like, no visible edges from these particles occur in the cascades. It is expected to see the edges for $\tilde{\chi}^0_2 \to \tilde{\ell}^\pm_R\ell^\mp$, $\tilde{\chi}^0_2 \to \tilde{\ell}^\pm_L\ell^\mp$, $\tilde{\chi}^0_3 \to \tilde{\ell}^\pm_R\ell^\mp$ and for $\tilde{\chi}^0_3 \to \tilde{\ell}^\pm_L\ell^\mp$ [140].

With a precise mass measurement of $\tilde{\chi}^0_1$,$\tilde{\chi}^0_2$, $\tilde{\ell}_{L,R}$ and $\tilde{\nu}$ from the ILC_{500} analysis, a clear identification and separation of the edges of the two gauginos at the LHC is possible without imposing specific model assumptions. We therefore assume a precision of about 2% for the measurement of $m_{\tilde{\chi}^0_3}$, in analogy to [137–139]:

$$m_{\tilde{\chi}^0_3} = 367 \pm 7\ \mathrm{GeV}. \tag{4.68}$$

The precise mass measurement of $\tilde{\chi}^0_3$ is compatible with the mass predictions of the ILC_{500} for the $\tilde{\chi}^0_3$ in the MSSM but not with the prediction of the small gaugino admixture, see Fig. 4.17 (right panel). The $\tilde{\chi}^0_3$ as predicted in the MSSM would not be visible in the decay cascades at the LHC. The other possible interpretation of the measured neutralino as the $\tilde{\chi}^0_4$ in the MSSM is incompatible with the cross section measurements at the ILC. We point out that a measurement of the neutralino masses $m_{\tilde{\chi}^0_1}$, $m_{\tilde{\chi}^0_2}$, $m_{\tilde{\chi}^0_3}$ which could take place at the LHC alone is not sufficient to distinguish the SUSY models since rather similar mass spectra could exist [134, 135]. Therefore the cross sections in different beam polarization configurations at the ILC have to be included in the analysis.

The obvious inconsistency of the combined results from the LHC and the ILC_{500} analyses and the predictions for the missing chargino/neutralino masses could motivate the immediate use of the low-luminosity but higher-energy option $\mathrm{ILC}_{650}^{\mathcal{L}=1/3}$ in order to resolve model ambiguities even at an early stage of the experiment and outline future search strategies at the upgraded ILC at 1 TeV. This would finally lead to the correct identification of the underlying model. The expected polarized and unpolarized cross sections, including the statistical error on the basis of one third of the luminosity of the ILC_{500}, are given in Table 4.7. The neutralino $\tilde{\chi}^0_3$ as well as the higgsino-like heavy neutralino $\tilde{\chi}^0_4$ and the chargino $\tilde{\chi}^\pm_2$ are now accessible at the $\mathrm{ILC}_{650}^{\mathcal{L}=1/3}$.

The cross sections together with the precisely measured masses $m_{\tilde{\chi}^0_4}$ and $m_{\tilde{\chi}^\pm_2}$ constitute the observables for a fit of the NMSSM parameters. This will be achieved by extending the fit program `Fittino` [141] to include also the NMSSM [142], where the SUSY particle spectrum is calculated with `SPheno` [143] and the Higgs spectrum with `NMHDECAY` [63].

4.8.5 Concluding remarks

We have presented an NMSSM scenario where the measurement of masses and cross sections in the neutralino and chargino sector as well as measurements in the Higgs sector do not allow a distinction from the MSSM at the LHC or at the ILC_{500} with $\sqrt{s} = 500$ GeV alone. Precision measurements of the neutralino branching ratio into the lightest Higgs particle and of the mass difference between the lightest and next-to-lightest SUSY particle [122] may give first evidence for the SUSY model but are difficult to realize in the presented scenario. Therefore the identification of the underlying model requires precision measurements of the heavier neutralinos by combined analyses of LHC and ILC and the higher energy but lower luminosity option of the ILC at $\sqrt{s} = 650$ GeV. This gives access to the necessary observables for a fit of the underlying NMSSM parameters.

4.9 Moderately light charged Higgs bosons in the NMSSM and CPV-MSSM

Rohini M. Godbole and Durga P. Roy

We discuss some aspects of the phenomenology of a light charged Higgs ($M_{H^+} \lesssim 150$ GeV), allowed at low and moderate values of $\tan\beta$, in the NMSSM and CP-violating MSSM (CPV-MSSM), respecting all the LEP-II bounds. In the NMSSM with the $H^\pm$ near its lower mass limit ($M_{H^+} \simeq 120$ GeV), and a light pseudoscalar ($M_{A_1^0} \simeq 50$ GeV) with a very significant doublet component, the charged Higgs boson is expected to decay dominantly via the standard $H^+ \to \tau^+\nu$ mode. One can probe this mass range via the $t \to bH^+ \to b\tau^+\nu$ channel at Tevatron and especially at LHC. For somewhat heavier charged Higgs boson ($M_{H^\pm} > 130$ GeV) the dominant decay via the $H^+ \to W^+\, A_1^0$ channel provides a probe for not only a light H^+ but also a light A_1^0 [144] in the moderate $\tan\beta$ region, where its dominant decay mode is into a $b\bar{b}$ final state. A similar situation also attains in the CP-violating MSSM as well. The CPV-MSSM allows the existence of a light neutral Higgs boson ($M_{H_1} \lesssim 50$ GeV) in the CPX scenario in the low $\tan\beta(\lesssim 5)$ region, which could have escaped the LEP searches due to a strongly suppressed $H_1 ZZ$ coupling. The light charged H^+ decays dominantly into the WH_1 channel again giving rise to a striking $t\bar{t}$ signal at the LHC, where one of the top quarks decays into the $bb\bar{b}W$ channel, via $t \to bH^\pm, H^\pm \to WH_1$ and $H_1 \to b\bar{b}$. The characteristic correlation between the $b\bar{b}$, $b\bar{b}W$ and $bb\bar{b}W$ invariant mass peaks helps reduce the SM background, drastically.

4.9.1 Moderately light $H^\pm$ in the NMSSM

As discussed in Section 4.1.2, the solution of the the so called μ-problem of the MSSM was the original motivation for the NMSSM. The effect of the additional complex singlet scalar S in the NMSSM on the charged Higgs phenomenology mainly comes through a relaxation of the mass limits of the A^0 and the H^+ in the MSSM. This arises from the modification of the MSSM mass relations between the doublet scalars $H_{1,2}$ and pseudoscalar A and the resulting modification of the H_1 mass bound. The masses of the $A_i^0, i = 1, 2$ and $H_i, i = 1, 3$ in terms of the various parameters of the NMSSM: the dimensionless parameters λ, κ appearing in the superpotential of Eq. (4.7) as well as the corresponding soft trilinear terms A_λ, A_κ and the vacuum expectation value of the singlet scalar field $\langle S\rangle = x = v_S/\sqrt{2}$, are given by Eqs. (4.16)–(4.19). In particular, the resulting upper bound of the lightest Higgs scalar mass including the radiative correction ϵ, is [25, 28, 29, 145–147]

$$M_{H_1}^2 \le M_Z^2 \cos^2(2\beta) + \frac{2\lambda^2 M_W^2}{g^2} \sin^2(2\beta) + \epsilon, \tag{4.69}$$

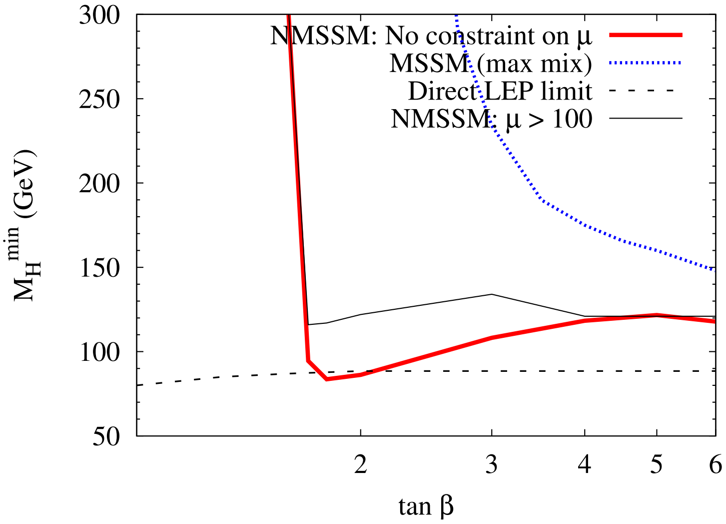

Fig. 4.18: The indirect lower bounds on the charged Higgs boson mass following from the LEP limits on the neutral Higgs bosons in the MSSM (Maximal Stop Mixing) and the NMSSM. The direct LEP limit on the charged Higgs boson mass is also shown for comparison .

where contribution specific to the NMSSM in addition to the terms in MSSM is given by the middle term. This is most pronounced in the low to moderate $\tan\beta$ region, where the MSSM mass bound coming from the first term of Eq. (4.69) is very small. Therefore it relaxes the MSSM bound on M_{H_1} and the resulting lower limit of M_{A_i}, most significantly over this range of $\tan\beta$. This in turn relaxes the lower limit of the charged Higgs mass, which is related to the doublet pseudoscalar mass via

$$M^2_{H^+} = M^2_A + M^2_W \left(1 - \frac{2\lambda^2}{g^2}\right) \tag{4.70}$$

along with a small radiative correction. This is helped further due to the additional (negative) contribution in Eq. (4.70). Note that the additional contributions of Eqs. (4.69) and (4.70) depend only on the $\hat{S}\hat{H}_u\hat{H}_d$ coupling λ, in the superpotential of Eq. (4.7). Therefore the Eqs. (4.69) and (4.70) hold also for the minimal nonminimal supersymmetric standard model (MNSSM), which assumes only this term in the superpotential [44, 45, 47]. Finally the upper bound of Eq. (4.69) will only be useful if one can find an upper limit on λ. Such a limit can be derived [25, 29, 145] from the requirement that all the couplings of the model remain perturbative upto some high energy scale, usually taken to be the GUT scale. Such an upper limit on λ has been estimated in [148] as a function of $\tan\beta$ using two-loop renormalization group equations.

For quantitative evaluation of the NMSSM Higgs spectrum we consider the complete Higgs potential as given in terms of these parameters in [55]. The lower limit of the $H^\pm$ mass has been estimated as a function of $\tan\beta$ in [148] by varying all these five NMSSM parameters over the allowed ranges, which include the constraints from LEP-2. The resulting $H^\pm$ mass limit is shown in Fig. 4.18 along with the most conservative MSSM limit, corresponding to maximal stop mixing, which gives the largest radiative correction ϵ. The NMSSM limit has practically no sensitivity to stop mixing. The LEP-2 mass limit from direct search of $H^+ \to \tau^+\nu$ events is also shown for comparison [109]. There is no limit from Tevatron in the moderate $\tan\beta$ region shown in Fig. 4.18.

One sees from Fig. 4.18 that even the most conservative MSSM limit implies $H^\pm$ mass ≥ 150 GeV (175 GeV) for $\tan\beta \leq 6$ (4). In contrast in the NMSSM one can have a $H^\pm$ mass $\lesssim 120$ GeV over this moderate $\tan\beta$ region, going down to the direct LEP-2 limit of 86 GeV at $\tan\beta \simeq 2$. Note however that requiring that the effective μ parameter $\mu_{eff} = \langle S\rangle\lambda$ be greater than 100 GeV, as favored

Table 4.8: Examples of dominant $H^{\pm} \to WA_1^0$ decay in the NMSSM. These decay branching fractions are shown along with the Higgs boson masses and the other model parameters.

$\tan\beta$	M_{H^+} (GeV)	M_{A_1} (GeV)	B_{A_1} (%)	λ, κ	$x = v_s/\sqrt{2}, A_\lambda, A_\kappa$ (GeV)
2	147	38	94	0.45, -0.69	224, -8, 2
3	159	65	83	0.33, -0.70	305, 40, 38
4	145	48	89	0.28, -0.70	563, 170, 85
5	150	10	91	0.26, -0.54	503, 109, 38

by the LEP chargino search, increases this mass limit to $\gtrsim$ 120 GeV [47]. The steep vertical rise at left reflects the well-known fixed-point solution at $\tan\beta = 1.55$, where the top Yukawa coupling blows up at the GUT scale. Thus allowing for possible intermediate scale physics one can evade the steep NMSSM mass limit at low $\tan\beta$ [149]. In contrast the MSSM limit holds independent of any intermediate scale physics ansatz.

We have investigated the neutral scalar and pseudoscalar Higgs spectrum of the NMSSM, when the $H^{\pm}$ lies near its lower mass limit ($M_{H^+} \simeq$ 120 GeV). The lightest scalar is dominantly singlet ($M_{H_1} \simeq$ 100 GeV), while the doublet scalars are relatively heavy ($M_{H_{2,3}} >$ 120 GeV). On the other hand there is often a light pseudoscalar ($M_{A_1^0} \simeq$ 50 GeV) with a very significant doublet component. Consequently a light charged Higgs boson of mass $\simeq$ 120 GeV is expected to decay dominantly via the standard $H^+ \to \tau^+\nu$ mode. Thus one can probe this mass range via the $t \to bH^+ \to b\tau^+\nu$ channel at Tevatron and especially at LHC. On the other hand a somewhat heavier charged Higgs boson ($M_{H^\pm} >$ 130 GeV) can dominantly decay via the $H^+ \to W^+ A_1^0$ channel [144]. In fact this seems to be a very favorable channel to probe for not only H^+ but also a light A^0 in the moderate $\tan\beta$ region, where the A^0 is expected to decay mainly in to the $b\bar{b}$ or $\tau^+\tau^-$ mode. Table 4.8 shows some illustrative samples of NMSSM Higgs spectra where H^+ decays dominantly into the $W^+A_1^0$ mode. These results are obtained by scanning the NMSSM parameter space. Note that in each case the effective μ parameter $\mu_{eff} = \lambda\langle S\rangle$ is greater than 100 GeV as favored by the LEP chargino limit. The decay branching fractions are shown along with the Higgs boson masses and the other model parameters.

4.9.2 Light $H^{\pm}$ in the CP-violating MSSM

Interestingly one can have a similar signal in the CP violating MSSM due to large scalar-pseudoscalar mixing. The CP-violating MSSM allows existence of a light neutral Higgs boson ($M_{H_1} \lesssim$ 50 GeV) in the CPX scenario in the low $\tan\beta$($\lesssim 5$) region, which could have escaped the LEP searches due to a strongly suppressed H_1ZZ coupling. The light charged H^+ decays dominantly into the WH_1 channel giving rise to a striking $t\bar{t}$ signal at the LHC, where one of the top quarks decays into the $bb\bar{b}W$ channel, via $t \to bH^{\pm}, H^{\pm} \to WH_1$ and $H_1 \to b\bar{b}$. The characteristic correlation between the $b\bar{b}$, $b\bar{b}W$ and $bb\bar{b}W$ invariant mass peaks helps reduce the SM background, drastically [62]. Note that this signal is identical to the NMSSM case discussed above.

As already mentioned, a combined analysis of all the LEP results, shows that a light neutral Higgs is still allowed in the CPX [150] scenario in the CPV-MSSM. The experiments provide exclusion regions in the $M_{H_1} - \tan\beta$ plane for different values of the CP-violating phase, with the various parameters taking value as given in the CPX scenario in Section 3.1, Eq. (3.13). Combining the results of Higgs searches from ALEPH, DELPHI, L3 and OPAL, the authors in Ref. [50, 151] have provided exclusion regions in the M_{H_1}–$\tan\beta$ plane as well as in the M_{H^+}–$\tan\beta$ plane. A more recent analysis of the LEP exclusion limits is given in Section 3.2 of this report. While the exact exclusion regions differ somewhat in the three analysis they all show that for phases $\Phi_{\rm CP} = 90°$ and $60°$ LEP cannot exclude the presence of a light Higgs boson at low $\tan\beta$, mainly because of the suppressed H_1ZZ coupling. The analysis

Table 4.9: Range of values for BR ($H^+ \to H_1 W^+$) and BR ($t \to bH^+$) for different values of $\tan\beta$ corresponding to the LEP allowed window in the CPX scenario, for the common phase $\Phi_{\rm CP} = 90°$, along with the corresponding range for the H_1 and H^+ masses. The quantities in the bracket in each column give the values at the edge of the kinematic region where the decay $H^+ \to H_1 W^+$ is allowed.

$\tan\beta$	3.6	4	4.6	5
$\mathrm{Br}(H^+ \to H_1 W^+)[\%]$	> 90 (87.45)	> 90 (57.65)	> 90 (50.95)	> 90 (46.57)
$\mathrm{Br}(t \to bH^+)[\%]$	~ 0.7	0.7 – 1.1	0.9 – 1.3	1.0 – 1.3
M_{H^+} [GeV]	< 148.5 (149.9)	< 139 (145.8)	< 130.1 (137.5)	< 126.2 (134)
M_{H_1} [GeV]	< 60.62 (63.56)	< 49.51 (65.4)	< 36.62 (57.01)	< 29.78 (53.49)

of Ref. [50] further shows that in the same region the $H_1 t\bar{t}$ coupling is suppressed as well. Thus this particular region in the parameter space can not be probed either at the Tevatron where the associated production W/ZH_1 mode is the most promising one; neither can this be probed at the LHC as the reduced $t\bar{t}H_1$ coupling suppresses the inclusive production mode and the associated production modes W/ZH_1 and $t\bar{t}H_1$, are suppressed as well. This region of Ref. [50] corresponds to $\tan\beta \sim 3.5 - 5, M_{H^+} \sim 125 - 140$ GeV, $M_{H_1} \lesssim 50$ GeV and $\tan\beta \sim 2 - 3, M_{H^+} \sim 105 - 130$ GeV$, M_{H_1} \lesssim 40$ GeV, for $\Phi_{CP} = 90°$ and $60°$ respectively. In the same region of the parameter space where $H_1 ZZ$ coupling is suppressed, the $H^+ W^- H_1$ coupling is enhanced because these two sets of couplings satisfy a sum-rule. Further, in the MSSM a light pseudo-scalar implies a light charged Higgs, lighter than the top quark.

Table 4.9 shows the behaviour of the M_{H^+}, M_{H_1} and the BR ($H^+ \to H_1 W^+$), for values of $\tan\beta$ corresponding to the above mentioned window in the $\tan\beta$–M_{H_1} plane, of Ref. [50]. It is to be noted here that indeed the $H^\pm$ is light (lighter than the top) over the entire range, making its production in t decay possible. Further, the $H^\pm$ decays dominantly into $H_1 W$, with a branching ratio larger than 47% over the entire range where the decay is kinematically allowed, which covers practically the entire parameter range of interest; viz. $M_{H_1} < 50$ GeV for $\Phi_{\rm CP} = 90°$. It can be also seen from the table that the BR($H^\pm \to H_1 W$) is larger than 90% over most of the parameter space of interest. So not only that H^+ can be produced abundantly in the t decay giving rise to a possible production channel of H_1 through the decay $H^\pm \to H_1 W^\pm$, but this decay mode will be the only decay channel to see this light ($M_{H^\pm} < M_t$) $H^\pm$. The traditional decay mode of $H^\pm \to \tau\nu$ is suppressed by over an order of magnitude and thus will no longer be viable. Thus the process

$$
\begin{array}{llllllll}
pp \to t & & & & + & \bar{t} & + & X \\
\quad \hookrightarrow & b\; H^+ & & & & \hookrightarrow \bar{b}\; W & & \\
& \quad \hookrightarrow & W & H_1 & & \quad \hookrightarrow q\bar{q}(\ell\nu) & & \\
& & \hookrightarrow \ell\nu(q\bar{q}) & \hookrightarrow b\bar{b} & & & &
\end{array}
$$

allows a probe of both the light H_1 **and** a light $H^\pm$ in this parameter window in the CP-violating MSSM in the CPX scenario.

As can be seen from the Fig. 4.19 the largest signal cross-section case is ~ 38 fb and the signal cross-section is $\gtrsim 20$ fb for $M_{H_1} \gtrsim 15$ GeV. It is clear from the right panel of the Fig. 4.19, that there is simultaneous clustering in the $m_{b\bar{b}}$ distribution around $\simeq M_{H_1}$ and in the $m_{b\bar{b}W}$ distribution around $M_{H^\pm}$. This clustering feature can be used to distinguish the signal over the standard model background.

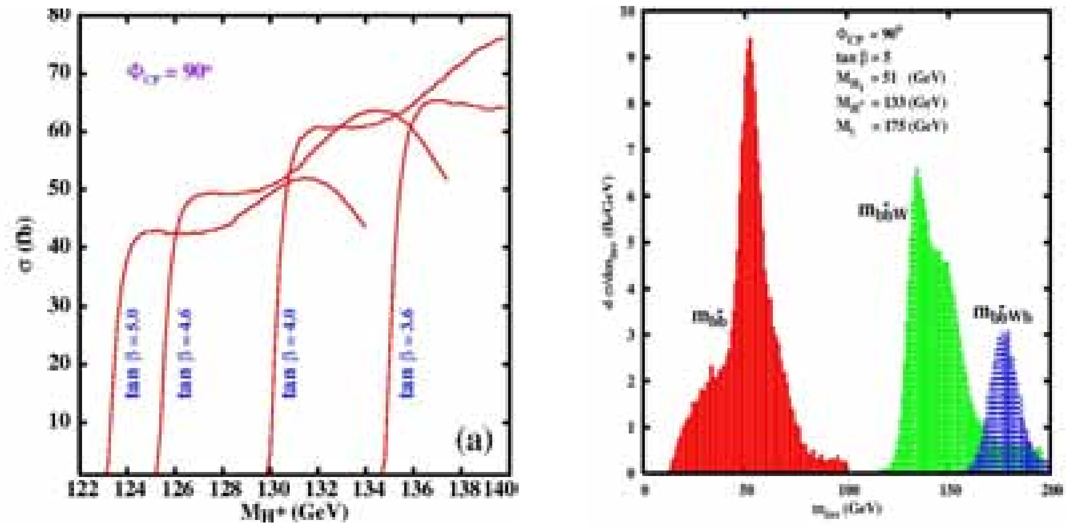

Fig. 4.19: Variation of the cross-section with M_{H^+} for four values of $\tan\beta = 3.6, 4, 4.6$ and 5 is shown in the left panel, for the CP-violating phase $\Phi_{\rm CP} = 90°$. These numbers should be multiplied by ~ 0.5 to get the signal cross-section to take into account the b tagging ef ciency. The right panel shows the $m_{b\bar{b}}, m_{b\bar{b}W}$ and the $m_{b\bar{b}Wb} = M_t$ invariant mass distributions, for this choice of CP-violating phase and $\tan\beta = 5, M_{H^+} = 133$ GeV, corresponding to a light neutral Higgs H_1 with mass $M_{H_1} = 51$ GeV M_t, M_W mass window cuts have been applied [62].

As a matter of fact the estimated background to the signal coming from the QCD production of $t\bar{t}b\bar{b}$ once all the cuts (including the mass window cuts) are applied, to the signal type events is less than 0.5 fb, in spite of a starting cross-section of 8.5 pb. The major reduction is brought about by requiring that the invariant mass of the $bbbW$ be within 25 GeV of M_t.

4.9.3 Summary

Thus in conclusion, both in the NMSSM and in the CPV-MSSM the moderately light charged Higgs that is allowed at moderately low values of $\tan\beta$, provides interesting and novel phenomenology at the LHC.

REFERENCES

[1] L. J. Hall, J. Lykken and S. Weinberg, Phys. Rev. **D27**, 2359 (1983).

[2] J. E. Kim and H. P. Nilles, Phys. Lett. **B138**, 150 (1984).

[3] G. F. Giudice and A. Masiero, Phys. Lett. **B206**, 480 (1988).

[4] E. J. Chun, J. E. Kim and H. P. Nilles, Nucl. Phys. **B370**, 105 (1992).

[5] I. Antoniadis, E. Gava, K. S. Narain and T. R. Taylor, Nucl. Phys. **B432**, 187 (1994), [hep-th/9405024].

[6] R. D. Peccei and H. R. Quinn, Phys. Rev. Lett. **38**, 1440 (1977).

[7] J. E. Kim, Phys. Rev. Lett. **43**, 103 (1979).

[8] A. R. Zhitnitsky, Sov. J. Nucl. Phys. **31**, 260 (1980).

[9] M. Dine, W. Fischler and M. Srednicki, Phys. Lett. **B104**, 199 (1981).

[10] D. J. Miller and R. Nevzorov, hep-ph/0309143.

[11] L. J. Hall and T. Watari, Phys. Rev. **D70**, 115001 (2004), [hep-ph/0405109].

[12] B. Feldstein, L. J. Hall and T. Watari, Phys. Lett. **B607**, 155 (2005), [hep-ph/0411013].

[13] M. Cvetic, D. A. Demir, J. R. Espinosa, L. L. Everett and P. Langacker, Phys. Rev. **D56**, 2861 (1997), [hep-ph/9703317].
[14] D. A. Demir and L. L. Everett, Phys. Rev. **D69**, 015008 (2004), [hep-ph/0306240].
[15] T. Han, P. Langacker and B. McElrath, Phys. Rev. **D70**, 115006 (2004), [hep-ph/0405244].
[16] S. F. King, S. Moretti and R. Nevzorov, hep-ph/0510419.
[17] M. Carena, A. Daleo, B. A. Dobrescu and T. M. P. Tait, Phys. Rev. **D70**, 093009 (2004), [hep-ph/0408098].
[18] F. Abe *et al.* (CDF Collaboration), Phys. Rev. Lett. **79**, 2192 (1997).
[19] V. M. Abazov *et al.* (D0 Collaboration), Phys. Rev. Lett. **87**, 061802 (2001), [hep-ex/0102048].
[20] P. Fayet, Nucl. Phys. **B90**, 104 (1975).
[21] H. P. Nilles, M. Srednicki and D. Wyler, Phys. Lett. **B120**, 346 (1983).
[22] J. M. Frere, D. R. T. Jones and S. Raby, Nucl. Phys. **B222**, 11 (1983).
[23] J. P. Derendinger and C. A. Savoy, Nucl. Phys. **B237**, 307 (1984).
[24] B. R. Greene and P. J. Miron, Phys. Lett. **B168**, 226 (1986).
[25] M. Drees, Int. J. Mod. Phys. **A4**, 3635 (1989).
[26] J. R. Ellis, J. F. Gunion, H. E. Haber, L. Roszkowski and F. Zwirner, Phys. Rev. **D39**, 844 (1989).
[27] U. Ellwanger, M. Rausch de Traubenberg and C. A. Savoy, Nucl. Phys. **B492**, 21 (1997), [hep-ph/9611251].
[28] P. N. Pandita, Z. Phys. **C59**, 575 (1993).
[29] S. F. King and P. L. White, Phys. Rev. **D52**, 4183 (1995), [hep-ph/9505326].
[30] D. J. Miller, R. Nevzorov and P. M. Zerwas, Nucl. Phys. **B681**, 3 (2004), [hep-ph/0304049].
[31] S. Y. Choi, D. J. Miller and P. M. Zerwas, Nucl. Phys. **B711**, 83 (2005), [hep-ph/0407209].
[32] Y. B. Zeldovich, I. Y. Kobzarev and L. B. Okun, Zh. Eksp. Teor. Fiz. **67**, 3 (1974).
[33] A. Vilenkin, Phys. Rep. **121**, 263 (1985).
[34] H. P. Nilles, M. Srednicki and D. Wyler, Phys. Lett. **B124**, 337 (1983).
[35] A. B. Lahanas, Phys. Lett. **B124**, 341 (1983).
[36] U. Ellwanger, Phys. Lett. **B133**, 187 (1983).
[37] J. Bagger and E. Poppitz, Phys. Rev. Lett. **71**, 2380 (1993), [hep-ph/9307317].
[38] J. Bagger, E. Poppitz and L. Randall, Nucl. Phys. **B426**, 3 (1994), [hep-ph/9405345].
[39] V. Jain, Phys. Lett. **B351**, 481 (1995), [hep-ph/9407382].
[40] S. A. Abel, Nucl. Phys. **B480**, 55 (1996), [hep-ph/9609323].
[41] C. F. Kolda, S. Pokorski and N. Polonsky, Phys. Rev. Lett. **80**, 5263 (1998), [hep-ph/9803310].
[42] S. A. Abel, S. Sarkar and P. L. White, Nucl. Phys. **B454**, 663 (1995), [hep-ph/9506359].
[43] C. Panagiotakopoulos and K. Tamvakis, Phys. Lett. **B446**, 224 (1999), [hep-ph/9809475].
[44] C. Panagiotakopoulos and A. Pilaftsis, Phys. Rev. **D63**, 055003 (2001), [hep-ph/0008268].
[45] C. Panagiotakopoulos and K. Tamvakis, Phys. Lett. **B469**, 145 (1999), [hep-ph/9908351].
[46] A. Dedes, C. Hugonie, S. Moretti and K. Tamvakis, Phys. Rev. **D63**, 055009 (2001), [hep-ph/0009125].
[47] C. Panagiotakopoulos and A. Pilaftsis, Phys. Lett. **B505**, 184 (2001), [hep-ph/0101266].
[48] R. Dermisek and J. F. Gunion, Phys. Rev. Lett. **95**, 041801 (2005), [hep-ph/0502105].
[49] R. Dermisek and J. F. Gunion, hep-ph/0510322.
[50] M. Carena, J. R. Ellis, S. Mrenna, A. Pilaftsis and C. E. M. Wagner, Nucl. Phys. **B659**, 145 (2003), [hep-ph/0211467].
[51] A. Menon, D. E. Morrissey and C. E. M. Wagner, Phys. Rev. **D70**, 035005 (2004), [hep-

ph/0404184].

[52] V. Barger, P. Langacker and H.-S. Lee, Phys. Lett. **B630**, 85 (2005), [hep-ph/0508027].

[53] J. F. Gunion, D. Hooper and B. McElrath, hep-ph/0509024.

[54] G. Belanger, F. Boudjema, C. Hugonie, A. Pukhov and A. Semenov, JCAP **0509**, 001 (2005), [hep-ph/0505142].

[55] M. Bastero-Gil, C. Hugonie, S. F. King, D. P. Roy and S. Vempati, Phys. Lett. **B489**, 359 (2000), [hep-ph/0006198].

[56] S. W. Ham, S. K. Oh, C. M. Kim, E. J. Yoo and D. Son, Phys. Rev. **D70**, 075001 (2004), [hep-ph/0406062].

[57] K. Funakubo, S. Tao and F. Toyoda, Prog. Theor. Phys. **114**, 369 (2005), [hep-ph/0501052].

[58] M. Carena, M. Quiros, M. Seco and C. E. M. Wagner, Nucl. Phys. **B650**, 24 (2003), [hep-ph/0208043].

[59] T. Konstandin, T. Prokopec, M. G. Schmidt and M. Seco, hep-ph/0505103.

[60] J. F. Gunion and H. E. Haber, Nucl. Phys. **B272**, 1 (1986).

[61] J. F. Gunion and A. Turski, Phys. Rev. **D40**, 2333 (1989).

[62] D. K. Ghosh, R. M. Godbole and D. P. Roy, Phys. Lett. **B628**, 131 (2005), [hep-ph/0412193].

[63] U. Ellwanger, J. F. Gunion and C. Hugonie, JHEP **02**, 066 (2005), [hep-ph/0406215].

[64] U. Ellwanger and C. Hugonie, hep-ph/0508022.

[65] J. F. Gunion, H. E. Haber and T. Moroi, Proc. Snowmass 1996, Snowmass Village, CO, 1996, eConf **C960625**, LTH095 (1996), [hep-ph/9610337].

[66] B. A. Dobrescu, G. Landsberg and K. T. Matchev, Phys. Rev. **D63**, 075003 (2001), [hep-ph/0005308].

[67] B. A. Dobrescu and K. T. Matchev, JHEP **09**, 031 (2000), [hep-ph/0008192].

[68] U. Ellwanger, J. F. Gunion and C. Hugonie, hep-ph/0111179.

[69] U. Ellwanger, J. F. Gunion, C. Hugonie and S. Moretti, hep-ph/0305109.

[70] U. Ellwanger, J. F. Gunion, C. Hugonie and S. Moretti, hep-ph/0401228.

[71] D. J. Miller and S. Moretti, hep-ph/0403137.

[72] U. Ellwanger, J. F. Gunion and C. Hugonie, JHEP **07**, 041 (2005), [hep-ph/0503203].

[73] R. Barbieri and G. F. Giudice, Nucl. Phys. **B306**, 63 (1988).

[74] R. Barate *et al.* (The LEP Working Group for Higgs Boson Searches), hep-ex/0602042.

[75] R. Barate *et al.* (The LEP Working Group for Higgs Boson Searches), Phys. Lett. **B565**, 61 (2003), [hep-ex/0306033].

[76] N. Marinelli (CMS Collaboration), Physics at LHC (PHLHC 04), Vienna, Austria, 2004, Czech. J. Phys. **55** (2005) suppl. B.

[77] A. D. Martin, V. A. Khoze and M. G. Ryskin, hep-ph/0507305.

[78] J. R. Forshaw, hep-ph/0508274.

[79] A. B. Kaidalov, V. A. Khoze, A. D. Martin and M. G. Ryskin, Eur. Phys. J. **C33**, 261 (2004), [hep-ph/0311023].

[80] J. F. Gunion, V. Khoze, A. de Roeck, M. Ryskin, work in progress.

[81] J. F. Gunion and M. Szleper, hep-ph/0409208.

[82] J. Dai, J. F. Gunion and R. Vega, Phys. Lett. **B315**, 355 (1993), [hep-ph/9306319].

[83] S. Baffioni, Clermont-Ferrand, France.

[84] S. Moretti and S. Munir, hep-ph/0603085.

[85] Z. Kunszt, S. Moretti and W. J. Stirling, Z. Phys. **C74**, 479 (1997), [hep-ph/9611397].

[86] V. Buscher and K. Jakobs, Int. J. Mod. Phys. **A20**, 2523 (2005), [hep-ph/0504099].

[87] W. W. Armstrong *et al.* (ATLAS Collaboration), ATLAS: Technical proposal for a general-purpose pp experiment at the Large Hadron Collider at CERN, CERN-LHCC-94-43.

[88] A. Bottino, N. Fornengo and S. Scopel, Phys. Rev. **D67**, 063519 (2003), [hep-ph/0212379].

[89] A. Bottino, F. Donato, N. Fornengo and S. Scopel, Phys. Rev. **D68**, 043506 (2003), [hep-ph/0304080].

[90] D. Hooper and T. Plehn, Phys. Lett. **B562**, 18 (2003), [hep-ph/0212226].

[91] C. L. Bennett *et al.*, Astrophys. J. Suppl. **148**, 1 (2003), [astro-ph/0302207].

[92] D. N. Spergel *et al.* (WMAP Collaboration), Astrophys. J. Suppl. **148**, 175 (2003), [astro-ph/0302209].

[93] G. Belanger, F. Boudjema, A. Pukhov and A. Semenov, micrOMEGAs2.0 and the relic density of dark matter in a generic model, in *Les Houches Physics at TeV colliders 2005, Beyond the Standard Model Working Group, summary report*, [hep-ph/0602198].

[94] U. Ellwanger and C. Hugonie, Eur. Phys. J. **C13**, 681 (2000), [hep-ph/9812427].

[95] U. Ellwanger and C. Hugonie, Eur. Phys. J. **C5**, 723 (1998), [hep-ph/9712300].

[96] G. Belanger, F. Boudjema, A. Pukhov and A. Semenov, Comput. Phys. Commun. **149**, 103 (2002), [hep-ph/0112278].

[97] G. Belanger, F. Boudjema, A. Pukhov and A. Semenov, Comput. Phys. Commun. **174**, 577 (2006), [hep-ph/0405253].

[98] T. Elliott, S. F. King and P. L. White, Phys. Lett. **B314**, 56 (1993), [hep-ph/9305282].

[99] U. Ellwanger and C. Hugonie, Eur. Phys. J. **C25**, 297 (2002), [hep-ph/9909260].

[100] S. W. Ham, S. K. Oh and B. R. Kim, Phys. Lett. **B414**, 305 (1997), [hep-ph/9612294].

[101] P. Langacker and J. Wang, Phys. Rev. **D58**, 115010 (1998), [hep-ph/9804428].

[102] J. Erler, P. Langacker and T.-j. Li, Phys. Rev. **D66**, 015002 (2002), [hep-ph/0205001].

[103] V. Barger, P. Langacker, H.-S. Lee and G. Shaughnessy, hep-ph/0603247.

[104] S. Weinberg, Phys. Rev. Lett. **40**, 223 (1978).

[105] F. Wilczek, Phys. Rev. Lett. **40**, 279 (1978).

[106] A. Sopczak, hep-ph/0502002.

[107] LEP Higgs Working Group for Higgs boson searches, hep-ex/0107031.

[108] LEP SUSY Working Group: ALEPH, DELPHI, L3 and OPAL Collaborations, LEPSUSYWG/01-03.1, see `http://lepsusy.web.cern.ch/lepsusy/`.

[109] Particle Data Group, S. Eidelman *et al.*, Phys. Lett. **B592**, 1 (2004).

[110] R. Barate *et al.* (ALEPH Collaboration), Eur. Phys. J. **C12**, 183 (2000), [hep-ex/9904011].

[111] P. Abreu *et al.* (DELPHI Collaboration), Phys. Lett. **B485**, 45 (2000), [hep-ex/0103025].

[112] J. Erler and P. Langacker, Phys. Lett. **B456**, 68 (1999), [hep-ph/9903476].

[113] K. S. Babu, C. F. Kolda and J. March-Russell, Phys. Rev. **D54**, 4635 (1996), [hep-ph/9603212].

[114] A. Aranda and C. D. Carone, Phys. Lett. **B443**, 352 (1998), [hep-ph/9809522].

[115] F. Franke and H. Fraas, Z. Phys. **C72**, 309 (1996), [hep-ph/9511275].

[116] F. Franke and H. Fraas, Int. J. Mod. Phys. **A12**, 479 (1997), [hep-ph/9512366].

[117] F. Franke, H. Fraas and A. Bartl, Phys. Lett. **B336**, 415 (1994), [hep-ph/9408217].

[118] S. Hesselbach, F. Franke and H. Fraas, Phys. Lett. **B492**, 140 (2000), [hep-ph/0007310].

[119] F. Franke and S. Hesselbach, Phys. Lett. **B526**, 370 (2002), [hep-ph/0111285].

[120] S. Hesselbach and F. Franke, hep-ph/0210363.

[121] S. Kraml and W. Porod, Phys. Lett. **B626**, 175 (2005), [hep-ph/0507055].

[122] J. F. Gunion and S. Mrenna, Phys. Rev. **D64**, 075002 (2001), [hep-ph/0103167].

[123] C. Hensel, *Search for nearly mass degenerate charginos and neutralinos in e^+e^- collisions*, Ph.D.

thesis, Hamburg University, 2002, DESY-THESIS-2002-047.
[124] S. Y. Choi, A. Djouadi, H. K. Dreiner, J. Kalinowski and P. M. Zerwas, Eur. Phys. J. **C7**, 123 (1999), [hep-ph/9806279].
[125] S. Y. Choi *et al.*, Eur. Phys. J. **C14**, 535 (2000), [hep-ph/0002033].
[126] S. Y. Choi, J. Kalinowski, G. Moortgat-Pick and P. M. Zerwas, Eur. Phys. J. **C22**, 563 (2001), [hep-ph/0108117].
[127] S. Y. Choi, J. Kalinowski, G. Moortgat-Pick and P. M. Zerwas, hep-ph/0202039.
[128] G. Moortgat-Pick, S. Hesselbach, F. Franke and H. Fraas, hep-ph/9909549.
[129] S. Hesselbach, F. Franke and H. Fraas, hep-ph/0003272.
[130] S. Hesselbach, F. Franke and H. Fraas, Eur. Phys. J. **C23**, 149 (2002), [hep-ph/0107080].
[131] G. Weiglein *et al.* (LHC/LC Study Group), hep-ph/0410364.
[132] T. Tsukamoto, K. Fujii, H. Murayama, M. Yamaguchi and Y. Okada, Phys. Rev. **D51**, 3153 (1995).
[133] J. L. Feng, M. E. Peskin, H. Murayama and X. Tata, Phys. Rev. **D52**, 1418 (1995), [hep-ph/9502260].
[134] G. Moortgat-Pick, S. Hesselbach, F. Franke and H. Fraas, JHEP **06**, 048 (2005), [hep-ph/0502036].
[135] G. Moortgat-Pick, S. Hesselbach, F. Franke and H. Fraas, hep-ph/0508313.
[136] A. Bartl, H. Fraas, W. Majerotto and B. Mosslacher, Z. Phys. **C55**, 257 (1992).
[137] G. Polesello, J. Phys. **G30**, 1185 (2004).
[138] K. Desch, J. Kalinowski, G. Moortgat-Pick, M. M. Nojiri and G. Polesello, JHEP **02**, 035 (2004), [hep-ph/0312069].
[139] G. Moortgat-Pick, K. Desch, J. Kalinowski, M. M. Nojiri and G. Polesello, hep-ph/0410121.
[140] G. Polesello, private communication.
[141] P. Bechtle, K. Desch and P. Wienemann, hep-ph/0506244.
[142] P. Bechtle *et al.*, in progress.
[143] W. Porod, Comput. Phys. Commun. **153**, 275 (2003), [hep-ph/0301101].
[144] M. Drees, M. Guchait and D. P. Roy, Phys. Lett. **B471**, 39 (1999), [hep-ph/9909266].
[145] S. F. King and P. L. White, Phys. Rev. **D53**, 4049 (1996), [hep-ph/9508346].
[146] U. Ellwanger and M. Rausch de Traubenberg, Z. Phys. **C53**, 521 (1992).
[147] T. Elliott, S. F. King and P. L. White, Phys. Rev. **D49**, 2435 (1994), [hep-ph/9308309].
[148] M. Drees, E. Ma, P. N. Pandita, D. P. Roy and S. K. Vempati, Phys. Lett. **B433**, 346 (1998), [hep-ph/9805242].
[149] M. Masip, R. Munoz-Tapia and A. Pomarol, Phys. Rev. **D57**, 5340 (1998), [hep-ph/9801437].
[150] A. Pilaftsis and C. E. M. Wagner, Nucl. Phys. **B553**, 3 (1999), [hep-ph/9902371].
[151] G. Abbiendi *et al.* (OPAL Collaboration), Eur. Phys. J. **C37**, 49 (2004), [hep-ex/0406057].